297 068

AFCRL-62-1008

THE OHIO STATE UNIVERSITY

RESEARCH FOUNDATION

1314 KINNEAR ROAD   COLUMBUS 12, OHIO

AN INTERFEROMETRIC-MODULATION ORDER-SEPARATOR FOR A FAR INFRARED SPECTROGRAPH

Miles Elliot Vance

ASTIA

FEB 27 1963

TISIA   A

NOTICES

Requests for additional copies by Agencies of the Department of Defense, their contractors, and other Government agencies should be directed to the:

ARMED SERVICES TECHNICAL INFORMATION AGENCY
ARLINGTON HALL STATION
ARLINGTON 12, VIRGINIA

Department of Defense contractors must be established for ASTIA services or have their "need-to-know" certified by the cognizant military agency of their project or contract.

All other persons and organizations should apply to the:

U.S. DEPARTMENT OF COMMERCE
OFFICE OF TECHNICAL SERVICES
WASHINGTON 25, D.C.

AFCRL-62-1008

AN INTERFEROMETRIC-MODULATION ORDER-SEPARATOR
FOR A FAR INFRARED SPECTROGRAPH

Miles Elliot Vance

The Ohio State University
Research Foundation
Columbus 12, Ohio

September 1962

FOREWORD

The body of this technical report is the dissertation of Dr. Miles Vance, which was written in partial fulfillment of the requirements for his Ph.D. degree (1962) from The Ohio State University. The research reported in the dissertation was supported, in part, by the Air Force Cambridge Research Laboratories through Contract AF 19(604)-4119 with The Ohio State University Research Foundation and by a grant from the National Science Foundation.

The interferometric modulator described in this report is now in constant use in the new far-infrared spectrometer at the University. Discussions of this modulator and spectrometer have been reported in the following papers at the Symposium on Molecular Structure and Spectroscopy at The Ohio State University, Columbus, June 1962:

> "An Interferometric Modulator For Use as a Pre-Monochromator in the Far Infrared," by M. E. Vance, E. E. Bell, P. B. Burnside and R. F. Rowntree.

> "A New Far-Infrared Submillimeter Spectrometer Utilizing Interferometric Modulation," by R. F. Rowntree, E. E. Bell, M. E. Vance and R. A. Oetjen.

This instrument has also been described at The International Symposium on Molecular Structure and Spectroscopy in Tokyo, Japan, September 1962, under the following title:

> "An Interferometric Modulation Order Separator for a Far-Infrared Spectrometer," by M. E. Vance, R. F. Rowntree, E. E. Bell, and R. A. Oetjen.

The basic design of this interferometric modulator was made by Dr. Phillips B. Burnside. It was inspired by the ideas and groundwork of Professor Ludwig Genzel (now at the University of Freiburg, W. Germany), and has benefited from many discussions among a group including, in addition to Dr. Burnside, Professors Ely E. Bell and Robert A. Oetjen, Dr. Miles E. Vance, Dr. Raymond L. Brown, and Mr. Robert F. Rowntree.

The tutorial style of this report, with its detailed derivations, is the result of a deliberate attempt to make the report especially useful to those many students and workers who will be using, adjusting, and designing this kind of device in the future.

CONTENTS

TABLES

ILLUSTRATIONS

CHAPTER I

INTRODUCTION

In 1954 John Strong reported the advantages of using a variable-
depth lamellar grating interferometer as a selective modulator of the
radiation emerging from a far infrared grating spectrometer, as well
as progress toward actual development of a complete working system[1].
In 1957 Genzel and Weber published an account of the theory, con-
struction and operation of such an interferometric modulator for the
far infrared[2,3]. Unlike the later interferometers of Strong[4-6] and
of Gebbie,[7,8] in which the path difference is increased at a slow,
constant rate and an interferogram is recorded requiring Fourier
transformation to obtain the spectrum, the path difference of the
Genzel instrument was varied periodically at 1/2 cps and a spectrum
was obtained directly. Also it was shown that the interferometric
modulator could be used advantageously as a radiation filter for either
a grating monochromator or a microwave harmonic generator[9]. This
dissertation contains a description of a similar instrument constructed

---

1. J. Strong, J. Opt. Soc. Am. 44, 352 (1954).

2. L. Genzel and R. Weber, Z. angew. Physik 10, 127 (1957).

3. L. Genzel and R. Weber, Z. angew. Physik 10, 195 (1957).

4. J. Strong, J. Opt. Soc. Am. 47, 354 (1957).

5. G. Vanasse, J. Strong, and E. Loewenstein, J. Opt. Soc.
   Am. 49, 309 (1959).

6. J. Strong and G. Vanasse, J. Opt. Soc. Am. 49, 844 (1959);
   50, 113 (1960).

7. H. Gebbie, G. Roland, and L. Delbouille, Nature 191, 264
   (1961).

8. H. Gebbie, N. Stone, and C. Walshaw, Nature 187, 765 (1960).

9. Genzel and Weber, Z. angew. Physik 10, 127 (1957).

at The Ohio State University, a formulation of the theory aimed at
analyzing possible errors in its operation, and a report on its
actual performance. This interferometric modulator, hereafter called
simply "the modulator", does not differ in principle from that of
Genzel, but it is designed primarily for use with a far infrared
grating monochromator and incorporates several design features for
facilitating its use in that way.

Principle of operation

The type of interferometric modulation discussed here may be
described in essence as wavelength-dependent modulation of radiation
intensity by two-beam interference. The beam-splitter employed is a
lamellar grating of variable depth X, two facets of which are shown
in Figure 1. Only the zeroth order of interference is used. Suppose
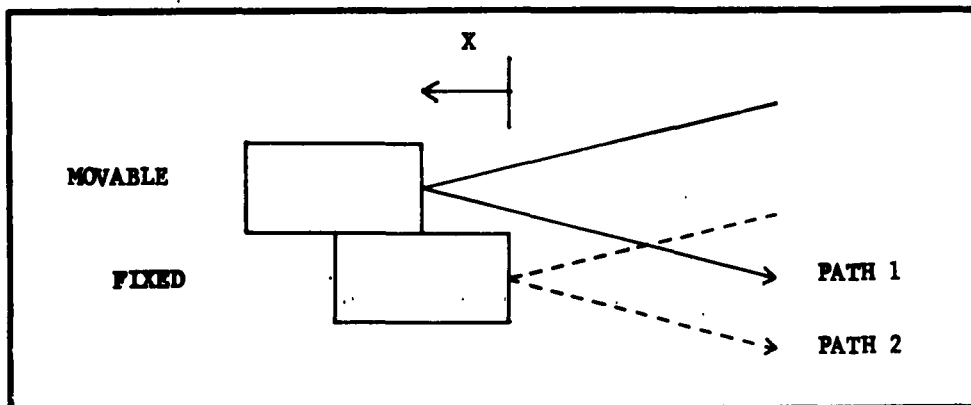
Fig. 1. Two facets of the lamellar grating.

a parallel beam of monochromatic radiation of wavelength λ falls on the
lamellar grating at a small angle of incidence so that the two reflected
beams follow the paths indicated in the figure. The path difference x
for the two beams is then approximately twice the grating depth:

$$x \doteq 2X \quad .$$

If X is increased from X = o, each time its value passes through a
multiple of $\lambda/2$ (x passes through a multiple of λ) constructive inter-

ference produces a maximum output power, while values falling midway be-
tween the maxima yield zero output power. The variation of the output
as a function of X will be shown later to be cosinusoidal as shown in
Figure 2. An abscissa labelled path difference is inserted below the
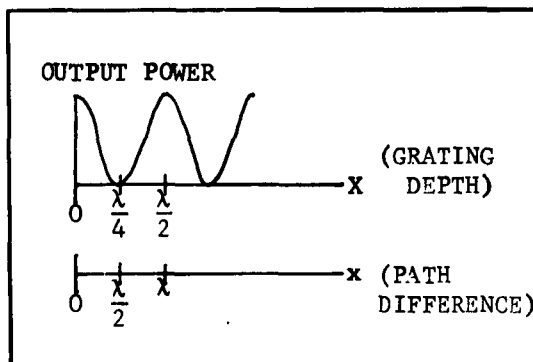
Fig. 2. The output power from the
lamellar grating as a function of
grating depth and of path difference,
for radiation of wavelength λ.

graph. A segment of the curve covering a distance $\lambda/2$ on the X axis or
λ on the x axis will be called a modulation cycle. Now suppose that X
is allowed to reach a maximum value X_m and to return to X = 0, so that
x increases from x = 0 to a maximum value x_m and returns to x = o.
This constitutes a complete grating cycle. Then if X_m is so chosen that
an integral number of modulation cycles occurs during one grating cycle,
the relationship

$$\frac{2x_m}{\lambda_n} = n = \text{an integer}$$

holds for $\lambda = \lambda_n$. For radiation of wavelength λ_n and for an idealized
grating cycle consisting of constant-speed motion from X = o to X = X_m,
instantaneous reversal, and return with the same constant speed during
a total time T the path difference variation x(t) and the output power
variation are plotted as functions of time in Figure 3 (a) and (b) re-
spectively. Since n modulation cycles occur in time T, the modulation
frequency f_n for wavelength λ_n is
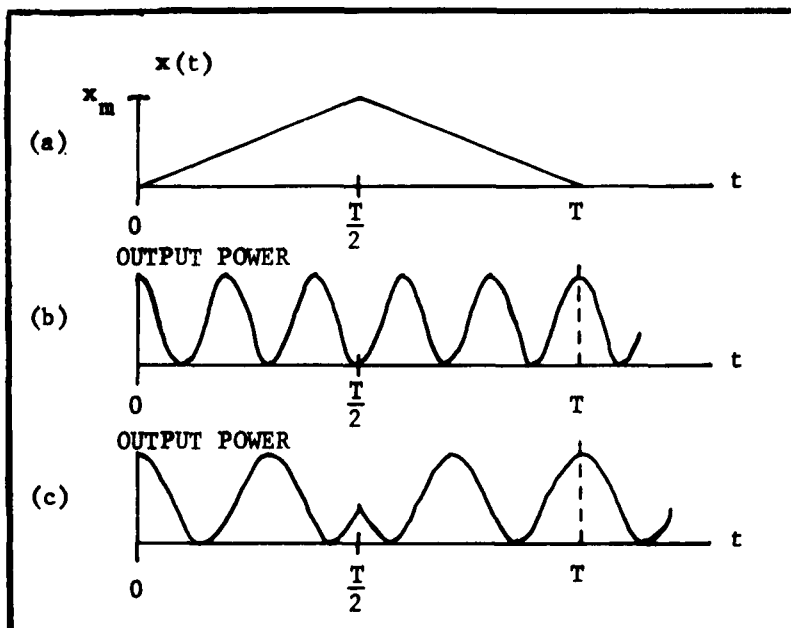
Fig. 3. (a) The path difference as a function of time. (b) The output power for wavelength λ_n, as a function of time. (c) The output power for a typical wavelength such that $\frac{2x_m}{\lambda}$ is not an integer.

$$f_n = \frac{n}{T} \ .$$

Also, since $n = \frac{2x_m}{\lambda_n} = 2x_m \nu_n$, where $\nu_n = \frac{1}{\lambda_n}$ is the wave number of the radiation, it follows that

$$f_n = \frac{2x_m}{T} \nu_n \ .$$

A detector placed at the point of interference of the focused output beams responds to this periodically varying radiant power, producing a similar electrical signal which may then be amplified, rectified and recorded.

For incident radiation of different wave numbers, the result can be understood most easily for the arrangement in which the input to the modulator is the output of a grating monochromator. This output may be

viewed r.pproximately as a group of discrete spectral lines having wave numbers

$$\nu, \ 2\nu, \ 3\nu, \ \ldots$$

If the monochromator is set in first order for wave number ν_n such that the modulator is adjusted for modulation at frequency f_n, then radiation of wave number

ν_n has modulation frequency $f_n \ = \ \dfrac{n}{T}$,

$2\nu_n$ " " " $2f_n \ = \dfrac{2n}{T}$,

$3\nu_n$ " " " $3f_n \ = \dfrac{3n}{T}$,

etc.

The virtue of this relationship is that all these modulation frequencies but one, say f_n, can be filtered out electrically by use of an amplifier with a bandpass of the order of f_n, thus discriminating against signals produced by the higher monochromator orders. A block diagram of this arrangement is found in Figure 4. The source spectrum can be scanned
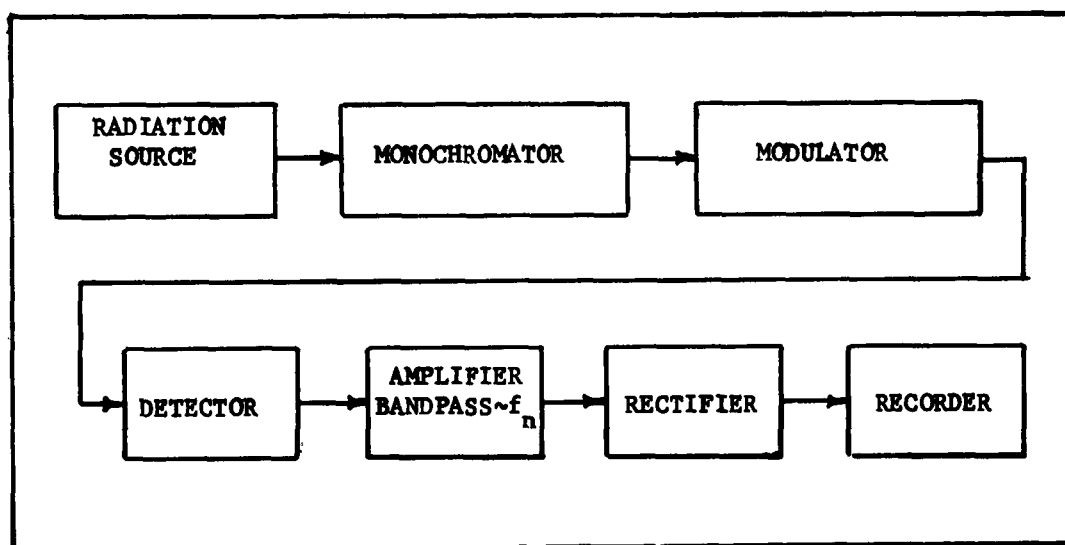
Fig. 4. A block diagram of a possible arrangement for using the modulator as a filter for a grating monochromator.

by varying the monochromator output λ_n and keeping the relation

$$2x_m = n \lambda_n$$

valid at all times by continuously changing x_m.

Now if the interferometric modulator is used alone as a spectrome-
ter, or even if monochromator "lines" of finite spectral width are to
be treated, the modulation effect for arbitrary wave numbers must be
taken account of. This requires the detailed calculations of chapter
III. However, it is evident that wave number

$$\nu_n = \frac{n}{2x_m} \quad \text{is modulated at frequency} \quad f_n = \frac{n}{T}$$

and at no other frequency; that

$$\nu_{n+1} = \frac{n+1}{2x_m} \quad \text{is modulated at frequency} \quad f_{n+1} = \frac{n+1}{T}$$

and at no other frequency; etc. A wave number between these integral
multiples of $\frac{1}{2x_m}$ produces a periodic variation in output power for
which the smallest period is T as shown in Figure 3(c); hence it is
modulated to some extent at all modulation frequencies $\frac{1}{T}, \frac{2}{T}, \frac{3}{T}, \dots$,
and in particular at frequency $\frac{n}{T}$ it is modulated, with reduced
effectiveness. Therefore, a curve representing the effectiveness of
modulation at a chosen frequency $f_n = \frac{n}{T}$, plotted against incident
radiation wave number ν, has a maximum value near the wave number
$\frac{n}{2x_m}$, must pass through zero at other integral multiples of $\frac{1}{2x_m}$,
and has a value between zero and the maximum value at other points.
The result of an exact calculation for the case n = 3 is depicted in
Figure 16, Chapter III. To select the single modulation frequency
$\frac{n}{T}$, requires an electrical filter or amplifier bandpass of the order
of $\frac{1}{T}$. In the instrument described here, the alternative of synchro-
nous rectification at the selected frequency $\frac{n}{T}$, preceded by a medium
bandpass ($< 3 \ f_n$) amplifier and followed by a low-pass filter, is em-
ployed. Figure 5 indicates this arrangement, in which the synchronous
rectifier is mechanically phased with the grating motion. This instru-
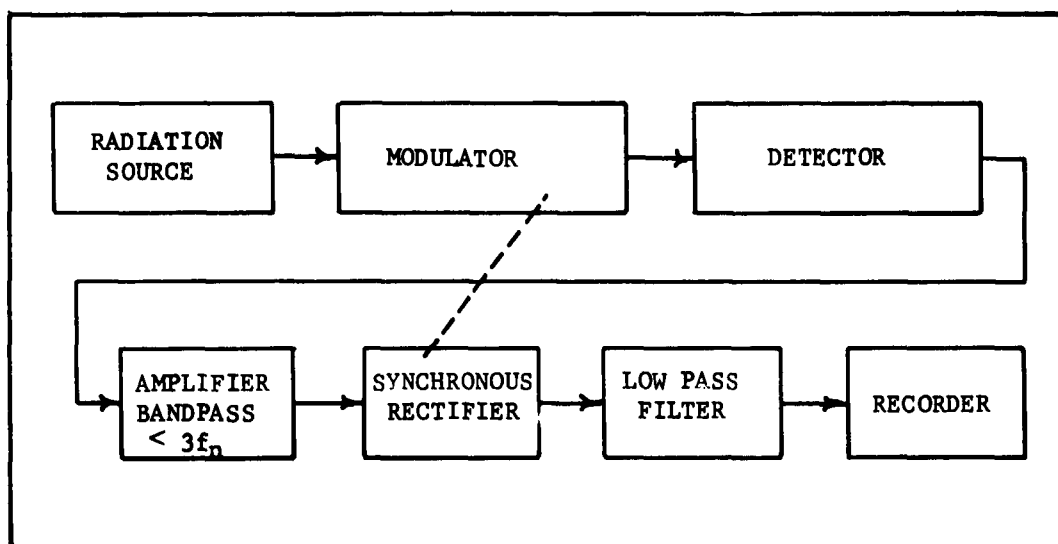
Fig. 5. A block diagram of the arrangement used in this investigation.

mentation can be used as shown, as a spectrometer with spectral band-pass characteristic of the modulator; or with the monochromator inserted in series with the modulator to utilize the narrow spectral bandpass of the monochromator.

Advantages of the modulator-spectrometer combination

The large potential radiation-gathering power (product of exit aperture area and solid angle subtended by beam-splitter) of inter-ferometers is well known[10]. Also, Jacquinot has pointed out that the greatest radiation-gathering power is obtained when the interferometer plates or beam-splitter have rotational symmetry and consist of semi-transparent plates, as in the Fabry-Perot interferometer, the Michelson interferometer and the SISAM[11,12,13]. In the far infrared at present,

10. J. Strong, Concepts of Classical Optics (W. A. Freeman and Company, San Francisco, 1958), p. 270.

11. P. Jacquinot, J. Phys. Rad. 19, 223 (1958).

12. P. Jacquinot, Reports on Progress in Physics 23, 267 (1960).

13. P. Connes, Optica Acta 4, 136 (1957); Revue D'Optique 38, 157 (1959), 38, 416 (1959), 39, 402 (1960).

however, the useful radiation-gathering power for both interferometers
and grating spectrometers is determined by the acceptance solid angle
and the receiver area of the detector. Assuming no source limitation,
if a grating spectrometer and an interferometer are each designed to
just accommodate the solid angle and receiver area of a given detector,
then the detected radiant flux per unit spectral bandpass is given in
each case by the product of the source spectral radiance and the radi-
ation-gathering power, and is therefore the same for both instruments.
The major difference is that the area of the interferometer beam-
splitter can be much smaller than the projected area of the spectrometer
grating. If detectors with significantly larger receiver areas and solid
angles become available, the interferometer may be more easily enlarged
to take advantage of them. If, in addition, the limiting noise of
the spectrometric system is detector noise, as in the far infrared, a
significant gain in signal-to-noise ratio for a given time of observa-
tion is realized by use of the Fourier transform method[14,15].

Under the present energy-limited, detector-limited conditions,
the transmission factors of instruments are of prime importance; hence
the choice of the lamellar grating instead of a semi-transparent mem-
brane beam-splitter. Interferometric filtering is expected to be more
efficient than the conventional reststrahlen and transmission filters.
The next consideration is convenience. The convenience of the present
method is in having a source of uniformly pure radiation in the range
100-1000µ, with immediate recording of the spectrum and with the
possibility of immediate comparison of signals with and without samples.
It is expected to be particularly useful in the measurement of trans-
mittances and reflectances of materials.

---

14. P. Fellgett, J. Phys. Rad. 19, 187 (1958).
15. J. Strong, J. Opt. Soc. Am. 47, 354 (1957).

CHAPTER II

MATHEMATICAL SUMMARY

The mathematical approach used in the theoretical parts of this dissertation has been adapted largely from a book by R. B. Blackman and J. W. Tukey[1] and one by M. J. Lighthill[2]. Below is a summary of the definitions and results which have been found useful in the mathematical description of the operation of the interferometric modulator. In general, proofs are not included, but in most cases an attempt is made to establish the reasonableness of the results.

1. Some definitions

The functions $F(t)$ and $P(f)$ with various subscripts and superscripts are used in a general sense in this chapter and are not to be confused with the same functions used later on to represent specific physical quantities.

A function $F(t)$ is an even function of t if $F(t) = F(-t)$, and is odd if $F(t) = -F(-t)$. If it is niether even nor odd it is a mixed function, having both an even and an odd part.

The symbol F.T. $\left[F(t)\right]$ means the (complex) Fourier transform of $F(t)$, while $\overline{F.T.}$ $\left[P(f)\right]$ means the inverse (complex) Fourier transform of $P(f)$. Cosine F.T. and sine F.T. refer to the cosine Fourier transform and the sine Fourier transform, respectively.

A one-sided function $F(t)$ is defined on $(0 < t < \infty)$, while a two-sided function $F(t)$ is defined on $(-\infty < t < \infty)$.

---

1. R. B. Blackman and J. W. Tukey, The Measurement of Power Spectra, (Dover Publications, Inc., New York, 1959), Appendix A.

2. M. J. Lighthill, Introduction to Fourier Analysis and Generalized Functions (Cambridge University Press, Cambridge, 1958).

2. Fourier transforms

Suppose F(t) is expanded as a Fourier integral[3]

$$F(t) = \int_{-\infty}^{\infty} \left[\int_{-\infty}^{\infty} F(\tau) \, e^{-2\pi i f \tau} \, d\tau \right] e^{+2\pi i f t} \, df \quad , \tag{2.1}$$

in which the real function F(t) represents a physical quantity defined on $(-\infty < t < \infty)$ and may be even, odd or mixed. The bracketed quantity in Eq. (2.1) is apparently the complex spectrum of F(t) when the latter is expressed as a complex Fourier integral, and may be called

$$P(f) = \int_{-\infty}^{\infty} F(t) \, e^{-2\pi i f t} \, dt = \text{F.T.} \left[F(t) \right] \quad . \tag{2.2}$$

Then Eq. (2.1) can be written

$$F(t) = \int_{-\infty}^{\infty} P(f) \, e^{+2\pi i f t} \, df = \overline{\text{F.T.}} \left[P(f) \right] \quad . \tag{2.3}$$

The functions F(t) and P(f) are said to form a Fourier transform pair. P(f) is in general complex. Since F(t) is real but mixed, Eq. (2.2) can be expressed in the form

$$P(f) = \int_{-\infty}^{\infty} \left[F^e(t) + F^o(t) \right] \left[\cos 2\pi ft - i \sin 2\pi ft \right] dt \quad ,$$

or

$$P(f) = P_r(f) + i \, P_i(f) \quad ,$$

where

$$P_r(f) = \int_{-\infty}^{\infty} F^e(t) \cos 2\pi \, ft \, dt \qquad P_i(f) = - \int_{-\infty}^{\infty} F^o(t) \sin 2\pi \, ft \, dt \quad . \tag{2.4}$$

Thus the real part of P(f) is even and the imaginary part of P(f) is odd. Returning to Eq. (2.3), it follows that only the real part of P(f) contributes to the even part of F(t), while only the imaginary part of P(f) contributes to the odd part of F(t). Also, $P_r(f)$ and $F^e(t)$ form a cosine transform pair and $P_i(f)$ and $F^o(t)$ are negative sine transforms of each other.

---

3. See e.g., L. A. Pipes, *Applied Mathematics for Engineers and Physicists* (McGraw-Hill Book Company, Inc., New York, 1946), p. 65.

3. Even functions

If F(t) happens to be even, then

$$P(f) = \int_{-\infty}^{\infty} F(t) e^{-2\pi i ft} \, dt = \int_{-\infty}^{\infty} F(t) (\cos 2\pi ft - i \sin 2\pi ft) \, dt$$

$$\int_{-\infty}^{\infty} F(t) \cos 2\pi ft \, dt \quad . \tag{2.5}$$

By a similar procedure,

$$F(t) = \int_{-\infty}^{\infty} P(f) \cos 2\pi ft \, df \quad . \tag{2.6}$$

The following inferences can be drawn:

    a. The cosine Fourier transform is equal to the complex transform and the inverse transform has the same form as the direct transform.

    b. P(f) is even

    c. P(f) is real if F(t) is real.

    Eq. (2.6) can also be written

$$F(t) = \int_{0}^{\infty} \left[2P(f) \right] \cos 2\pi ft \, df \quad . \tag{2.7}$$

Suppose F(t) to be an even function represented both by Eq. (2.3) and by Eq. (2.7). In the first case the spectrum of F(t) is P(f) and is defined for positive and negative frequencies. In (2.7) on the other hand, the spectrum is 2 P(f), defined for positive frequencies only and thus physically measurable.

4. Odd functions

Analogous relations hold for the Fourier transforms of odd functions. If F(t) is odd, then

$$P(f) = \int_{-\infty}^{\infty} F(t) e^{-2\pi i ft} \, dt = -i \int_{-\infty}^{\infty} F(t) \sin 2\pi ft \, dt \tag{2.8}$$

and

$$F(t) = \int_{-\infty}^{\infty} P(f) e^{2\pi i ft} \, dt = i \int_{-\infty}^{\infty} P(f) \sin 2\pi ft \, df \quad . \tag{2.9}$$

5. __Convolution__

Let

$$P_1(f) = \int_{-\infty}^{\infty} F_1(t) \, e^{-2\pi i f t} \, dt = \text{F.T.} \left[F_1(t) \right],$$

$$P_2(f) = \int_{-\infty}^{\infty} F_2(t) \, e^{-2\pi i f t} \, dt = \text{F.T.} \left[F_2(t) \right],$$

and

$$P(f) = \int_{-\infty}^{\infty} F(t) \, e^{-2\pi i f t} \, dt = \text{F.T.} \left[F(t) \right]. \qquad (2.10)$$

Then if $F(t) = F_1(t) \cdot F_2(t)$ \qquad (2.11)

the Fourier transforms are related, according to the convolution theorem, by

$$P(f) = \int_{-\infty}^{\infty} P_1(f-f') P_2(f') \, df', \qquad (2.12)$$

which is written symbolically as

$$P(f) = P_1(f) * P_2(f). \qquad (2.13)$$

Also,

$$P(f) = P_2(f) * P_1(f). \qquad (2.14)$$

Since the distributive law holds for multiplication of the time functions, it must also hold for convolution of the frequency functions. That is,

$$P_1 * P_2 * P_3 = \left[P_1 * P_2 \right] * P_3 = P_1 * \left[P_2 * P_3 \right]. \qquad (2.15)$$

However, the order of convolution and multiplication cannot in general be interchanged. That is,

$$\text{F.T.} \left[F_1(t) \cdot \left\{ F_2(t) * F_3(t) \right\} \right] = P_1(f) * \left\{ P_2(f) \cdot P_3(f) \right\}$$

$$\neq \left\{ P_1(f) * P_2(f) \right\} \cdot P_3(f). \qquad (2.16)$$

Since

$$\text{F.T.} \left[F_1(t) + F_2(t) \right] = \text{F.T.} \left[F_1(t) \right] + \text{F.T.} \left[F_2(t) \right]$$

$$= P_1(f) + P_2(f),$$

it follows that

$$\text{F.T.}\left\{\left[F_1(t) + F_2(t)\right] \cdot \left[F_3(t) + F_4(t)\right]\right\}$$
$$= \left[P_1(f) + P_2(f)\right] * \left[P_3(f) + P_4(f)\right] \quad ,$$

where $F_3(t)$ and $P_3(f)$ are a transform pair and $F_4(t)$ and $P_4(f)$ are a transform pair.

The convolution relation also holds without alteration for the inverse transforms.

6. The Dirac delta function[4]

The Dirac delta function is not a function in the ordinary sense, but is defined in terms of the result of integrating its product with other functions between the limits $-\infty$ and ∞. The defining integral is

$$\int_{-\infty}^{\infty} \delta(t) \, F(t) \, dt = F(0) . \tag{2.17}$$

In order for (2.17) to be true, $\delta(t)$ must evidently have the characteristics

$$\delta(t) = 0 \qquad t \neq 0 \tag{2.18}$$

and

$$\int_{-\infty}^{\infty} \delta(t) \, dt = 1 . \tag{2.19}$$

Furthermore, a delta function at $t = t_o$ has the property

$$\int_{-\infty}^{\infty} \delta(t - t_o) \, F(t) \, dt = F(t_o) . \tag{2.20}$$

The statement

$$\delta(t - t_o) \, F(t) = F(t_o) \, \delta(t - t_o) \tag{2.21}$$

means that each side of the equation gives the same result when used as the integrand in Eq. (2.20). Since the height of the delta function is

---

4. In addition to the general references cited for this chapter M. Born and E. Wolf, _Principles of Optics_ (Pergamon Press, New York, 1959) p. 752, contains a helpful discussion of this function.

infinite it cannot be legitimately graphed as a function of t but it is customary to do so, giving it unit height. The quantity $\delta(t-t_0)F(t)$ is then graphed with the height $F(t_0)$ given by Eq. (2.20).

Using the definition (2.13) and the property (2.20) yields

$$\delta(t - t_0) * F(t) = \int_{-\infty}^{\infty} \delta(t - t_0 - t')F(t')dt' = F(t - t_0). \qquad (2.22)$$

The Fourier transform of $\delta(t)$ is shown by Lighthill[5] to be

$$\text{F.T.} \left[\delta(t)\right] = 1. \qquad (2.23)$$

Therefore,

$$\overline{\text{F.T.}} \left[1\right] = \delta(t) = \text{F.T.} \left[1\right]. \qquad (2.24)$$

From Eq. (2.17) it follows that

$$\text{F.T.} \left[\delta(t - t_0)\right] = \int_{-\infty}^{\infty} \delta(t - t_0)e^{-2\pi ift}dt = e^{-2\pi it_0 f}. \qquad (2.25)$$

Therefore,

$$\overline{\text{F.T.}} \left[e^{-2\pi it_0 f}\right] = \delta(t - t_0). \qquad (2.26)$$

Also

$$\overline{\text{F.T.}} \left[\delta(f - f_0)\right] = \int_{-\infty}^{\infty} \delta(f - f_0)e^{+2\pi ift} df = e^{2\pi if_0 t} \qquad (2.27)$$

and

$$\text{F.T.} \left[e^{2\pi if_0 t}\right] = \delta(f - f_0). \qquad (2.28)$$

---

5. Lighthill, op. cit., p. 19.

In the present work the convention is adhered to that transforms of time functions are direct transforms and transforms of frequency functions are inverse transforms. From Eqs. (2.27) and (2.28) it follows that

$$\overline{\text{F.T.}} \left[\frac{\delta(f - f_0) + \delta(f + f_0)}{2} \right] = \cos 2\pi f_0 t \qquad (2.29)$$

$$\text{F.T.} \left[\cos 2\pi f_0 t \right] = \tfrac{1}{2} \left[\delta(f - f_0) + \delta(f + f_0) \right] \qquad (2.30)$$

and

$$\overline{\text{F.T.}} \left[\frac{\delta(f - f_0) - \delta(f + f_0)}{2i} \right] = \sin 2\pi f_0 t \qquad (2.31)$$

$$\text{F.T.} \left[\sin 2\pi f_0 t \right] = \tfrac{1}{2i} \left[\delta(f - f_0) - \delta(f + f_0) \right] . \qquad (2.32)$$

The shifting property Eq. (2.22) of the delta function can be used to show that

$$\text{F.T.} \left[F(t - t_0) \right] = \text{F.T.} \left[F(t) * \delta(t - t_0) \right]$$

$$= e^{-2\pi i t_0 f} \text{F.T.} \left[F(t) \right] . \qquad (2.33)$$

7. The Dirac comb

An infinite row of Dirac deltas, or a Dirac comb, can be written

$$F(t) = \sum_{q = -\infty}^{\infty} \delta(t - qT) . \qquad (2.34)$$

By generalized function theory, Lighthill[6] shows rigorously that its

---

6. Lighthill, op. cit., p. 67.

Fourier transform is also a Dirac comb,

$$P(f) = \frac{1}{T} \sum_{q=-\infty}^{\infty} \delta\left(f - \frac{q}{T}\right) . \tag{2.35}$$

This transform pair is shown in Figure 6.
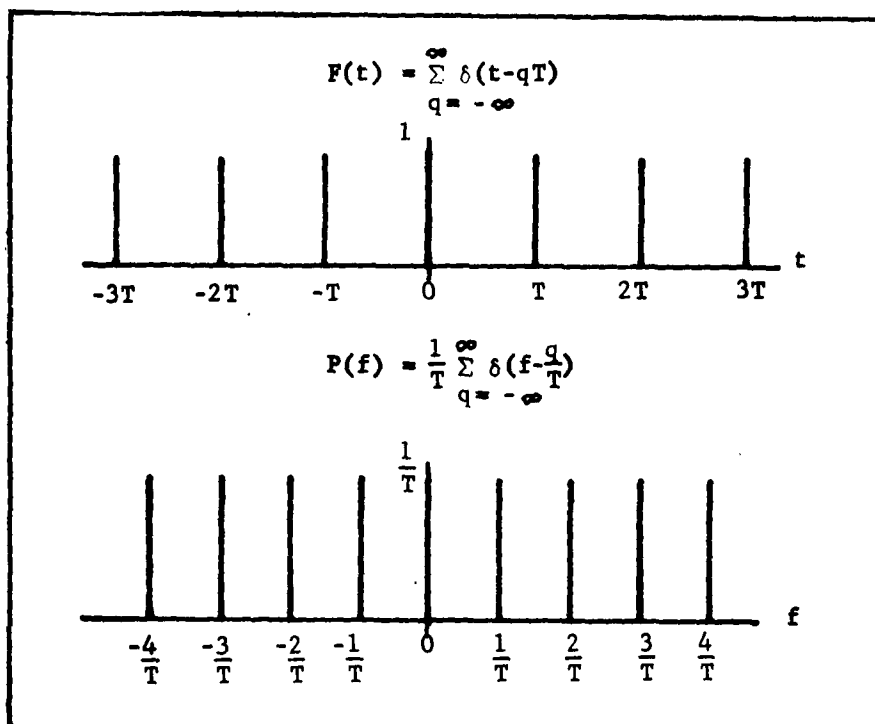
Fig. 6. The Fourier transform of a
Dirac comb is another Dirac comb.
Both combs are supposed to extend
from $-\infty$ to ∞ .

8. Periodic functions.

The Dirac comb may be used in constructing a periodic function $F(t)$ from a function $F_0(t)$ which vanishes outside the interval $\left(-\frac{T}{2} < t < \frac{T}{2}\right)$ as follows:

$$F(t) = F_0(t) * \sum_{q=-\infty}^{\infty} \delta(t - qT). \tag{2.36}$$

The Fourier transform, or spectrum, of $F(t)$ is

$$P(f) = P_0(f) \cdot \frac{1}{T} \sum_{q=-\infty}^{\infty} \delta(f - \frac{q}{T}), \tag{2.37}$$

or

$$P_r(f) + iP_i(f) = \left[P_{or}(f) + iP_{oi}(f) \right] \frac{1}{T} \sum_{q=-\infty}^{\infty} \delta(f - \frac{q}{T}), \tag{2.38}$$

where $P_r(f)$ is the Fourier transform of the even part of $F(t)$, while $iP_i(f)$ is the Fourier transform of the odd part and similar definitions hold for $P_{or}(f)$ and $iP_{oi}(f)$. Illustrative, but not necessarily accurate, examples of $F_0(t)$, $P_0(f)$, $F(t)$, and the real and imaginary parts of $P(f)$ are drawn in Fig. 7. The deltas in Fig. 7(c) and (d) are given heights equal to the value of the multiplying function, as explained below Eq. (2.21).

9. Fourier series

If Eq. (2.37) is written

$$P(f) = \frac{1}{T} \sum_{q=-\infty}^{\infty} P_0(f) \ \delta(f - \frac{q}{T}), \tag{2.39}$$

its inverse Fourier transform can be expressed

$$F(t) = \frac{1}{T} \sum_{q=-\infty}^{\infty} \overline{F.T.} \left[P_0(f) \ \delta(f - \frac{q}{T}) \right] \tag{2.40}$$

$$= \frac{1}{T} \sum_{q=-\infty}^{\infty} P_0(\frac{q}{T}) \ e^{2\pi i \frac{q}{T} t} .$$
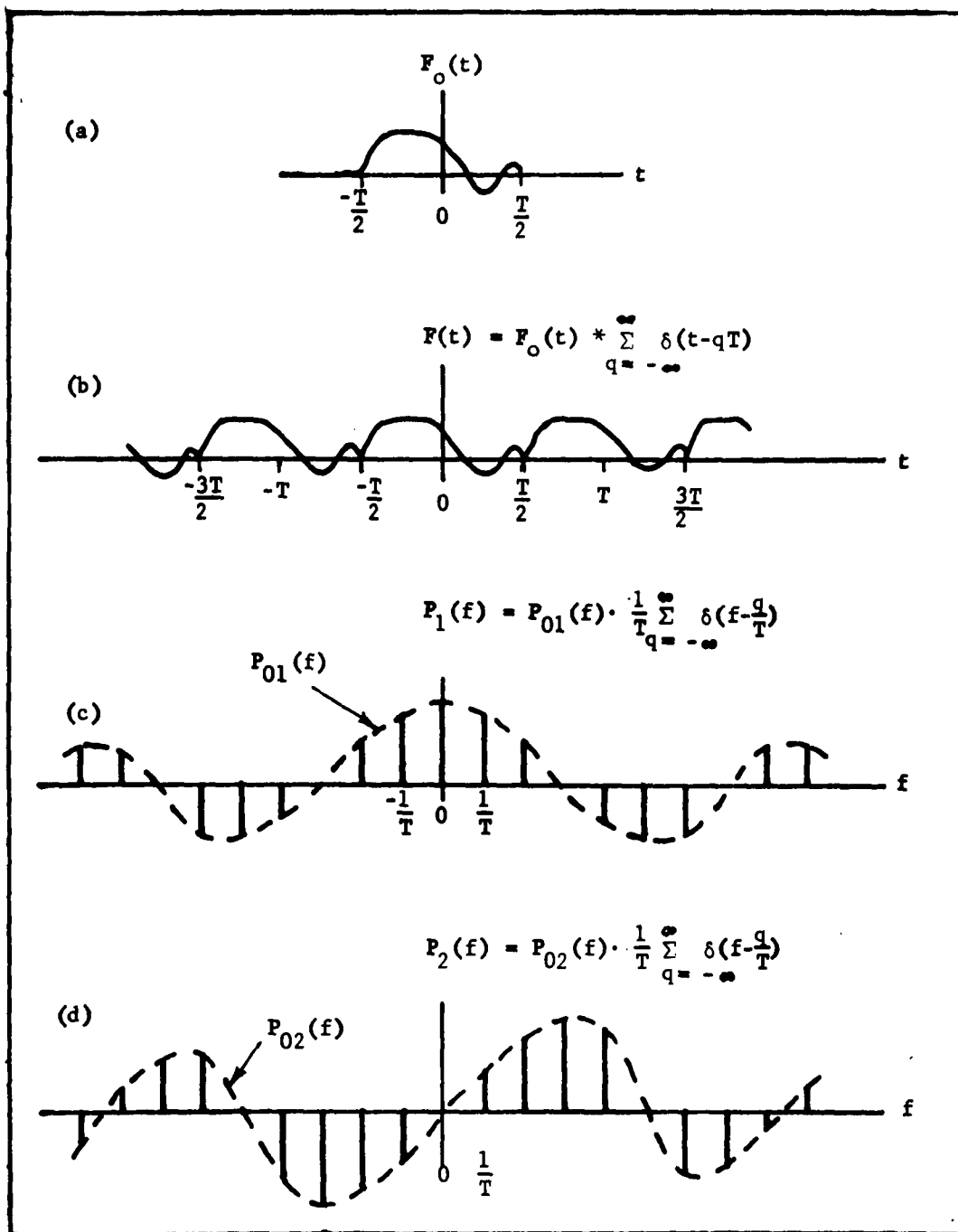
Fig. 7. The Fourier transform of a periodic function. (a) The function on its fundamental interval. (b) The periodic function. (c) The real part of the transform. (d) The imaginary part of the transform.

But since the Fourier series for $F(t)$ based on the period T is

$$F(t) = \sum_{q = -\infty}^{\infty} c_q \, e^{2\pi i \frac{q}{T} t} , \tag{2.41}$$

it follows that

$$c_q = \frac{1}{T} P_o \left(\frac{q}{T} \right) . \tag{2.42}$$

Thus the Fourier series coefficients of a periodic function can be obtained from its Fourier transform, and the heights and locations of the delta functions in Fig. 7 correspond to the amplitudes and frequencies, respectively, of the Fourier components of $F(t)$.

10. Some useful transform pairs

The function

$$U_T(t) = 1 \qquad (-\tfrac{T}{2} < t < \tfrac{T}{2})$$

$$= 0 \qquad |t| > \tfrac{T}{2} \tag{2.43}$$

has Fourier transform

$$\text{F.T.} \left[U_T(f) \right] = \int_{-\frac{T}{2}}^{\frac{T}{2}} e^{-2\pi i f t} \, dt = \frac{T \sin \pi T f}{\pi T f} = T \text{ dif } T f, \tag{2.44}$$

where the function

$$\text{dif } Tf = \frac{\sin \pi Tf}{\pi Tf} \tag{2.45}$$

has the approximate shape shown in Figure 8 and has the properties:

$$\text{dif } o = 1 \tag{2.46}$$

$$\text{dif } p = 0 \qquad p = 1,2,3,4,\ldots \tag{2.47}$$

$$\text{dif } Tf = \text{dif } (-Tf) \tag{2.48}$$

If two such rectangular functions are convolved, the result is the triangular function

$$\frac{T}{2} \ V_T(t) = U_{\frac{T}{2}}(t) * U_{\frac{T}{2}}(t) \quad , \tag{2.49}$$

or

$$V_T(t) = 1 - \frac{2}{T} \ |t| \qquad (-\frac{T}{2} < t < \frac{T}{2})$$

$$= 0 \qquad \qquad |t| > \frac{T}{2} \quad . \tag{2.50}$$

From Eq. (2.49) the Fourier transform of $V_T(t)$ is

$$\text{F.T.} \ \left[V_T(f) \right] = \frac{2}{T} \ \left[\frac{T}{2} \ \text{dif} \ \frac{Tf}{2} \right]^2 = \frac{T}{2} \ \text{dif}^2 \ \frac{Tf}{2} \ . \tag{2.51}$$

These pairs appear in Figure 8.
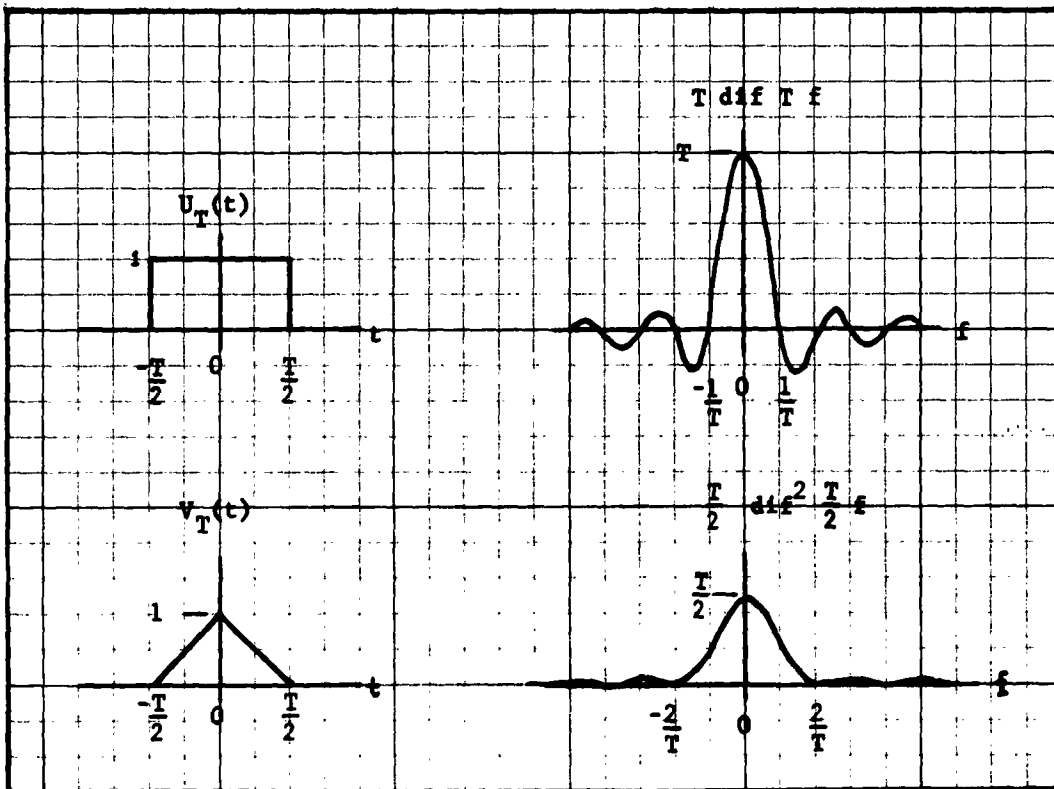
Fig. 8. The functions $U_T(t)$ and $V_T(t)$ with their Fourier transforms.

11. An infinite series needed in Chapter V

To obtain Eq. (5.88) it is necessary to perform the summation

$$\sum_{q=-\infty}^{\infty} \text{dif } Nb(y - {}^q/_b)$$

(2.52)

for odd N.

A single term is

$$\frac{\sin(\pi N\, by - \pi\, Nq)}{\pi N\, by - \pi\, Nq} = \frac{\sin \pi N\, by}{N} \cdot \frac{(-1)^q}{\pi\, by - q\pi} \quad .$$

But

$$\sum_{q=-\infty}^{\infty} \frac{(-1)^q}{\pi\, by - q\pi} = \frac{1}{\pi\, by} + \sum_{q=1}^{\infty} (-1)^{q-1} \frac{2\, \pi\, by}{q^2 \pi^2 - (\pi\, by)^2} = \csc \pi\, by$$

is a standard series expansion.[7] Hence

$$\sum_{q=-\infty}^{\infty} \text{dif } N\, b\, (y - \frac{q}{b}) = \frac{\sin \pi N\, by}{N} \cdot \frac{1}{\sin \pi\, by} = \frac{\text{dif } N\, by}{\text{dif } by} \quad .$$

(2.53)

7. E. P. Adams and R. L. Hippisley, Smithsonian Mathematical Formulae and Tables of Elliptic Functions (Smithsonian Institution, Washington, 1922), p. 129.

CHAPTER III

THEORY: THE IDEALIZED CASE

This chapter contains a formulation of the theory of operation
of the interferometric modulator under the restrictions of idealized,
error-free, geometry and kinematics of the instrument.

The input spectrum

Suppose $P_0(\nu')$ is the spectrum of the radiant power incident
on the beam splitter of the interferometer and for analytical purposes
is artificially defined as a real, even function of the wave number ν'
on the interval $(-\infty < \nu' < \infty)$. Under this definition, the total
incident power is

$$\int_{-\infty}^{\infty} P_0(\nu')\, d\nu' \quad . \tag{3.1}$$

The detector input

The interferometer separates the incoming wave front into two
parts, introduces a path difference x between these parts, and super-
poses them at the detector. The resultant radiant power depends on
the path difference, the wave number of the radiation, and constant
geometrical factors. The power transmission function may thus be
denoted by $L_0(x, \nu')$ and the total power reaching the detector for a
given path difference is

$$F_0 (x) = \int_{-\infty}^{\infty} P_0(\nu')\, L_0(x, \nu')\, d\nu' \quad , \text{ which,} \tag{3.2}$$

22

plotted as a function of x, is the **interferogram** corresponding to the input spectrum $P_o(\nu')$.

Operation with the path difference extending to infinity

An ideal two-beam interferometer separates the incoming beam of radiation represented by the wave function

$$a_o \, e^{i(\omega t - 2\pi\nu'\zeta)}$$

where a_o is the amplitude, ω is the angular frequency, and ν' is the wave number of the radiation, and ζ is a coordinate along the direction of propagation, into two beams of equal amplitude represented by the wave functions

$$\tfrac{1}{2} \, a_o \, e^{i(\omega t - 2\pi\nu'\zeta)}$$

and

$$\tfrac{1}{2} \, a_o \, e^{i(\omega t - 2\pi\nu'\zeta - 2\pi\nu'x)} \, .$$

These two beams are then superposed and the result is represented by the sum of the two wave functions

$$a_1 = \tfrac{1}{2} a_o \, e^{i(\omega t - 2\pi\nu\zeta)} \left[1 + e^{-i2\pi\nu'x} \right].$$

The average output radiant power relative to the average input power is then

$$\frac{a_1 a_1^*}{a_o a_o^*} = \tfrac{1}{2} + \tfrac{1}{2} \cos 2\pi\nu'x \, . \qquad (3.3)$$

However, it is convenient to take for the __transmission function__ in this case

$$L_o(x, \nu') = \cos 2\pi\nu'x \qquad , \qquad (3.4)$$

since, as will be shown later, the constant term does not influence the results. Equation (3.2) then becomes

$$F_o(x) = \int_{-\infty}^{\infty} P_o(\nu') \cos 2\pi \, x\nu'd\nu' \; . \qquad (3.5)$$

In the notation explained in chapter II, this can be written

$$F_o(x) = F.T. \left[P_o(\nu') \right] \qquad , \qquad (3.6)$$

and consequently, by Eqs. (2.5) and (2.6),

$$P_o(\nu') = F.T. \left[F_o(x) \right] \qquad ; \qquad (3.7)$$

the input spectrum and the interferogram form a Fourier transform pair. Equations (3.6) and (3.7) would be applicable if an interferogram $F_o(x)$ of infinite extent were obtained by increasing the path difference indefinitely. The incident spectrum $P_o(\nu')$ could then be retrieved unmodified, by Fourier transformation of $F_o(x)$. The even, two-sided function $F_o(x)$ would be obtained by direct measurement on the interval $(-\infty < x < \infty)$ or by measurement on $(0 < x < \infty)$ only and construction of the required even function by the condition

$$F_o(x) = F_o(-x). \qquad (3.8)$$

__Change of variables to time and frequency__; Definition of __F(t)__ and __F(t,f)__

If the path difference x is supposed to vary at a constant rate v from zero to a value x_m in a time $\frac{T}{2}$, then as a function of time t,

$$x(t) = vt = \frac{2x_m}{T} t. \tag{3.9}$$

The product $\nu'x$ becomes

$$\nu'x = \frac{2x_m \nu'}{T} t = f't \quad , \tag{3.10}$$

where $f' = \frac{2x_m \nu'}{T} = v\nu' \quad . \tag{3.11}$

Equation (3.4) then leads to

$$L_o(x,\nu') = L(t,f') = \cos 2\pi f't, \tag{3.12}$$

in which it is apparent that f' is the frequency of the cosinusoidal variation of the transmitted power for radiation of wave number ν'. The quantity $L(t,f')$ may be called the __modulation function__ of the interferometer and f' the __modulation frequency__ for radiation of wave number ν'. In terms of t and f' equations (3.6) and (3.7) become:

$$\sqrt{v}F_o(x) = F(t) = \int_{-\infty}^{\infty} P(f') \cos 2\pi tf' \, df' = F.T. \left[P(f') \right] \tag{3.13}$$

$$\frac{1}{\sqrt{v}} P_o(\nu') = P(f') = \int_{-\infty}^{\infty} F(t) \cos 2\pi f't \, dt = F.T. \left[F(t) \right] \quad . \tag{3.14}$$

That is, the __interferogram function__ $F(t)$ and the __modulation frequency spectrum__ $P(f')$ form a Fourier transform pair in the time and frequency domains. For the case of monochromatic input radiation of positive wave number ν, positive modulation frequency f, and unit power, the input modulation frequency spectrum may be expressed as

$$P(f',f) = \frac{1}{2}\left[\delta(f' - f) + \delta(f' + f)\right] , \qquad (3.15)$$

according to Eq. (2.30). Then

$$F(t,f) = F.T. \left[P(f',f)\right] = \cos 2\pi ft , \qquad (3.16)$$

by Eq. (2.29). This transform pair is illustrated in Figure 9.
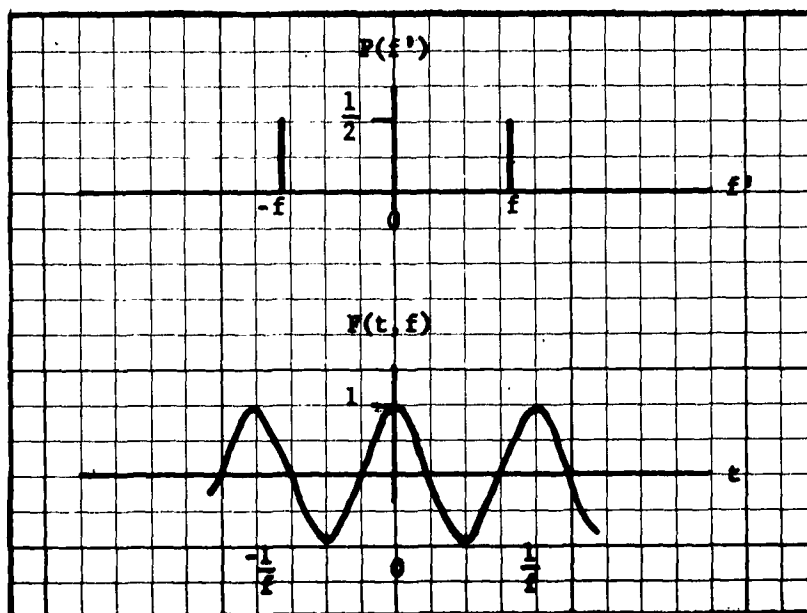
Fig. 9. The Fourier transform pair $P(f',f)$, $F(t,f)$ for infinite variation of path difference.

Operation with finite path difference; Definition of $F_1(t)$ and $F_1(t,f)$

Naturally it is not possible to increase the path difference to infinity in practice. Rather, $F_0(x)$ is measured on the finite interval $(-x_m < x < x_m)$ and is assumed to vanish outside this interval. Or,

as pointed out earlier, the measurement is made for the range

$(o < x < x_m)$ and the even function constructed by use of equation (3.8).

The corresponding time interval is $(-T/2 < t < T/2)$ and an inter-

ferogram function $F_1(t)$ vanishing outside this range can be constructed

by use of the function $U_T(t)$ defined by Eq. (2.43):

$$F_1(t) = F(t) \cdot U_T(t) \quad . \tag{3.17}$$

The Fourier transform of (3.17) is

$$P_1(f') = P(f') * T \text{ dif } T f' \quad , \tag{3.18}$$

by Eqs. (2.13) and (2.44). The apparent spectrum $P_1(f')$ obtained

by Fourier transformation of the measured interferogram $F_1(t)$ is

proportional to the convolution of the input spectrum with the function

T dif T f', which is then by definition the **spectral window** for the

interferometer used in this way.

It is also of interest to know the form of the spectrum obtained

from the instrument when it is presented with an input spectrum consist-

ing of a single spectral line of wave number ν . This apparent

spectrum will be called the **instrumental line shape** and it is obtained

mathematically in the present case by calculating P_1 for the input

spectrum $P(f',f)$ given by Eq. (3.15). The instrumental line shape is

then

$$P_1(f',f) = \frac{1}{2} \left[\delta (f' - f) + \delta (f' + f) \right] * T \text{ dif } Tf'$$

$$= \frac{T}{2} \left[\text{dif } T(f' - f) + \text{dif } T(f' + f) \right] \tag{3.19}$$

and the corresponding interferogram function is

$$F_1(t,f) = \cos 2\pi \, ft \cdot U_T(t) \,.$$ (3.20)

The instrumental line shape $P_1(f',f)$ for an interferometer used in this way differs somewhat in shape from the spectral window T dif Tf' but for some purposes the difference is negligible. These two functions, along with $F_1(t,f)$, are exhibited in Figure 10.
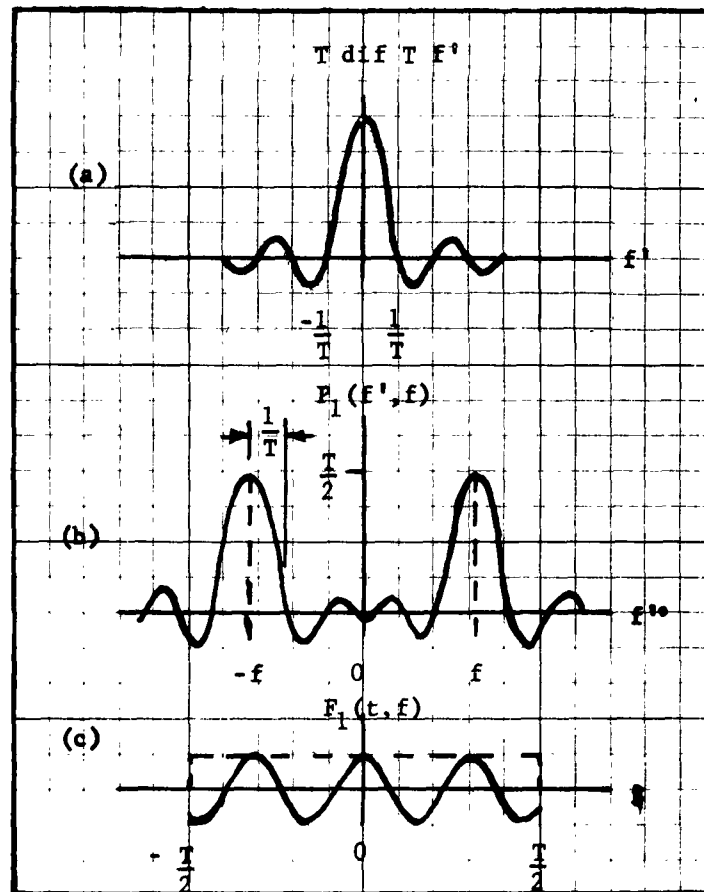
Fig. 10. The spectral window (a), the instrumental line shape (b), and the interferogram function (c), for limited path difference.

An estimate of the resolving power may be obtained, in analogy
with the Rayleigh definition, by the assumption that two neighboring
dif functions can be just distinguished if the first zero of the one
coincides with the maximum value of the other. Since the zeros of
dif T f' and therefore those of $P_1(f',f)$ have the uniform spacing
$\Delta f' = \frac{1}{T}$ along f', and since by Eq. (3.11) this corresponds to a
spacing $\Delta \nu' = \frac{1}{2x_m}$ along ν', the resolving power as defined above
is given by

$$\frac{\nu'}{\Delta \nu'} = 2\, x_m \, \nu' \ . \tag{3.21}$$

This resolving power may be thought of as the number of wavelengths
contained in twice the maximum path difrerence. It is convenient
to use this definition of the resolving power when the instrumental
line shape is a dif curve, but the analogy with the Rayleigh definition
can be drawn in different ways.[1-4] It will be shown in the chapter
describing apodization that for comparing the interferometer with a
grating spectrometer it is more appropriate to define the resolving
power as just one half the value obtained here.

1. J. Connes, J. phys. radium <u>19</u>, 197 (1958).

2. P. Jacquinot, Reports on Progress in Physics <u>23</u>, 267 (1960).

3. L. Genzel and R. Weber, Z. angew. Physik <u>10</u>, 127 (1957).

4. John Strong and G. A. Vanasse, J. Opt. Soc. Am. <u>49</u>, 844 (1959).

Periodic variation of path difference; Definition of $F_0(t)$ and $F_2(t,f)$

The foregoing analysis applies directly to nonperiodic inter-ferometry. However, the results are useful in extending the investiga-tion to periodic interferometric modulation. Suppose the path difference x is increased, at a constant rate, from zero to x_m during time $\frac{T}{2}$ as in equation (3.9), then is decreased at the same rate for a time $\frac{T}{2}$, becoming zero again at time T. This will be referred to as the one-sided mode of operation of the interferometer. If this process is repeated indefinitely, the result is a periodic function of time as shown in Figure 11(a), and the origin of time may be chosen so that it is an even function of period T. That is,

$$x(t) = \frac{2\,x_m}{T}\,\left| t \right| \qquad (-\frac{T}{2} < t < \frac{T}{2}) \ , \qquad (3.22)$$

with appropriately modified definitions for other time intervals. Or, the variation of x can be between $-x_m$ and $+x_m$, in which case the definition is

$$x(t) = \frac{2\,x_m}{T}\,t \qquad (-\frac{T}{2} < t < \frac{T}{2}) \ , \qquad (3.23)$$

for the interval indicated. This will be called the two-sided mode of operation. Figure 11(c) depicts this alternative. In both cases, however, the transmission function becomes an even periodic function of period 2 x_m, defined as follows for the fundamental interval:

$$L_0(x,\nu') = \cos 2\pi\nu'x \qquad (-x_m < x < x_m). \qquad (3.24)$$

The modulation function becomes an even periodic function of period T defined thus on its fundamental interval:
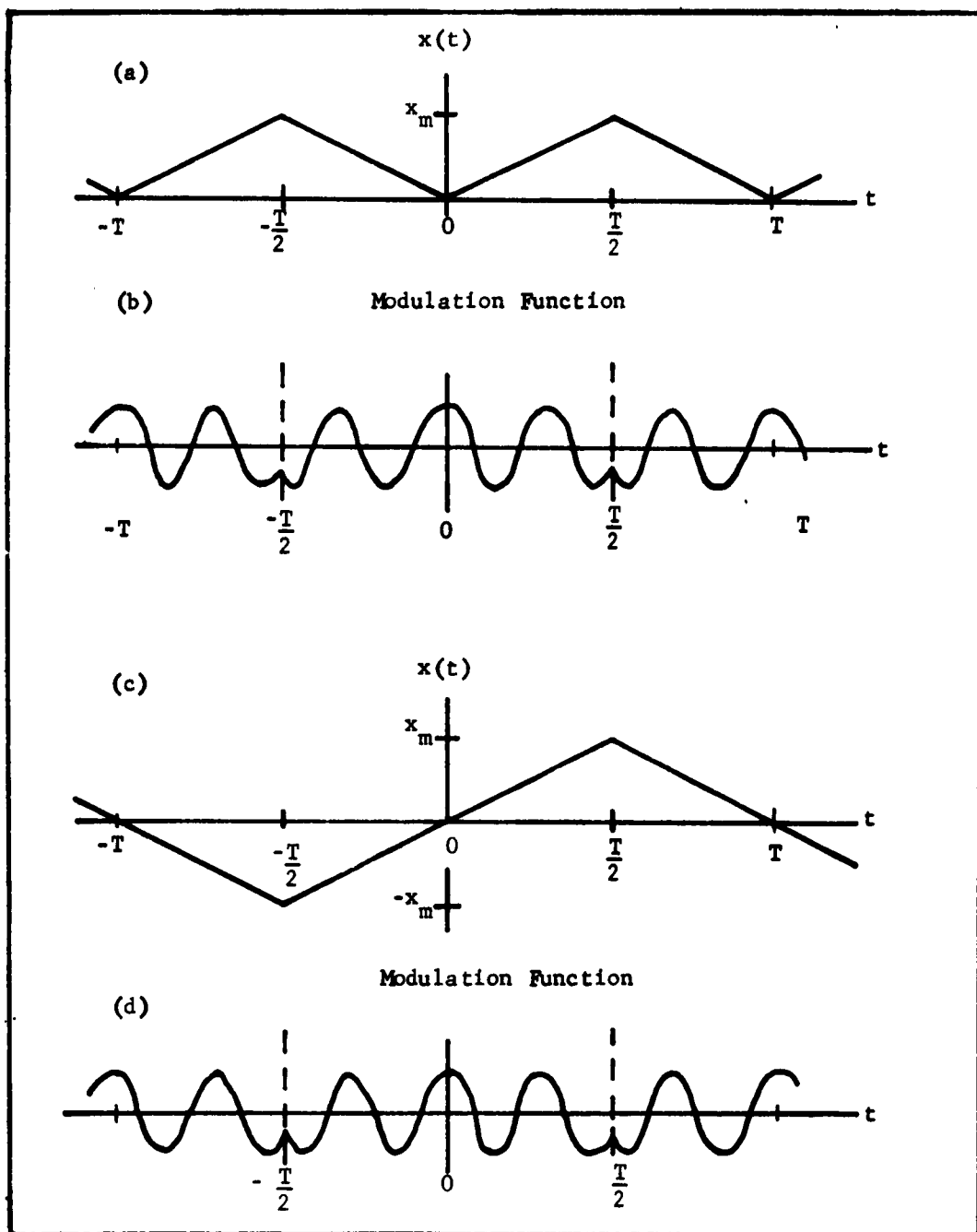
Fig. 11. (a) <u>One-sided</u> operation: the path difference periodically varied between the values zero and x_m. (b) The modulation function corresponding to (a) for an arbitrary wave number of radiation. (c) <u>Two-sided</u> operation: the path difference periodically varied between $- x_m$ and x_m. (d) The corresponding modulation function.

$$L(t,f') = \cos 2\pi f't \qquad (-\tfrac{T}{2} < t < \tfrac{T}{2}) . \qquad (3.25)$$

This is illustrated in Figure 11(b) and (d). Hence the interferogram function, being a superposition of these modulation functions for the various wavelengths of radiation, also becomes an even periodic function of period T. This periodic interferogram function can be defined for all values of t by means of the technique discussed in section 8, chapter II, as

$$F_2(t) = F_1(t) * \sum_{q=-\infty}^{\infty} \delta(t - qT) . \qquad (3.26)$$

Fourier transformation yields

$$
\begin{aligned}
P_2(f') &= P_1(f') \cdot \frac{1}{T} \sum_{q=-\infty}^{\infty} \delta(f' - \tfrac{q}{T}) \\
&= \frac{1}{T} \sum_{q=-\infty}^{\infty} P_1(\tfrac{q}{T}) \, \delta(f' - \tfrac{q}{T}) . \qquad (3.27)
\end{aligned}
$$

The quantity $F_2(t)$ is the modulation envelope of the radiant power input to the detector as a function of time, while $P_2(f')$ is its modulation frequency spectrum.

For monochromatic input radiation of wave number ν , with modulation frequency f, $P_1(f',f)$ is given by equation (3.19), so that $P_2(f')$ becomes

$$P_2(f',f) = \frac{1}{2} \sum_{q=-\infty}^{\infty} \left[\text{dif } T \, (\tfrac{q}{T} - f) + \text{dif } T \, (\tfrac{q}{T} + f) \right] \, \delta(f' - \tfrac{q}{T}) , \qquad (3.28)$$

which appears in Figure 12 for a value of f near $\frac{3}{T}$. For the interferogram function, Eqs. (3.20) and (3.26) yield

$$F_2(t,f) = \left[(\cos 2\pi \, f \, t) \cdot U_T(t) \right] * \sum_{q=-\infty}^{\infty} \delta(t - q \, T) , \qquad (3.29)$$
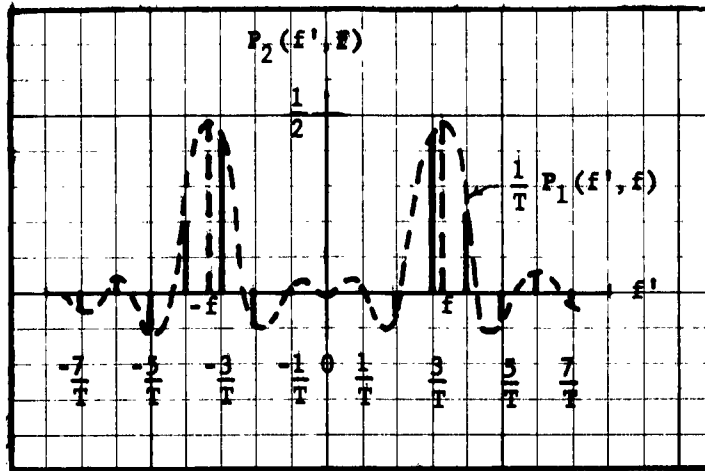
Fig. 12. The modulation frequency spectrum of the periodic input to the detector for radiation of wave number ν. The input modulation frequency spectrum $\frac{1}{2}\left[\delta(f'-f) + \delta(f'+f)\right]$ and the envelope $\frac{1}{T} P_1(f',f)$ are shown as broken curves.

which has the same form as the periodic modulation function in Figure 11. By use of Eq. (2.42) the qth Fourier series coefficient for $F_2(t,f)$ is easily obtainable from Eq. (3.28) as

$$c_q = \frac{1}{2}\left[\text{dif } T(f - \frac{q}{T}) + \text{dif } T(f + \frac{q}{T})\right].$$

Detection and Amplification; Definition of $F_3(t)$

The detector is assumed to produce a voltage signal proportional to the input radiant power, for modulation frequencies within the passband of the detector. The amplifier passband being finite also,

the effect of the detection-amplification system is to impose an overall bandwidth w on the frequency function $P_2(f')$. For purposes of analysis the amplifier gain and the detector sensitivity are set equal to unity within this passband. It will be shown later that no undesirable effects result from phase changes of the signal during amplification. The result of this bandwidth restriction is the elimination of some of the higher harmonics present in the detector input. The fact that the gain of the real amplifier and detector system is not constant from zero to $^w/_2$ is of minor importance, it will be seen. Under this circumstance the voltage output of the amplifier can be reasonably approximated by:

$$P_3(f') = U_w(f') \cdot P_2(f')$$

$$= \frac{1}{T} \sum_{q=-q'}^{q'} P_1(\frac{q}{T}) \delta(f' - \frac{q}{T}), \qquad (3.30)$$

where $\qquad \frac{2q'}{T} < w \leqslant \frac{2(q'+1)}{T}$. $\qquad (3.31)$

The graph of $P_3(f')$ for the monochromatic case appears in Figure 14(a), in which $\frac{1}{2} U_w(f')$ and $P(f',f)$ are indicated by the broken lines. The passband w is less than $2(\frac{3n}{T})$ in this figure. The transform of $P_3(f')$ is

$$F_3(t) = w \text{ dif } wt * F_2(t) .$$

$$= \frac{1}{T} \sum_{q=-q'}^{q'} P_1(\frac{q}{T}) e^{2\pi i \frac{q}{T} t} \qquad (3.32)$$

Synchronous rectification;
Definition of $F_4(t)$, $F_5(t)$, and $F_5(t,f)$

From the continuum of modulation frequencies f' the processes of periodic path difference variation, and detection and amplification select the discrete set

$$\frac{q}{T} , \quad q = 0, \pm 1, \pm 2, \ldots, \pm q' , \tag{3.33}$$

from which a particular positive member

$$f_n = \frac{n}{T} \tag{3.34}$$

is chosen for the frequency of synchronous rectification. Synchronous rectification at frequency $\frac{n}{T}$ can be accomplished, in the time domain, by multiplying the function to be rectified by the function

$$R_0(t) = \left[2U_{\frac{T}{2n}}(t) - U_{\frac{T}{n}}(t) \right] * \sum_{k=-\infty}^{\infty} \delta\left(t - k\frac{T}{n}\right) , \tag{3.35}$$

shown in Figure 13 for n = 3, and selecting the zero frequency
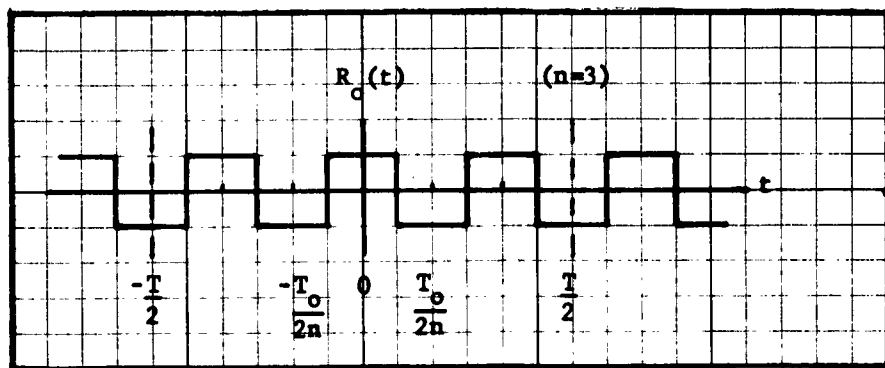
Fig. 13. The rectification function illustrated for n = 3.

component of the result. The Fourier transform of $R_0(t)$ is

$$R(f') = \left[\frac{2T}{2n} \text{ dif } \frac{T}{2n}f' - \frac{T}{n} \text{ dif } \frac{T}{n} f'\right] \cdot \frac{n}{T} \sum_{k=-\infty}^{\infty} \delta(f' - k\frac{n}{T})$$

(3.36)

$$= \sum_{k=-\infty}^{\infty} (\text{dif } \frac{k}{2} - \text{dif } k) \, \delta(f' - k\frac{n}{T}) \ ,$$

which appears in Figure 14(b). The values of the coefficients

$(\text{dif } \frac{k}{2} - \text{dif } k)$ are shown in parentheses in the figure. For even

values of k these coefficients vanish.

In the time domain, the signal after this first step of rectification is thus

$$F_4(t) = F_3(t) \cdot R_0(t) \ ,$$

(3.37)

while the resulting frequency spectrum is

$$P_4(f') = P_3(f') * R(f') \ .$$

(3.38)

The zero frequency component is selected by means of an electrical filter which rejects all frequencies $\geq \frac{1}{T}$. That is, the output frequency spectrum of this filter is

$$P_5(f') = P_4(f') \cdot U_{w_0}(f') \ .$$

(3.39)

The bandwidth w_0 is made less than $\frac{2}{T}$.

The quantity $P_5(f')$ is the D.C. input to the recorder. By the use of equations (3.38), (3.36) and (3.30) it can be evaluated analytically as follows:

$$P_5(f') = \left[P_3(f') * R(f') \right] \cdot U_{W_0}(f')$$

$$= \left\{ \left[\frac{1}{T} \sum_{q=-q'}^{q'} P_1^*\left(\frac{q}{T}\right) \delta\left(f'-\frac{q}{T}\right) \right] * \sum_{k=-\infty}^{\infty} (\text{dif}\,\frac{k}{2} - \text{dif}\,k) \delta\left(f'-k\frac{n}{T}\right) \right\} \cdot$$

$$U_{W_0}(f')$$

$$= \frac{1}{T} \sum_{q=-q'}^{q'} \sum_{k=-\infty}^{\infty} (\text{dif}\,\frac{k}{2} - \text{dif}\,k)\, P_1\left(\frac{q}{T}\right) \delta\left(f' - \frac{q}{T} - \frac{kn}{T}\right) \cdot U_{W_0}(f') .$$

$$(3.40)$$

The presence of the low pass filter function $U_{W_0}(f')$ now requires that

$$\delta\left(f' - \frac{q}{T} - \frac{kn}{T}\right) = \delta(f') ,$$

or

$$q = -kn , \qquad\qquad (3.41)$$

where n is a positive integer and k a positive or negative integer. Then

$$P_5(f') = \left[\frac{1}{T} \sum_k (\text{dif}\,\frac{k}{2} - \text{dif}\,k)\, P_1\left(\frac{-kn}{T}\right) \right] \delta(f') \qquad (3.42)$$

and

$$F_5(t) = \left[\frac{1}{T} \sum_k (\text{dif}\,\frac{k}{2} - \text{dif}\,k)\, P_1\left(\frac{-kn}{T}\right) \right] . \qquad (3.43)$$

The limits on k are determined by (3.41); that is, $k = -\,^{q}/_{n}$.
In turn, q is limited by the detector-amplifier bandwidth according to equations (3.30) and (3.31). If the detector-amplifier bandwidth

is restricted so that

$$\frac{w}{2} < \frac{3n}{T} \qquad (3.44)$$

then $|q| < 3n$ and $k = 0, \pm 1, \pm 2$. Of these values only $k = \pm 1$ contribute to $F_5(t)$, which reduces to

$$F_5(t) = \frac{2}{\pi T}\left[P_1(\frac{-n}{T}) + P_1(\frac{n}{T})\right] = \frac{2}{\pi T}\left[P_1(f_n) + P_1(-f_n)\right] \qquad (3.45)$$

For input radiation of wave number ν and formal modulation frequency

f, insertion of $P_1(f',f) = P_1(\pm f_n, f)$ from equation (3.19) into equation

(3.45) yields

$$F_5(t,f) = \frac{2}{\pi}\left[\text{dif } T(f - f_n) + \text{dif } T(f + f_n)\right]. \qquad (3.46)$$

The result (3.46) can also be obtained graphically by consideration

of Figures 14 and 15. The appropriate frequency functions for the

monochromatic input case are

$$P_3(f',f) = \left\{\frac{1}{2}\left[\text{dif } T(f'-f)+\text{dif } T(f'+f)\right] * \sum_{q=-\infty}^{\infty} \delta(f'-\frac{q}{T})\right\} \cdot U_w(f'), \qquad (3.47)$$

$$P_4(f',f) = P_3(f',f) * R(f') , \qquad (3.48)$$

$$P_5(f',f) = P_4(f',f) \cdot U_{w_o}(f') . \qquad (3.49)$$

The convolution of $P_3(f',f)$ with $R(f')$ means that the kth term of

$R(f')$ shifts the whole spectrum $P_3(f',f)$ a distance $\frac{kn}{T}$ to the right

along the axis of f' and alters the magnitude and sign, and then the

results for all k are added to get $P_4(f',f)$. The sum of all the

contributions at $f' = 0$ then yields $P_5(f',f)$. For example, Figure

14(c) shows that the $k = 1$ term of $R(f')$ shifts $P_3(f',f)$ a distance

$\frac{n}{T}$ to the right and multiplies it by $\frac{2}{\pi}$. This places the $f' = -\frac{n}{T}$

line of $P_3(f',f)$ exactly at $f' = 0$. The value of this line,

obtained from (3.47), is

$$\frac{1}{2}\left[\text{dif } T(f - \frac{n}{T})+\text{dif } T(f + \frac{n}{T})\right] ,$$

Fig. 14. Graphical representation of the process
of synchronous rectification of the detector-amplifier
output, in the frequency domain. In each graph the
heavy vertical lines represent the frequency components
corresponding to the ordinate label; the broken-line
rectangles represent filter functions. Input radiation
of wave number ν is chosen so that its modulation
frequency f is near the frequency $\frac{n}{T}$ of synchronous
rectification. The case $n = 3$ is illustrated.

(a) The detector-amplifier output. The two vertical
dotted lines represent the input $\frac{1}{2} \left[\delta(f'-f) + \delta(f'+f) \right]$.

(b) The frequency spectrum of the rectification
function. It extends from $-\infty$ to ∞. (c) The
convolution of the $k = 1$ term of $R(f')$ with $P_3(f',f)$.

(d) The convolution of the $k = -1$ term of $R(f')$ with
$P_3(f',f)$. (e) The contributions from the $k = \pm 3$ terms
of $R(f')$.

(a) $P_3(f',f)$ $\frac{1}{2}U_w(f')$

(b) $R(f')$

(c) $P_3(f',f) * \frac{2}{\pi}\delta(f'-\frac{n}{T})$ $(k=+1)$

(d) $P_3(f',f) * \frac{2}{\pi}\delta(f'-\frac{n}{T})$ $(k=-1)$

(e) $P_3(f',f) * \left[\frac{-2}{3\pi}\delta(f'-\frac{3n}{T})\frac{2}{3\pi}\delta(f'-\frac{3n}{T})\right]$
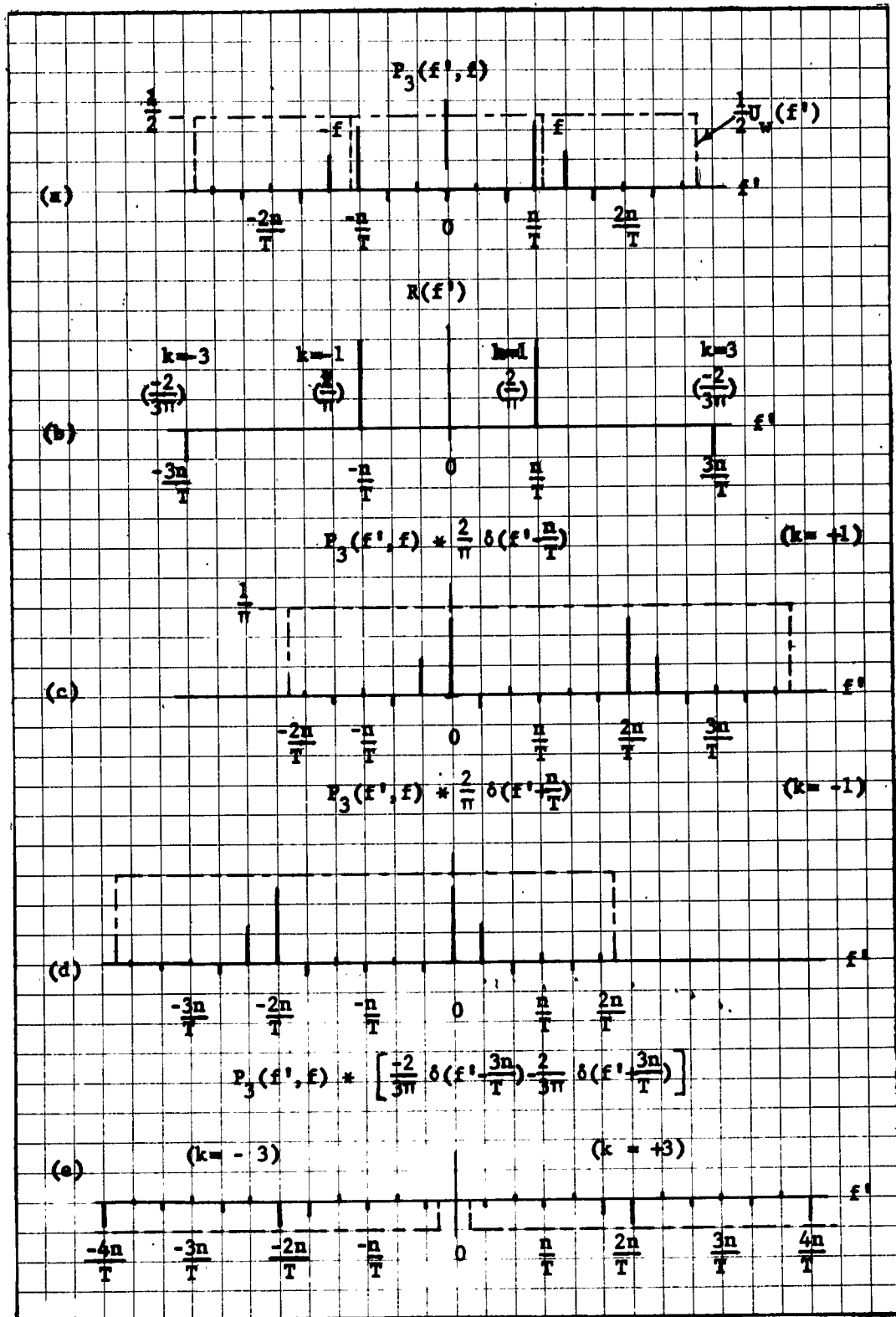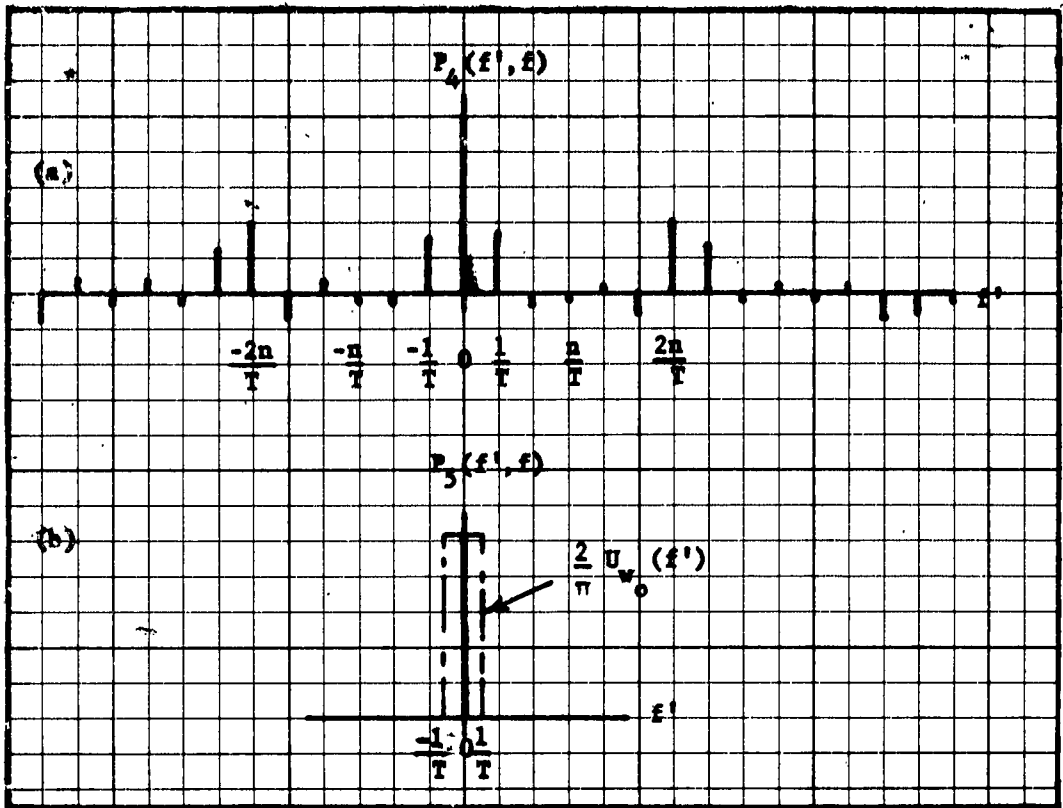
Fig. 15. (a) The frequency spectrum of the signal after the first step of synchronous rectification. (b) The final D.C. signal to the recorder.

which must be multiplied by $\frac{2}{\pi}$ to find the absolute contribution to the zero frequency component of $P_4(f',f)$. Similarly, the $k = -1$ term produces a shift of $-\frac{n}{T}$, places the $f' = \frac{n}{T}$ line of $P_3(f',f)$ at $f' = 0$, and produces a contribution equal to that of the $k = 1$ term. The $k = 3$ term translates $P_3(f',f)$ a distance $\frac{3n}{T}$ to the right, inverts it and multiplies it by the factor $\frac{2}{3\pi}$. As can be seen in Figure 14(e), choosing $W/2$ less than $\frac{3n}{T}$ prevents the $k = \pm 3$ and higher terms in $R(f')$ from contributing to the zero

frequency component of $P_4(f',f)$, so that the total D.C. signal is

$$\frac{2}{\pi}\left[\text{dif } T(f-\frac{n}{T})+\text{dif } T(f+\frac{n}{T})\right]$$

in agreement with equation (3.46). The possibility of having

a substantial $f'=\frac{1}{T}$ component in $P_4(f',f)$, as in Figure 15(a),

emphasizes the necessity for the post-rectification low pass

filter $U_{W_O}(f')$, shown, along with $P_5(f',f)$ in Figure 15(b).

The response function $\underline{S_O(f,f_n)}$,
the spectral response $\underline{S_O(\nu,\nu_n)}$,
and the instrumental line shape $\underline{S_O(\lambda_n,\lambda)}$

Because of the factor $\frac{1}{2}$ in the lamellar grating output,

equation (3.3), the recorded output relative to unit monochromatic

power incident on the lamellar grating is, under the assumption

of unit detector sensitivity, unit amplifier gain and no losses

by imperfect image formation, $\frac{1}{2}F_5(t,f)$. By use of equation (3.34)

this may be written:

$$\frac{1}{2}F_5(t,f)=\frac{1}{\pi}\left[\text{dif }\frac{n}{f_n}(f-f_n)+\text{dif }\frac{n}{f_n}(f+f_n)\right]\ . \tag{3.50}$$

The response function $\underline{S_O(f,f_n)}$. --

It is now convenient to define a new response function

$$S_O(f,f_n)=\frac{\pi}{2}F_5(t,f)\ =\ \text{dif }\frac{n}{f_n}(f-f_n)+\text{dif }\frac{n}{f_n}(f+f_n) \tag{3.51}$$

which makes clear the dependence on f and f_n and has very nearly

unit peak value, at least for $n\geqslant 3$. This function is plotted

versus f in Figure 16, for a = 3.
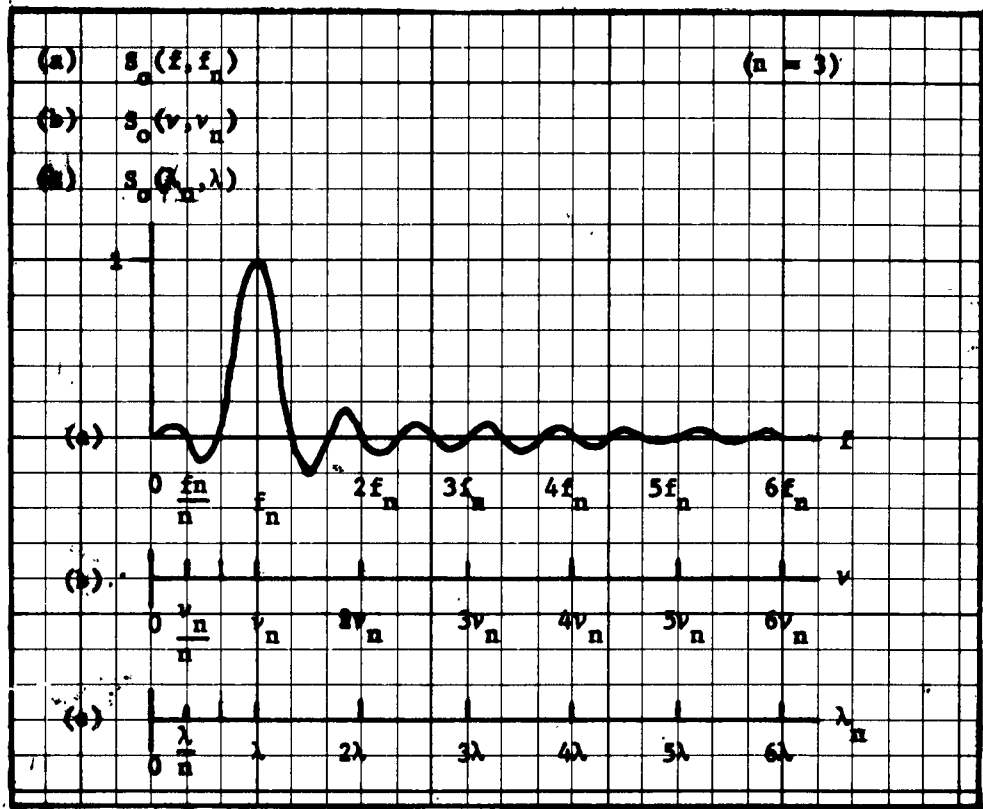
Fig. 16. The response function, the spectral response, and the instrumental line shape all have the same shape when plotted versus the appropriate variables. The ordinate label (a) and the abscissa (a) refer to the response function $S_0(f, f_n)$; the ordinate label (b) and the abscissa (b) refer to the spectral response $S_0(\nu, \nu_n)$; the ordinate label (c) and the abscissa (c) refer to the instrumental line shape $S_0(\lambda_n, \lambda)$. The case shown is for n = 3.

The spectral response $S_0(\nu, \nu_n)$.-- According to equation (3.11), f is formally defined as

$$f = \frac{2x_m}{T} \nu \quad .$$

(3.52)

The argument of the first dif function in equation (3.51) can be written

$$fT - n = 2x_m \nu - n$$

The peak value of the signal occurs for a value of f very near that for which the argument of the dif function vanishes; that is, approximately for

$$f = f_n$$

or

$$\nu = \nu_n = \frac{n}{2x_m} \, , \tag{3.53}$$

which defines ν_n as the wave number for which the modulator is adjusted for maximum response. The argument of the first part of (3.51) can now be expressed as

$$\frac{n}{\nu_n} \ (\nu - \nu_n) \, ,$$

so that equation (3.51) can be written in terms of ν and ν_n:

$$S_0(\nu , \nu_n) = \text{dif} \ \frac{n}{\nu_n} \ (\nu - \nu_n) + \text{dif} \ \frac{n}{\nu_n} \ (\nu + \nu_n) \quad . \tag{3.54}$$

For a given ν_n, determined by the values of n and x_m, $S_0(\nu , \nu_n)$ gives the output signal as a function of the variable input wave number ν. In the present work this will be called the spectral response of the instrument. It is equivalent to the "spectral reflected power" introduced by Genzel and Weber.[5] As is evident

5. L. Genzel and R. Weber, B. angew. Physik 10, 127 (1957).

from Figure 16, the spectral response as a function of ν has the same shape as $S_0(f,f_n)$. If the input spectrum as a function of positive wave number ν is $2P_0(\nu)$, then the total signal produced by this spectrum, for a given value of ν_n, is

$$S_0(\nu_n) = \int_0^\infty 2P_0(\nu)\, S_0(\nu,\nu_n)\, d\nu . \qquad (3.55)$$

The instrumental line shape $S_0(\lambda_n, \lambda)$. -- The apparent spectrum of a monochromatic line of fixed wave number ν can be obtained from (3.54) by holding ν constant and allowing ν_n to vary. The resulting instrumental line shape can be written

$$S_0\left(\frac{1}{\nu_n}, \frac{1}{\nu}\right) = \operatorname{dif} n\nu \left(\frac{1}{\nu_n} - \frac{1}{\nu}\right) + \operatorname{dif} n\nu \left(\frac{1}{\nu_n} + \frac{1}{\nu}\right) , \qquad (3.56)$$

or, in terms of the input wavelength $\lambda = \frac{1}{\nu}$ and the wavelength scanning variable $\lambda_n = 1/\nu_n$,

$$S_0(\lambda_n, \lambda) = \operatorname{dif} \frac{n}{\lambda}(\lambda_n - \lambda) + \operatorname{dif} \frac{n}{\lambda}(\lambda_n + \lambda) . \qquad (3.57)$$

Figure 16 suffices to illustrate this function, since it has the same form, as a function of λ_n and λ , as has the spectral response, as a function of ν and ν_n.

The effect on the idealized output of a grating spectrometer.

If the input spectrum is the idealized instantaneous output of a grating spectrometer, i.e., a series of monochromatic lines having wave numbers which are integral multiples of the first order wave number, and if the wave number of this first spectrometer order is maintained equal to the wave number of peak response ν_n of the

modulator, then

$$\nu = p \, \nu_n \qquad p = 1, 2, 3, \ldots \qquad (3.58)$$

and

$$S_0(\nu, \nu_n) \doteq S_0(p \, \nu_n, \nu_n) = \text{dif } n(p - 1) + \text{dif } n(p + 1) \qquad (3.59)$$

$$= 1 \qquad (p = 1)$$

$$= 0 \qquad (p = 2, 3, 4, \ldots) \ .$$

This result is also apparent from inspection of Figure 16. It should be pointed out that this complete blocking of the unwanted monochromator orders occurs only for perfect interferometric modulation of monochromatic input lines, and is also contingent on fulfillment of the electrical filtering conditions

$$\frac{W}{2} < \frac{3n}{T} \quad \text{and} \quad W_0 < \frac{2}{T} \ .$$

CHAPTER IV

THEORY: A MORE GENERAL TREATMENT

In chapter III the transmission function was assumed to be
cosinusoidal, at least during each grating cycle. In the present
chapter this restriction is removed and a method outlined for
obtaining the resulting response function, retaining the idealized
electrical filtering and rectification functions. Several
examples are treated in detail.

Arbitrary transmission function

Equation (3.2),

$$F_0(x) = \int_{-\infty}^{\infty} P_0(\nu') \, L_0(x, \nu') \, d\nu' , \qquad (3.2)$$

gives the interferogram function for arbitrary transmission function
$L_0(x, \nu')$, which is a real, but not necessarily even, function of
x. $P_0(\nu')$ is the wave number spectrum of the incident radiant
power. The transformation

$$x = x(t) \qquad (4.1)$$

$$f' = \frac{2x_m}{T} \quad \nu' = v\nu' \qquad (3.11)$$

suggests the definition

$$L(t,f') = L_0(x,\nu') . \qquad (4.2)$$

The interferogram as a function of time may then be expressed as

47

$$F(t) = \int_{-\infty}^{\infty} P(f') \, L(t,f') \, df' \quad, \tag{4.3}$$

where $P(f')$ is proportional to $P_0(\nu')$, in consequence of the definition (3.11) of f', which is formally retained even though $L(t,f')$ is no longer necessarily periodic with frequency f' within the time interval T.

A detector with infinite modulation frequency passband would respond to the power $F(t)$ and produce a proportional signal voltage. Thus $F(t)$ may also be regarded as a time-varying voltage, with frequency spectrum $P'(f'')$ given by

$$P'(f'') = F.T. \left[F(t) \right] \quad,$$

with $F(t)$ given by the integral (4.3). Since $F(t)$, according to Eq. (4.3) is real, but not necessarily even, $P'(f'')$ is in general complex. The remainder of the analysis consists in calculating the successive forms of this frequency spectrum as the maximum path difference is limited, the path difference is varied periodically, etc.

The interferogram function for a finite time interval is again

$$F_1(t) = F(t) \cdot U_T(t) \tag{3.17}$$

and the corresponding frequency spectrum is

$$P_1(f'') = F.T. \left[F_1(t) \right] . \tag{4.4}$$

The function $F_1(t)$ is obtained from Eq. (4.3) as

$$F_1(t) = \int_{-\infty}^{\infty} P(f') \, L(t,f') \cdot U_T(t) \, df'$$

$$= \int_{-\infty}^{\infty} P(f') \, L_1(t,f') \, df' \, , \qquad (4.5)$$

where

$$L_1(t,f') = U_T(t) \cdot L(t,f') \qquad (4.6)$$

is the modulation function on the fundamental interval $(-\frac{T}{2} < t < \frac{T}{2})$.

Equations (3.17) and (4.4) comprise a transform pair formally identical to the pair $F_1(t)$, $P_1(f')$ of Eqs. (3.17) and (3.18). Also, no confusion results if f'' is replaced by f' in Eq. (4.4). For periodic variation of path difference, with the same electrical filtering and synchronous rectification, therefore, the analysis proceeds exactly as in the idealized case. That is, the recorded signal is given by Eq. (3.40) as

$$P_5(f') = \left[\left\{ \left[P_1(f') \cdot \frac{1}{T} \sum_{q=-\infty}^{\infty} \delta(f' - \frac{q}{T}) \right] \cdot U_W(f') \right\} * R(f') \right] \cdot U_{W_0}(f') \, , \qquad (3.40)$$

which leads once more to

$$F_5(t) = \frac{2}{\pi T} \left[P_1(f_n) + P_1(-f_n) \right] \, . \qquad (3.45)$$

However, now P_1 is obtained from $L_1(t,f')$ by use of Eqs. (4.4) and (4.5) as

$$P_1(f') = \text{F.T.} \left[\int_{-\infty}^{\infty} P(f') \, L_1(t,f') \, df' \right] \, . \qquad (4.7)$$

For the monochromatic case, equations (3.15) and (4.7) become

$$P(f',f) = \frac{1}{2} \left[\delta(f' - f) + \delta(f' + f) \right] \qquad (3.15)$$

$$P_1(f',f) = \frac{1}{2} \text{ F.T. } \left[L_1(t,f) + L_1(t,-f) \right] \quad . \tag{4.8}$$

Equations (3.45), (3.15) and (4.8) allow calculation of the normalized output signal $S(f,f_n)$ from

$$S(f,f_n) = \frac{\pi}{2} \ F_5(t,f)$$

$$= \frac{1}{T} \left[P_1(f_n,f) + P_1(-f_n,f) \right] \quad . \tag{4.9}$$

In the event that $L_1(t,f')$ is an even function of both t and f',
F.T. $\left[L_1(t,f) \right]$ is an even function of both f' and f and

$$P_1(f',f) = \text{F.T. } \left[L_1(t,f) \right] \quad , \tag{4.10}$$

$$S(f,f_n) = \frac{2}{T} P_1(f_n,f) \quad . \tag{4.11}$$

Thus, on the assumption of flawless electrical filtering and rectification, the analysis of errors or other departures from perfect cosinusoidal modulation reduces to the calculation of the Fourier transform of $L_1(t,f)$, the transmission function during the fundamental period. This function $L_1(t,f)$ may be even, odd, or of mixed parity with respect to t = 0 so that its transform, hence $S(f,f_n)$, may have a real part, corresponding to the even part of L_1 and an imaginary part corresponding to the odd part of L_1. It will be found that synchronous rectification eliminates the imaginary part of $S(f,f_n)$.

As before, the spectral response $S(\nu, \nu_n)$ and the instrumental

line shape $S(\lambda_n, \lambda)$ are obtained from $S(f,f_n)$ by use of the definition (3.52).

Constant term in $L_1(t,f)$

If the modulation function contains a constant additive term L_1^o , which is usually the case, equations (4.5), (4.10) and (4.11) give for the constant part:

$$L_1^o \, (t,f') = L_1^o \, U_T(t) \, ,$$

$$P_1^o(f',f) = L_1^o \, T \text{ dif } Tf',$$

and

$$S^o(f,f_n) = 2L_1^o \text{ dif } Tf_n = 0.$$

Apodization

The spectral response of equation (3.54) is not optimum for spectroscopic purposes because of the prominent subsidiary maxima and minima, or feet. These can be considerably diminished by a suitable modification of the modulation function $L_1(t,f)$. This apodization can be accomplished by altering the radiation intensity itself, but, as pointed out by Happ and Genzel[1] and by Jacquinot,[2] it is preferable to introduce the apodizing function after detection and amplification so that detector noise is altered along with the

1. H. Happ and L. Genzel, Infrared Physics 1, 39 (1961).

2. P. Jacquinot, Reports on Progress in Physics 23, 267 (1960).

signal. If the detector-amplifier passband is infinite, the time variation of the radiant power falling on the detector is faithfully reproduced as an electrical voltage and equations (4.5) and (4.6) then apply equally well to the radiation or to the amplifier output. In this case the modified transmission function becomes

$$L_1(t,f') = L(t,f') \cdot A(t) , \qquad (4.12)$$

where $A(t)$ is the apodizing function, which vanishes outside the interval $(-\frac{T}{2} < t < \frac{T}{2})$.

As an example suppose

$$A(t) = V_T(t)$$

and

$$L(t,f') = 1 + \cos 2\pi f't ,$$

where $V_T(t)$ and its transform are given by Eqs. (2.50) and (2.51). Provided that the filter $U_w(f')$ is inserted after apodization, equation (4.10) yields

$$P_1(f',f) = \left\{\delta(f') + \frac{1}{2}\left[\delta(f'-f) + \delta(f'+f)\right]\right\} * \frac{T}{2}\,\mathrm{dif}^2\,\frac{Tf'}{2}$$

$$= \frac{T}{2}\,\mathrm{dif}^2\,\frac{Tf'}{2} + \frac{T}{4}\left[\mathrm{dif}^2\,\frac{T}{2}(f'-f) + \mathrm{dif}^2\,\frac{T}{2}(f'+f)\right] .$$

From equation (4.11),

$$S(f,f_n) = \mathrm{dif}^2\frac{Tf_n}{2} + \frac{1}{2}\left[\mathrm{dif}^2\,\frac{T}{2}(f-f_n) + \mathrm{dif}^2\,\frac{T}{2}(f+f_n)\right] .$$

$$= \mathrm{dif}^2\,\frac{Tf_n}{2} + \frac{1}{2}\,S_1(f,f_n) \qquad (4.13)$$

where

$$s_1(f,f_n) = \text{dif}^2 \, \frac{T}{2}(f-f_n) + \text{dif}^2 \, \frac{T}{2}(f+f_n) \tag{4.14}$$

The first term in (4.14) has the constant value $\text{dif}^2 \frac{n}{2}$ and arises from the constant term in $L(t,f')$. In practice the latter constant term does not appear in the electrical signal, so that only multiplying the radiation signal itself by $A(t)$ can produce a term like $\text{dif}^2 \frac{n}{2}$ in the response function. The result (4.14) is plotted in Figure 17, neglecting the $\text{dif}^2 \frac{n}{2}$ term. The feet are
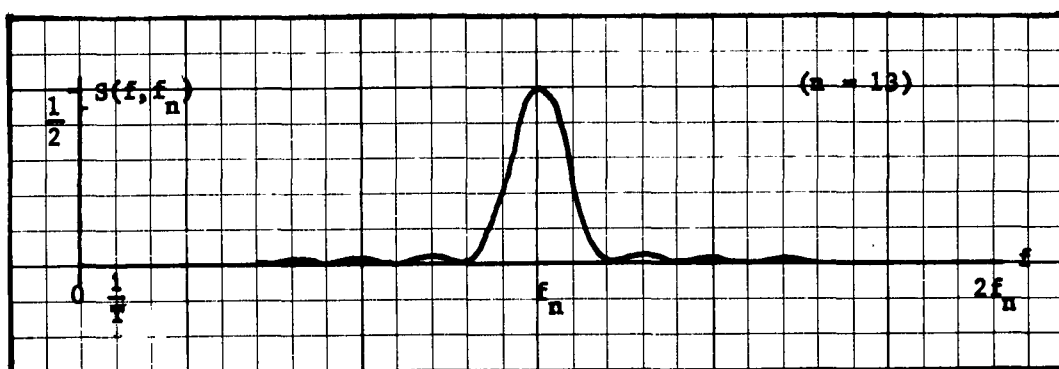
Fig. 17. The response function with triangular apodization applied after infinitely broad-band detection and amplification.

diminished at the expense of broadening and lowering of the principal maximum. In an interval on the f-axis including the principal maximum and a fairly large number of subsidiary maxima, this curve differs only slightly from the intensity distribution of a diffracting grating. On the basis of this similarity it is reasonable to define the Rayleigh resolving power of the instrument using the spectral response obtained for this triangular apodization.

That is,

$$\frac{\nu_n}{\Delta \nu} = \frac{f_n}{\Delta f} = \frac{n/T}{2/T} = \frac{n}{2} \quad . \tag{4.15}$$

Since $\Delta \nu = 1/x_m$, the resolving power is also $x_m \nu_n$, the number of wavelengths contained in the maximum path difference. Even more effective apodization can be obtained by suitable choice of apodizing function.[3]

When the apodization is introduced after a detector and amplifier with finite passband, the resulting time function can be written

$$F_A(t,f) = F_3(t,f) \cdot \left[A(t) * \sum_{\ell = -\infty}^{\infty} \delta(t - \ell T) \right] \quad ,$$

for monochromatic input radiation. If $A_1(f')$ is the Fourier transform of $A(t)$, the transform of $F_A(t,f)$ is

$$P_A(f',f) = P_3(f',f) * \left[A_1(f') \cdot \frac{1}{T} \sum_{\ell = -\infty}^{\infty} \delta(f' - \frac{\ell}{T}) \right] \quad .$$

Examination of Figure 18 shows that the convolution of these two modified Dirac combs would yield a finite sum of terms which would contribute to the final signal $S(f,f_n)$. For values of f within the detector-amplifier passband, the resulting $S(f,f_n)$ would not differ

---

3. See e.g.: Happ and Genzel, Infrared Physics 1, 39 (1961); R. B. Blackman and J. W. Tukey, The Measurement of Power Spectra (Dover Publications, Inc. New York, 1959), p. 95.
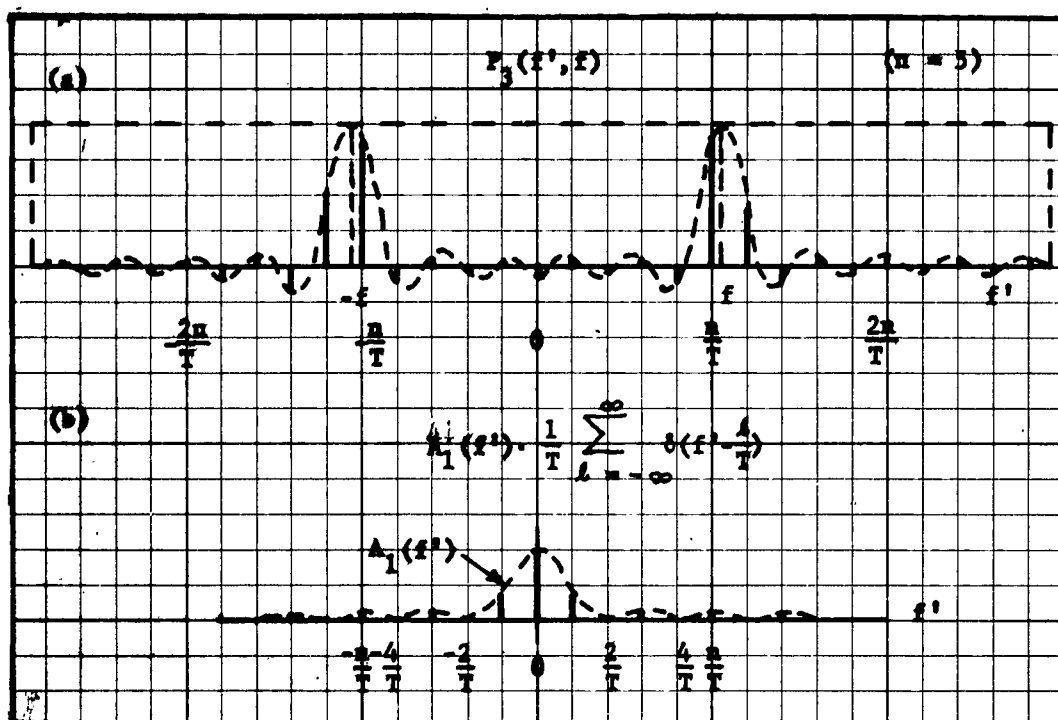
Fig. 18. The frequency functions involved in computing the response function for apodization applied after finite-pass-band detection and amplification. (a) The frequency spectrum of the amplified signal before apodization. (b) The frequency spectrum of the apodizing function.

appreciably from the form of A_1. For other values of f, the curve $S(f, f_n)$ would pass through zero at intervals of $\frac{1}{T}$ and it would have more resemblance to a dif curve.

Translation of limits of variation of path difference

Suppose that the linear reciprocating grating motion takes place between the limits X_0 and $X_m + X_0$ instead of the limits 0 and X_m. The path difference variation then takes place in the interval $(x_0 < x < x_m + x_0)$. The path difference as a function of time becomes

$$x(t) = \frac{2x_m}{T} \, |t| + x_0 \qquad (-\tfrac{T}{2} < t < \tfrac{T}{2}) \quad , \tag{4.16}$$

which is shown in Figure 19. If there are no other departures

$$x(t) = x_0 + \frac{2x_m}{T}\,|t|$$

Modulation Function
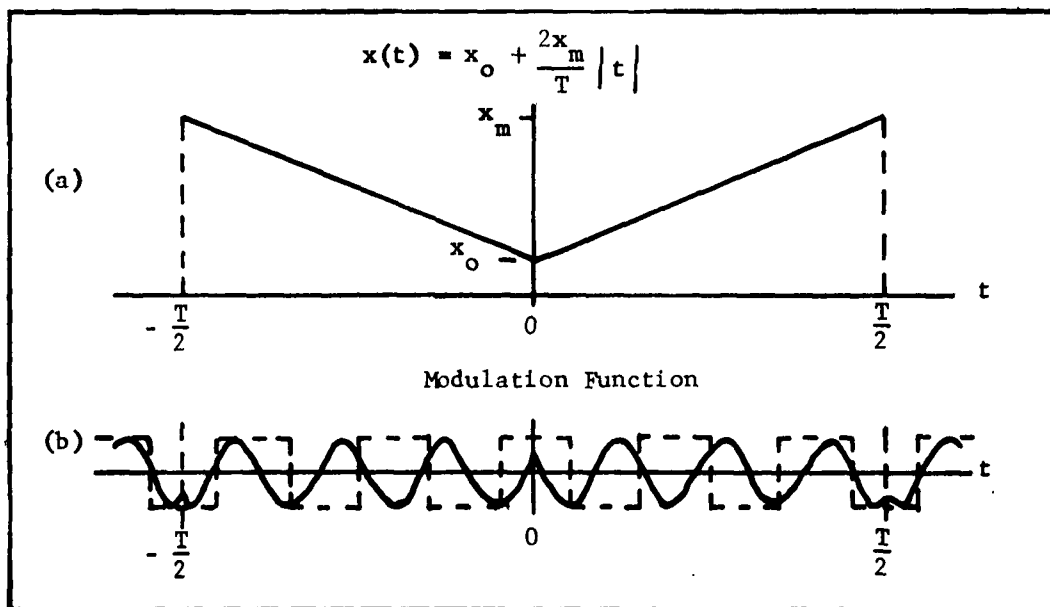
Fig. 19. (a) The path difference as a function of time for one-sided operation within the limits $(x_0 < x < x_m + x_0)$. (b) The corresponding modulation function for a selected wave number.

from the idealized treatment, the modulation function for this case is, by Eqs. (4.6) and (4.16),

$$L_1(t,f) = U_T(t) \cdot \cos 2\pi f(\,|t| + \epsilon\,) \quad , \tag{4.17}$$

where

$$f = \frac{2x_m \nu}{T} \tag{3.52}$$

$$\epsilon f = x_0 \nu \quad . \tag{4.18}$$

Eqs. (3.52) and (4.18) also imply:

$$\epsilon = \frac{x_0}{2x_m} T .$$ (4.19)

Another useful relation, deduced from Eqs. (4.19) and (3.53) is

$$\frac{\epsilon}{T/n} = \frac{x_0}{\lambda_n} = \gamma ,$$ (4.20)

which defines the number γ. Figure 19 shows that L_1 is an even function of t and of f, with a cusp at $t = 0$ as well as at $t = \pm\frac{T}{2}$. If it is assumed that the rectification function $R_0(t)$ remains centered on $t = 0$, then Eqs. (4.10) and (4.11) still apply and all that is required is the Fourier transform of $L_1(t,f)$. For this calculation $L_1(t,f)$ may be expressed as

$$L_1(t,f) = \cos 2\pi f(t + \epsilon) \cdot U_{\frac{T}{2}}(t - \frac{T}{4})$$

$$+ \cos 2\pi f(t - \epsilon) \cdot U_{\frac{T}{2}}(t + \frac{T}{4}) .$$ (4.21)

Then, using Eq. (2.33),

$$P_1(f',f) = F.T. \left[L_1(t,f) \right]$$

$$= \left\{ e^{2\pi i \epsilon f'} \cdot \frac{1}{2} \left[\delta(f'-f) + \delta(f'+f) \right] \right\} * \left\{ e^{-2\pi i \frac{T}{4} f'} \cdot \frac{T}{2} \text{ dif } \frac{Tf'}{2} \right\}$$

$$+ \left\{ e^{-2\pi i \epsilon f'} \cdot \frac{1}{2} \left[\delta(f'-f) + \delta(f'+f) \right] \right\} * \left\{ e^{2\pi i \frac{T}{4} f'} \cdot \frac{T}{2} \text{ dif } \frac{Tf'}{2} \right\} .$$

This reduces to

$$P_1(f',f) =$$

$$\frac{T}{2}\left\{ \cos 2\pi\left[(\epsilon + \frac{T}{4})f - \frac{Tf'}{4}\right] \text{dif } \frac{T}{2}(f'-f) + \cos 2\pi\left[(\epsilon + \frac{T}{4})f + \frac{T}{4}f'\right] \right.$$

$$\left. \cdot \text{dif } \frac{T}{2}(f'+f) \right\} \qquad (4.22)$$

Finally

$$S(f,\frac{n}{T}) = \cos 2\pi (\epsilon + \frac{T}{4}) f \cos \frac{n\pi}{2}\left[\text{dif } \frac{T}{2}(f - \frac{n}{T}) + \text{dif } \frac{T}{2}(f + \frac{n}{T})\right]$$

$$+ \sin 2\pi (\epsilon + \frac{T}{4}) f \sin \frac{n\pi}{2}\left[\text{dif } \frac{T}{2}(f - \frac{n}{T}) - \text{dif } \frac{T}{2}(f + \frac{n}{T})\right] .$$

$$(4.23)$$

Setting $\epsilon = 0$ in Eq. (4.23) converts it to Eq. (3.51) as expected. Another particular case of interest for the modulator as designed is n = 1, 5, 9, 13, 17,..., when Eq. (4.23) becomes

$$S(f,f_n) = \sin 2\pi (\epsilon + \frac{T}{4}) f \left[\text{dif } \frac{n}{2f_n}(f - f_n) - \text{dif } \frac{n}{2f_n} (f + f_n)\right] .$$

$$(4.24)$$

The definition (4.20) allows the sine factor of Eq. (4.24) to be written $\sin 2\pi(\gamma + \frac{n}{4}) \frac{f}{f_n}$.

The symmetrical, two-sided operation of the modulator such that the grating depth varies between positive and negative values of equal magnitude can now be treated as a special case of the one-sided operation. Setting $x_0 = -\frac{x_m}{2}$ makes Eq. (4.16) describe the

symmetrical motion depicted in Figure 20.

$$x(t) = -\frac{x_m}{2} + \frac{2x_m}{T}\left|t\right|$$
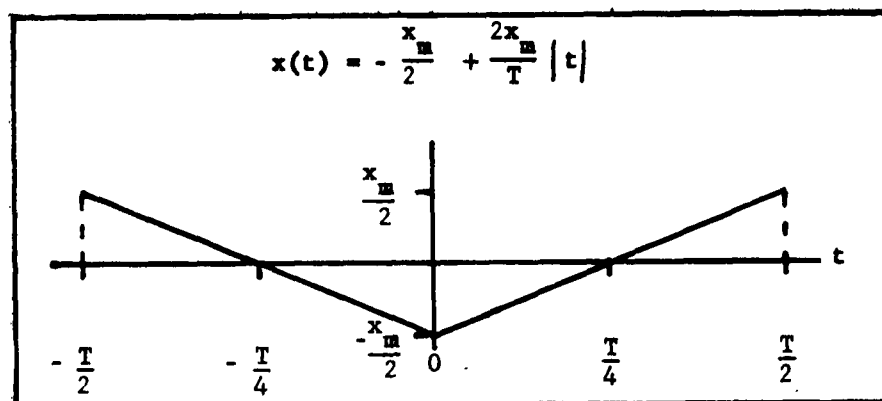
Fig. 20. The path difference for two-sided operation as a special case of one-sided operation.

The magnitude of the maximum path difference is now just half the former value. That is

$$x_m' = \frac{x_m}{2} \qquad (4.25)$$

Since $n = 2x_m \, \nu_n$ and $n' = 2x_m' \nu_n$ it follows that

$$n' = {}^n\!/_2 \; . \qquad (4.26)$$

The time for one grating cycle is now

$$T' = \frac{T}{2} \; . \qquad (4.27)$$

The modulation frequency for wave number ν_n remains the same:

$$\frac{n'}{T'} = \frac{n}{T} \qquad (4.28)$$

From Eq. (4.19), ϵ becomes $-\frac{T}{4}$, which inserted into Eq. (4.23) gives

$$S(f, \tfrac{n}{T}) = \cos \tfrac{n\pi}{2} \left[\text{dif } \tfrac{T}{2}(f - \tfrac{n}{T}) + \text{dif } \tfrac{T}{2}(f + \tfrac{n}{T}) \right]$$

or

$$S(f, \tfrac{n'}{T'}) = \cos n'\pi \left[\text{dif } T'(f - \tfrac{n'}{T'}) + \text{dif } T'(f + \tfrac{n'}{T'}) \right] \tag{4.29}$$

To make Eq. (4.29) correspond exactly with the response function for two-sided operation given in Eq. (3.51), n should be chosen to be even (e.g. n = 26, n' = 13) and if n' is odd the rectification function $R_0(t)$ must be shifted by $T/2n$ along the t axis. This simply changes the sign of Eq. (4.29) so that a positive peak response is obtained for $f = \frac{n'}{T'}$.

The response function $S(f,\frac{n'}{T'})$ for two-sided operation with a displacement x_0' from symmetric operation, corresponding to a path difference interval $(-x_m + x_0' < x < x_m + x_0')$, can be derived from Eq. (4.23) by setting

$$x_0 = -\frac{x_m}{2} + x_0' ,$$

or

$$\epsilon = -\frac{T}{4} + \epsilon' ,$$

where

$$\epsilon' = \frac{x_0' T}{2 x_m} . \tag{4.30}$$

The result is

$$S(f, \tfrac{n'}{T'}) = \cos 2\pi\epsilon' f \cos n'\pi \left[\text{dif } T'(f - \tfrac{n'}{T'}) + \text{dif } T'(f + \tfrac{n'}{T'}) \right]$$

$$+ \sin 2\pi\epsilon' f \sin n'\pi \left[\text{dif } T'(f - \tfrac{n'}{T'}) - \text{dif } T'(f + \tfrac{n'}{T'}) \right] .$$

$$(4.31)$$

For n' odd, and if the rectifier is properly phased,

$$S(f, \tfrac{n'}{T'}) = (\cos 2\pi\epsilon' f) \left[\text{dif } T'(f - \tfrac{n'}{T'}) + \text{dif } T'(f + \tfrac{n'}{T'}) \right] .$$

$$(4.32)$$

Since the symbols x_m', n', T' and ϵ' merely represent an arbitrary consistent set of values of x_m, n, T, and ϵ, and since $\frac{n'}{T'} = f_n$, no confusion should result if the primes are dropped in Eq. (4.32), yielding

$$S(f, f_n) = (\cos 2\pi\epsilon f) \left[\text{dif } \tfrac{n}{f_n}(f - f_n) + \text{dif } \tfrac{n}{f_n}(f + f_n) \right] . \quad (4.33)$$

This becomes

$$S(f, f_n) = \cos 2\pi \gamma \tfrac{f}{f_n} \, S_0(f, f_n) , \qquad (4.34)$$

when definitions (4.20) and (3.51) are used.

Now in the limit as ϵ approaches zero, Eq. (4.24), for the one-sided mode, and Eq. (4.33), for the two-sided mode, approach the same expression for the same value of n. In this limit the resolving power is the same in the two cases. The cosine and dif factors of Eq. (4.33) are plotted in Figure 21(a) for n = 13 and values of ϵ such that γ = 1/3, 1/4, 1/6, and 1/12. The factors of

Eq. (4.24) are graphed in Figure 21(b) for n = 13 and $\gamma = 1/12$

Although a more detailed study of these curves will be found in

chapter VIII, it can be seen immediately that the more rapidly

varying sinusoidal factor in Eq. (4.24) makes the spectral response

for the one-sided case more sensitive to a small displacement

from mirror position.

This derivation of $S(f,f_n)$ for the two-sided mode from the

expression for the one-sided mode neglects the fact that the

fundamental period of the modulation function is not T but 2T,

hence a $\frac{1}{2T}$ frequency component is in general introduced into

the rectifier output by the presence of x_0. The results stated

are correct if this $\frac{1}{2T}$ component is removed by the post-rectifica-

tion filter.

Fig. 21. The effect on the response function of a translation of the limits of variation of the path difference. (a) Two-sided operation, n = 13. The response function is obtained for various values of γ by multiplying the solid curve by the appropriate broken curve. (b) One-sided operation, n = 13. $S(f, f_n)$ for $\gamma = 1/12$ calculated as the product of the solid curve and the broken curve.
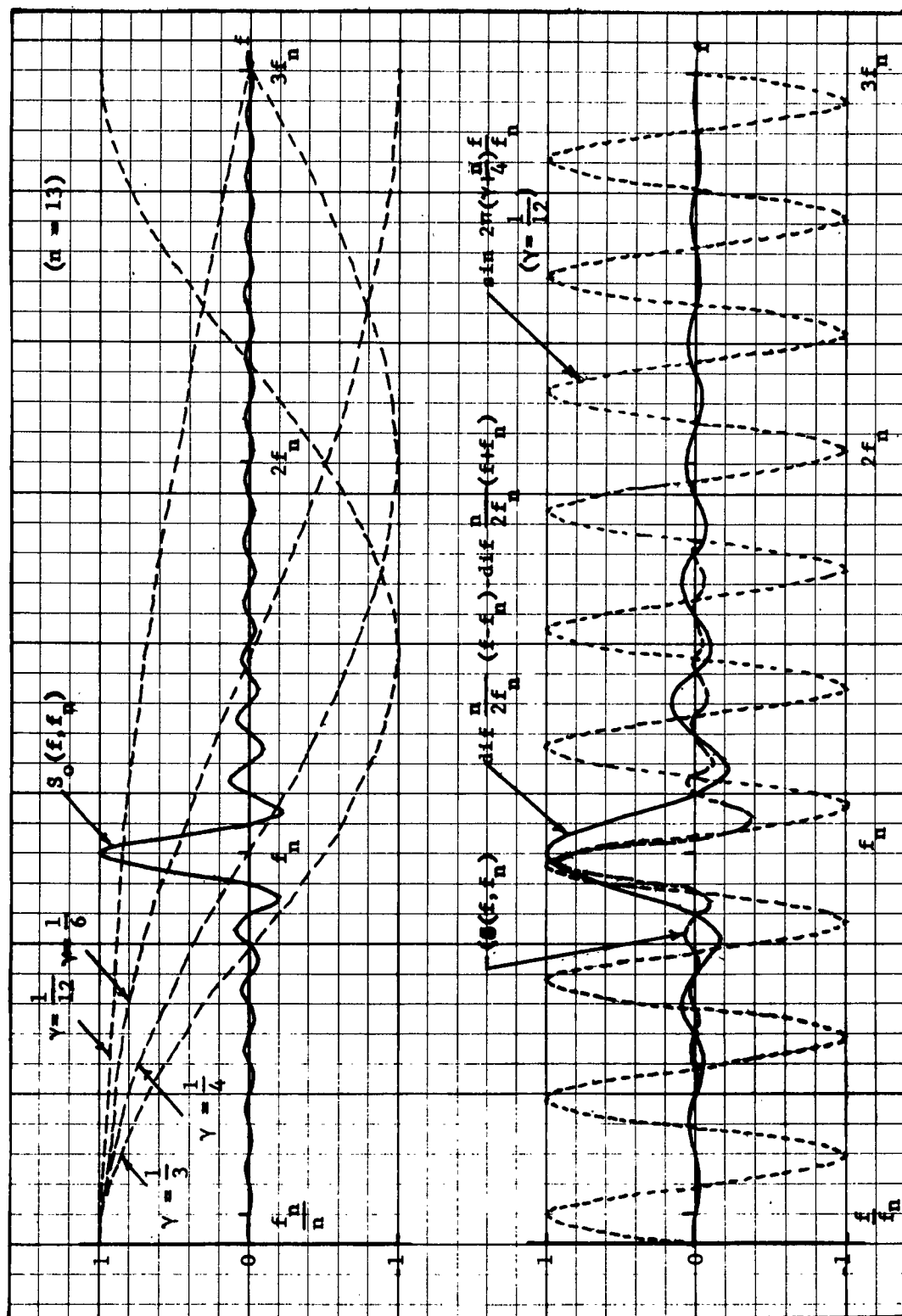
Effect of an irregularity in path difference
variation repeated with period 2T

For calculating the effects of mechanical imperfections in the grating drive arrangement, it is useful to obtain an expression for the increment $\Delta S(f,f_n)$ of signal associated with the special irregular portions of the path difference curve $x(t)$ illustrated in Figure 22 for the two-sided mode of operation. In this case,
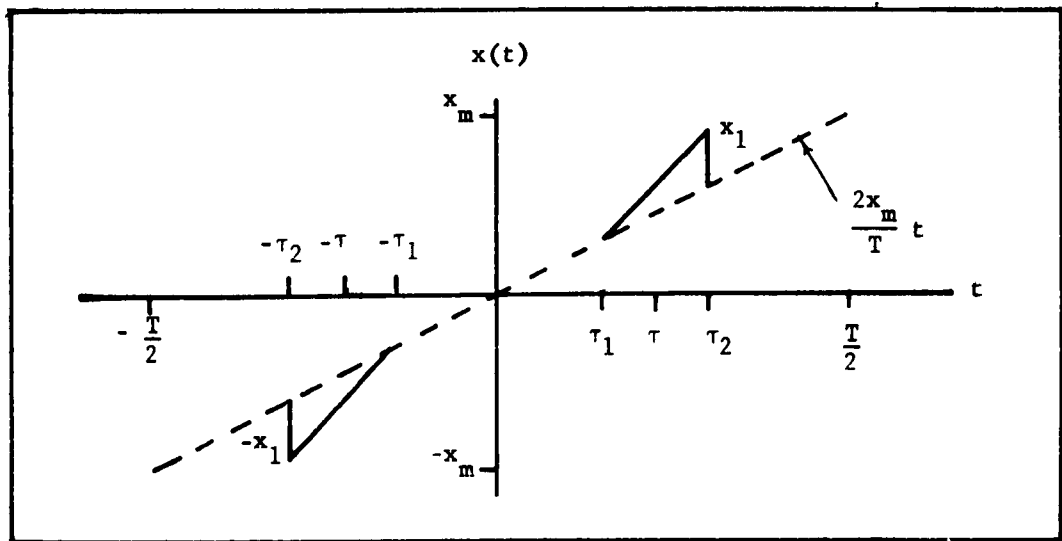
Fig. 22. Irregularities in the path difference variation on the intervals $(\tau_1 < t < \tau_2)$ and $(-\tau_2 < t < -\tau_1)$.

the period of the path difference curve is 2T and the irregularities shown are therefore supposed to recur with period 2T. The irregularity on the interval $(0 < t < \frac{T}{2})$ is a straight line segment limited to the interval $(\tau_1 < t < \tau_2)$. The equation of the straight line coincident with the segment (continuous line) in question is

$$x(t) = \left[\frac{2x_m}{T} + \frac{x_1}{\tau_2 - \tau_1}\right]t - \frac{\tau_1}{\tau_2 - \tau_1}x_1 \quad . \tag{4.35}$$

The midpoint of the segment is at

$$\tau = \frac{\tau_1 + \tau_2}{2} , \tag{4.36}$$

and the duration is the absolute value of

$$\tau_0 = \tau_2 - \tau_1 \quad . \tag{4.37}$$

The quantities τ_1 and τ_2 are regarded as always positive, while x_1 is positive for $t > 0$ when the segment lies above the usual path difference curve $\frac{2x_m}{T}$ t and is negative when it lies below. For $t < 0$, x_1 is positive when the segment lies below the curve $\frac{2x_m}{T}$ t. The calculations will be carried through for a segment lying on ($\tau_1 < t < \tau_2$). Then the results for a corresponding segment lying on (- $\tau_2 < t < \tau_1$) can be obtained by replacing τ, τ_0, τ_1, τ_2, and x_1 by - τ, - τ_0, - τ_1, - τ_2, and $-x_1$, respectively, in Eq. (4.35). With the definitions

$$v = \frac{2x_m}{T} , v_1 = \frac{x_1}{\tau_0} , \tag{4.38}$$

Eq. (4.35) becomes

$$x(t) = (v + v_1)t - \tau_1 v_1 .$$

Then

$$2\pi v x(t) = 2\pi f(1 + \frac{v_1}{v})(t - \frac{\tau_1}{1 + \frac{v}{v_1}})$$

$$= 2\pi\mu f(t + \epsilon) \qquad (4.39)$$

where

$$\mu = 1 + \frac{v_1}{v} \quad , \quad \epsilon = \frac{-\tau_1}{1 + v/v_1} \qquad (4.40)$$

The transmission function is to be zero outside the interval ($\tau_1 < t < \tau_2$) and may be expressed as

$$L_1(t,f') = \underset{|\tau_0|}{U} \quad (t - \tau) \cos 2\pi \mu f'(t + \epsilon). \qquad (4.41)$$

Because of the 2T periodicity it is necessary to go back to (3.26) and rewrite it for this case:

$$F_2(t) = F_1(t) * \sum_{q=-\infty}^{\infty} \delta(t - 2qT), \qquad (4.42)$$

where, according to Eq. (4.5),

$$F_1(t) = \int_{-\infty}^{\infty} P(f')L_1(t,f') \, df' . \qquad (4.5)$$

Then by Fourier transformation

$$P_2(f') = P_1(f') \cdot \frac{1}{2T} \sum_{q=-\infty}^{\infty} \delta(f' - \frac{q}{2T})$$

$$= \frac{1}{2T} \sum_{q=-\infty}^{\infty} P_1(\frac{q}{2T}) \delta(f' - \frac{q}{2T}) .$$

When this expression for $P_2(f')$ is inserted into Eq. (3.40), it is observed that a factor $\frac{1}{2}$ is introduced and that the spacing of the delta functions is $\frac{1}{2T}$ instead of $\frac{1}{T}$. If the bandpass v_0 is further

restricted so that $w_0 < \frac{1}{T}$, then the response function for this 2T periodicity is the same as if the irregularity were repeated with period T, except for the factor of $\frac{1}{2}$. The usual procedure can be used, then, to calculate the response function.

Since $L_1(t,f) = L_1(t,-f)$, it follows that

$$P_1(f',f) = F.T. \left[L_1(t,f) \right]$$

$$= |\tau_0| \left\{ \text{dif } \tau_0 f' \ e^{-2\pi i \tau f'} \right\} * \left\{ e^{2\pi i \epsilon f'} \ \frac{1}{2} \left[\delta(f' - \mu f) \right. \right.$$

$$\left. \left. + \delta(f' + \mu f) \right] \right\}$$

$$= \frac{|\tau_0|}{2} \ e^{2\pi i \epsilon \mu f} \ \text{dif} \left[\tau_0 (f' - \mu f) \right] \ e^{-2\pi i \tau (f' - \mu f)}$$

$$+ \frac{|\tau_0|}{2} \ e^{-2\pi i \epsilon \mu f} \ \text{dif} \left[\tau_0 (f' + \mu f) \right] \ e^{-2\pi i \tau (f' + \mu f)} .$$

By (4.9), since $P_1(f',f) \neq P_1(-f',f)$, the contribution to the response function is, when the factor $\frac{1}{2}$ mentioned above is inserted,

$$\Delta S(f,f_n) = \frac{|\tau_0|}{2T} \left\{ \cos 2\pi \left[(\tau + \epsilon)\mu f - \tau f_n \right] \text{dif } \tau_0 \mu (f - \frac{f_n}{\mu}) \right.$$

$$\left. + \cos 2\pi \left[(\tau + \epsilon) \mu f + \tau f_n \right] \text{dif } \tau_0 \mu (f + \frac{f_n}{\mu}) \right\} .$$

$$(4.43)$$

A useful special case of Eq. (4.43) is the contribution $\Delta S_0(f,f_n)$ to the signal associated with the time interval τ_0 centered about the point $t = \tau$ of each 2T period, with the usual

path difference $x(t) = \frac{2x_m}{T} t$. This result is obtained by setting $x_1 = 0$, which implies that $\epsilon = 0$ and $\mu = 1$, in Eq. (4.43). Then

$$\Delta S_0(f,f_n) \quad \frac{|\tau_0|}{2T} \left[\cos 2\pi \tau(f - f_n) \text{ dif } \tau_0(f - f_n) \right.$$

$$\left. + \cos 2\pi \tau(f + f_n) \text{ dif } \tau_0(f + f_n) \right] .$$

(4.44)

The total signal $S(f,f_n)$ in the presence of an irregularity of the type being considered arises from a transmission function of the form

$$U_T(t) \cos 2\pi ft - U_{|\tau_0|} (t - \tau) \cos 2\pi ft + U_{|\tau_0|} (t - \tau) \cos 2\pi \mu f(t+\epsilon).$$

Then

$$S(f,f_n) = S_0(f,f_n) - \Delta S_0(f,f_n) + \Delta S(f,f_n) ,$$

(4.45)

and the net contribution attributable to the departure from the idealized grating motion is

$$\Delta S(f,f_n) \quad - \Delta S_0(f,f_n) .$$

(4.46)

THE LAMELLAR GRATING

The lamellar grating with variable depth consists of two plane reflecting gratings arranged as in Figure 23 which is a cross section parallel to the plane of incidence. One grating remains fixed while the other moves parallel to n_o, the normal to the grating, producing
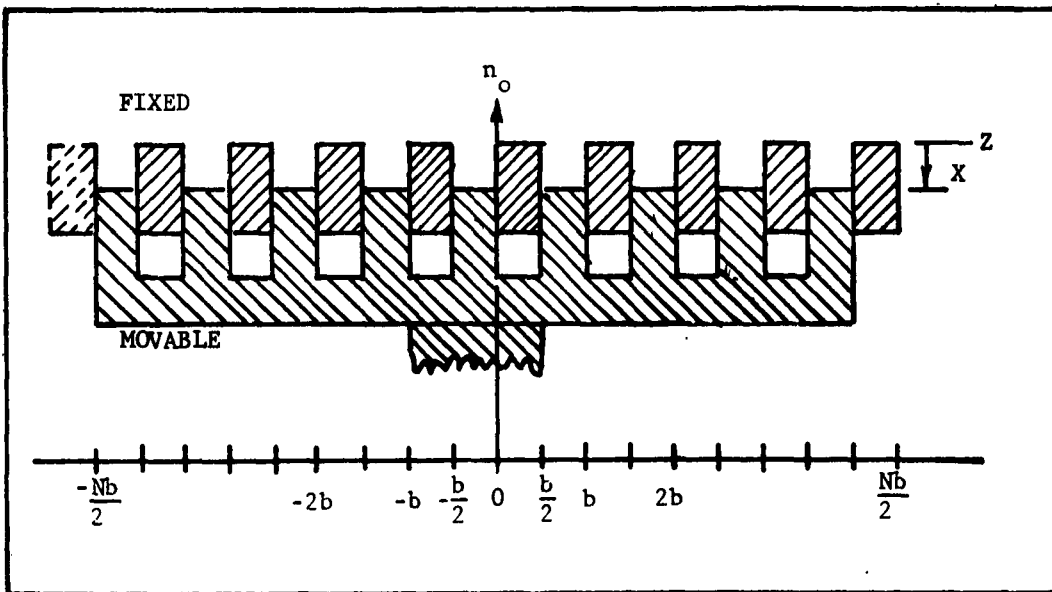
Fig. 23. A cross section of the lamellar grating.

a grating depth X, which is considered as positive when the movable grating lies below the fixed grating in the figure. Each facet has width b/2 and length ℓ , while each of the N complete periods of the

grating contains one facet of the movable and one facet of the fixed grating, so that the grating period is b. The total grating width is then Nb, excluding the extreme left facet, drawn with broken lines in the figure, to indicate that it is to be masked and does not affect the diffraction pattern.

The first grating that is to be used in the modulator has the following measurements:

b = 1 in.	Nb = 9 in.
N = 9	ℓ = 7 in.

A collimated beam is incident on the grating at an angle of about 10° with respect to n_0 and the diffracted radiation of most interest leaves the grating at an angle of about 10°. Under these conditions, polarization effects should be small.[1] The conditions for the validity of Kirchhoff's diffraction theory are[2]

a) size of aperture (single facet) $>>$ wavelength,

b) object and image distances $>>$ size of aperture.

Although the grating described is designed primarily for wavelengths less than 1mm, even for 2mm radiation the wavelength is about one sixth of the facet width of 1/2 inch, and the first condition is met reasonably well. The second condition is strictly fulfilled by the use

---

1. See e.g., M. Born and E. Wolf, Principles of Optics (Pergamon Press, New York, 1959), p. 388 and p. 614.

2. Ibid., p. 377.

of a collimated beam. In fact, this also allows use of the Fraunhofer approximation.[3]

Figure 24 shows a single period of the grating, on which is incident a parallel beam at angle α, with wave front $\overline{OA}$. The diffracted beam leaves the grating at angle β and has wave front
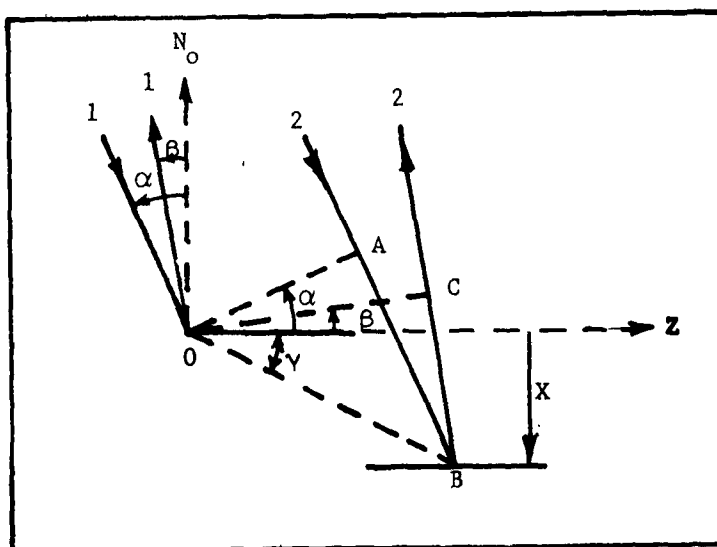
Fig. 24. Two adjacent facets of the lamellar grating showing the geometrical relationship of paths 1 and 2 with the facets.

$\overline{OC}$. Angles measured counterclockwise from n_0 are positive, while those measured clockwise are negative. The distance traversed in going from wave front $\overline{OA}$ to wave front $\overline{OC}$ along path 1 is zero, while that traversed along path 2 is

---

3. Ibid., p. 383.

$$x = \overline{AB} + \overline{BC}$$

$$= \overline{OB} \sin (\alpha + \gamma) + \overline{OB} \sin (\beta + \gamma)$$

$$= \overline{OB} \quad \sin \alpha \cos \gamma + \cos \alpha \sin \gamma + \sin \beta \cos \gamma + \cos \beta \sin \gamma$$

$$= z \sin \alpha + X \cos \alpha + z \sin \beta + X \cos \beta$$

$$= z (\sin \alpha + \sin \beta) + X (\cos \alpha + \cos \beta). \qquad (5.1)$$

This is the optical path for the movable grating. For the fixed grating, $X = 0$ and the optical path is

$$x = z(\sin \alpha + \sin \beta). \qquad (5.2)$$

The difference in path for the two gratings is then $X(\cos \alpha + \cos \beta)$. In particular, for radiation in zeroth order, $\beta = -\alpha$ and the path difference becomes

$$2 X \cos \alpha . \qquad (5.3)$$

Since the incident radiation is a uniform parallel beam, it may be represented by the complex scalar wave function

$$e^{i(\omega t - 2\pi \nu \zeta)}$$

where ν is the wave number, ζ is a coordinate along the direction of the beam, and ω is the angular frequency of the wave. For any plane grating, the part of the optical path

$$z(\sin \alpha + \sin \beta)$$

applies to all points of the grating. The wave diffracted from position z of the grating is then of the form

$$e^{i(\omega t - 2\pi \nu \zeta)} \quad e^{-2\pi i z \nu (\sin \alpha + \sin \beta)} .$$

If the grating causes an additional amplitude or phase variation in the diffracted wave, as a function of z, this property can be described by a transmission function $T(z)$, characteristic of the grating. The wave diffracted at z in direction β is then represented by

$$T(z)\; e^{i(\omega t - 2\pi\nu\zeta)}\; e^{-2\pi i z\nu(\sin\alpha + \sin\beta)} .$$

All the waves diffracted in direction β are superimposed in the focal plane of the telescope, giving a resultant wave function

$$A = A_0\; e^{i(\omega t - 2\pi\nu\zeta)} ,$$

where

$$A_0 = \int_{-\infty}^{\infty} T(z)\; e^{-2\pi i z\nu(\sin\alpha + \sin\beta)}\; dz .$$

Since the time average of the intensity associated with this wave function is proportional to

$$AA^* = A_0 A_0^* , \tag{5.4}$$

the interest lies in the quantity A_0.

Setting

$$y = \nu(\sin\alpha + \sin\beta) \tag{5.5}$$

yields

$$A_0(y) = \int_{-\infty}^{\infty} T(z)\; e^{-2\pi i y z}\; dz = F.T. \left[T(z) \right] . \tag{5.6}$$

The complex periodic function $T(z)$ can be expressed in terms of the period b of the grating, the total width Nb, and the transmission

function $G(z)$ of a single period:

$$T(z) = G(z) * \left\{ \left[\sum_{q=-\infty}^{\infty} \delta(z - bq) \right] \cdot U_{Nb}(z) \right\} \tag{5.7}$$

for N odd.

Then by Fourier transformation,

$$A_0(y) = \text{F.T.} \left[G(z) \right] \cdot \left\{ \left[\frac{1}{b} \sum_{q=-\infty}^{\infty} \delta(y - \frac{q}{b}) \right] * Nb \text{ dif } Nby \right\}$$

$$= \text{F.T.} \left[G(z) \right] \cdot \frac{N \text{ dif } N b y}{\text{dif } b y} \tag{5.8}$$

This is the amplitude distribution function for any plane grating used with collimated radiation. If "shadowing" of some facets by others is neglected, this expression is also valid for a lamellar grating.

For the lamellar grating, according to Eq. (5.1) and (5.2), the additional phase factor produced by the movable grating is

$$e^{-i\gamma_0} \tag{5.9}$$

in which

$$\gamma_0 = 2\pi \nu X(\cos\alpha + \cos\beta). \tag{5.10}$$

The first grating produces no additional phase factor, and all facets are assumed to be perfectly reflecting. So, for a complete period consisting of one facet of each grating,

$$G(z) = e^{-i\gamma_0} \qquad (-\frac{b}{2} < z < 0)$$

$$= 1 \qquad (0 < z < b/2) .$$

That is,

$$G(z) = \delta\left(z - \frac{b}{4}\right) * U_{\frac{b}{2}}(z) + e^{-i\gamma_0}\left[\delta\left(z + \frac{b}{4}\right) * U_{\frac{b}{2}}(z)\right]$$

$$= \left[\delta\left(z - \frac{b}{4}\right) + e^{-i\gamma_0}\,\delta\left(z + \frac{b}{4}\right)\right] * U_{\frac{b}{2}}(z) \tag{5.11}$$

and

$$\text{F.T.}\left[G(z)\right] = \left[e^{-2\pi i\frac{b}{4}y} + e^{-i\gamma_0 + 2\pi i\frac{b}{4}y}\right] \cdot \frac{b}{2}\,\text{dif}\,\frac{b}{2}\,y \,. \tag{5.12}$$

According to Eq. (5.8), then, the quantity $A_0(y)$ for the whole grating is

$$A_0(y) = \frac{N\,\text{dif}\,N\,by}{\text{dif}\,by} \cdot \frac{b}{2}\,\text{dif}\,\frac{b}{2}\,y \cdot \left[e^{-\pi i\frac{b}{2}y} + e^{-i\gamma_0 + \pi i\frac{b}{2}y}\right] \,. \tag{5.13}$$

The time average of the intensity is proportional to

$$A_0 A_0^{\,*} = \left[N\,b\,\text{dif}\,\frac{b}{2}\,y \cdot \frac{\text{dif}\,N\,by}{\text{dif}\,by}\right]^2 \frac{1 + \cos(\pi\,by - \gamma_0)}{2} \,, \tag{5.14}$$

where

$$y = \nu(\sin\alpha + \sin\beta) \tag{5.5}$$

$$\gamma_0 = 2\pi\,\nu\,X(\cos\alpha + \cos\beta) \,. \tag{5.10}$$

For purposes of normalization, it is assumed that, for radiation of wave number ν and angle of incidence α, unit intensity (average power per unit width) is incident on the whole grating. Then the average incident power is Nb. If no radiation is absorbed by the grating, then

$$\int_{y_1}^{y_2} A_o A_o^* \, dy = Nb \, , \tag{5.15}$$

in which the limits of integration are determined by the value of y for which sin β ± 1.

At "mirror position", when X = 0, Eq. (5.14) reduces to

$$A_o A_o^* = (N \, b)^2 \, dif^2 \, N \, by \, , \tag{5.16}$$

and

$$\int_{y_1}^{y_2} A_o A_o^* \, dy = Nb \int_{y_1}^{y_2} N \, b \, dif^2 \, N \, by \, dy \, . \tag{5.17}$$

The standard integral

$$\int_{-\infty}^{\infty} N \, b \, dif^2 \, N \, by \, dy = 1 \tag{5.18}$$

is a very close approximation to the integral in Eq. (5.17) as long as

$$y_1 = \nu \, (\sin\alpha + 1) >> \frac{1}{Nb}$$

and

$$\left|y_2\right| = \left|\nu \, (\sin\alpha - 1)\right| >> \frac{1}{Nb}$$

or

$$\frac{1}{Nb\nu} = \frac{\lambda}{Nb} << \left|\sin\alpha \pm 1\right| \, ,$$

or

$$\frac{\lambda}{Nb} << 1 \quad \text{and} \quad \left|\sin\alpha\right| << 1 \, . \tag{5.19}$$

These conditions are fulfilled in practice. For example, for

Nb = 22.86 cm, λ = 4.5 cm, and sin $\alpha \doteq$ 0,

$$\left| y_1 \right| \doteq \left| y_2 \right| \doteq \frac{5}{Nb} \, ,$$

and

$$\int_{y_1}^{y_2} N \, b \, dif^2 \, N \, by \, dy \doteq .982$$

Equation (5.15) thus holds very nearly exactly, and equation (5.14) can be written

$$\frac{A_o A_o^*}{Nb} = \frac{Nb}{2} \left[dif \, \frac{b}{2} \, y \cdot \frac{dif \, N \, by}{dif \, bt} \right]^2 \left[1 + \cos(\pi by - \gamma_o) \right] ,$$
$$(5.20)$$

where

$$\int_{y_1}^{y_2} \frac{A_o A_o^*}{Nb} \, dy \doteq 1 . \qquad (5.21)$$

In Eq. (5.20) the expression

$$D(y) = \frac{Nb}{2} \left[dif \, \frac{b}{2} \, y \cdot \frac{dif \, N \, by}{dif \, by} \right]^2 \qquad (5.22)$$

represents the intensity distribution for a plane grating having period b and facet width b/2, exhibiting the characteristic absence of even orders other than the zeroth. The graph of this function appears in Figure 25(a). The other factor in Eq. (5.20),

$$1 + \cos 2 \pi \left[\frac{by}{2} \, (\sin \alpha + \sin \beta) - \nu X (\cos \alpha + \cos \beta) \right] ,$$
$$(5.23)$$

(a)

$$D(y) = \frac{Nb}{2} \, \text{dif}^2 \, \frac{by}{2} \cdot \frac{\text{dif}^2 \, Nby}{\text{dif}^2 by}$$

$\frac{Nb}{2}$ ——

−3   −1   0   +1   +3

INTERFERENCE
ORDERS

$\frac{Nb}{2} \, \text{dif}^2 \, \frac{by}{2}$

$-\frac{4}{b}$ $-\frac{3}{b}$ $-\frac{2}{b}$ $-\frac{1}{b}$ 0 $\frac{1}{b}$ $\frac{2}{b}$ $\frac{3}{b}$ $\frac{4}{b}$ y

$\frac{1}{Nb}$

(b)

$$1 + \cos \, (\pi by - \gamma_o)$$

$(\gamma_o = 0)$
$(X = 0)$

1 ◄

$-\frac{1}{b}$ 0 $\frac{1}{b}$ y

(c)

$(\gamma_o = \frac{\pi}{2})$

$$1 + \cos \, (\pi by - \gamma_o)$$

$(X = \frac{\lambda}{4(\cos\alpha + \cos\beta)} \doteq \frac{\lambda}{8})$

$-\frac{1}{b}$ 0 $\frac{1}{b}$ y
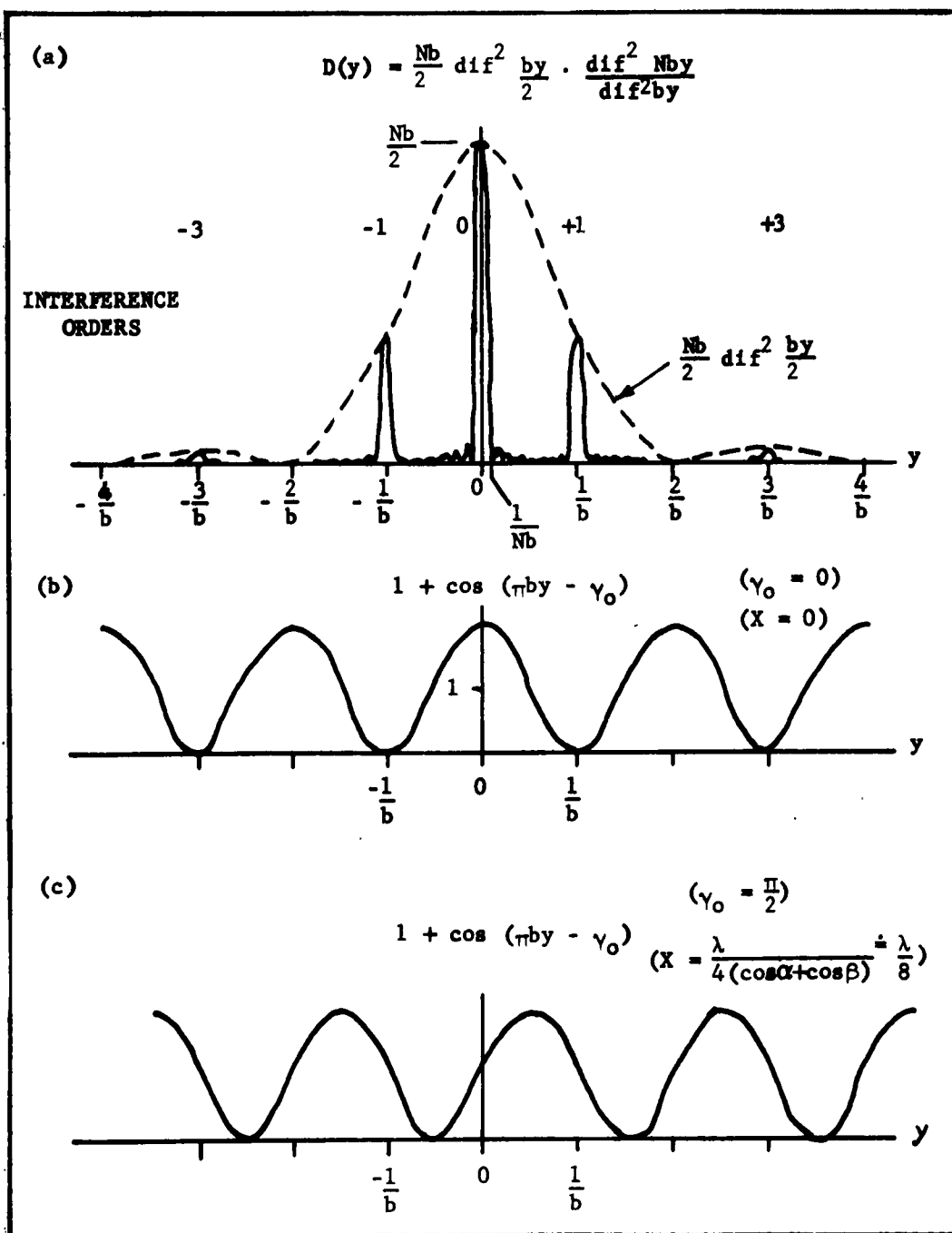
Fig. 25. A sketch of the diffraction pattern for a lamellar grating.
(a) D(y), the diffraction pattern for a single plane grating having
period b, fact width b/2 and N facets. (b) The factor by which D(y)
must be multiplied to take into account the interaction of the two
gratings. $\gamma_o = 0$. (c) The same factor for $\gamma_o = \pi/2$, $X \doteq \lambda/8$.

describes the interaction of the two gratings. It is a periodic
function of the grating depth X, for fixed values of ν, α and β.
It is very nearly a periodic function of y for fixed ν and X. When
X = 0, this is a true periodicity, as illustrated in Figure 25(b).
For successive values of X, the resultant diffraction pattern is
obtained sufficiently exactly by translating the cosine curve of
Figure 25(b) along y and multiplying it by D(y). Thus the diffracted
power passes back and forth between the zeroth order and the odd
orders of the grating as X is varied, i.e. the zeroth order power
is 180° out of phase with the odd order power.

Let X be a periodic function of time as in the one-sided mode
of operation, such that

$$x(t) = \frac{2X_m}{T} \left| t \right| . \qquad (-\frac{T}{2} < t < \frac{T}{2}). \qquad (5.24)$$

Then the time-varying part of $A_0 A_0^* / Nb$ becomes

$$U_T(t) \cdot D(y) \cos \left[2\pi \frac{2X_m}{T} (\cos \alpha + \cos \beta) \nu \left| t \right| - \pi by \right].$$

This is the transmission function for the lamellar grating for radia-
tion of wave number ν, incident at angle α and diffracted at angle β.
For fixed α it may be written

$$\frac{1}{2} L_\beta (t,f) = U_T(t) \cdot D(y) \cdot \cos 2\pi f (\left| t \right| + \tau) , \qquad (5.25)$$

where

$$f = \frac{2X_m \nu}{T} (\cos \alpha + \cos \beta) \qquad (5.26)$$

$$\epsilon = -\frac{\sin\alpha + \sin\beta}{\cos\alpha + \cos\beta} \frac{b \, T}{4X_m} \qquad (5.27)$$

$$y = \nu(\sin\alpha + \sin\beta) . \qquad (5.5)$$

For a given ν, the modulation frequency f varies by a very small amount under the maximum variation of both α and β permitted by normal slit widths. For example, with 20mm slits, and 100 cm focal lengths, and $\alpha = 10^\circ$,

$$\frac{\Delta f}{f} = \frac{\Delta(\cos\alpha + \cos\beta)}{\cos\alpha + \cos\beta} \doteq \sin\alpha \, \Delta\alpha \doteq 1.5 \times 10^{-3} .$$

This[4] corresponds to a negligibly small variation in $S(f, f_n)$. Therefore, it is reasonable to set

$$f = \frac{4X_m \, \nu \cos\alpha}{T} = \frac{2x_m \, \nu}{T} , \qquad (5.28)$$

as in Eq. (3.52). On the other hand, the relative phase $2\pi \epsilon f = -\pi$ by of the modulation is seen to vary continuously and linearly with y. In Figure 26 the function $\frac{1}{2} L_\beta (t, f)$ is plotted versus y, versus $(\sin\alpha + \sin\beta)$ and versus $(\sin\alpha + \sin\beta) \bar{F}$, which corresponds to transverse displacements in the plane of the exit slit if $\bar{F}$ is the telescope focal length. In this graph, t is chosen to be zero.

---

4. The same calculation gives the range of wave numbers leaving the exit slit and having the same modulation frequency. That is,

$$\frac{\Delta\nu}{\nu} = \frac{\Delta\lambda}{\lambda} = \frac{\Delta(\cos\alpha + \cos\beta)}{\cos\alpha + \cos\beta} ,$$

corresponding to a passband which is small compared with either the modulator or monochromator passbands.
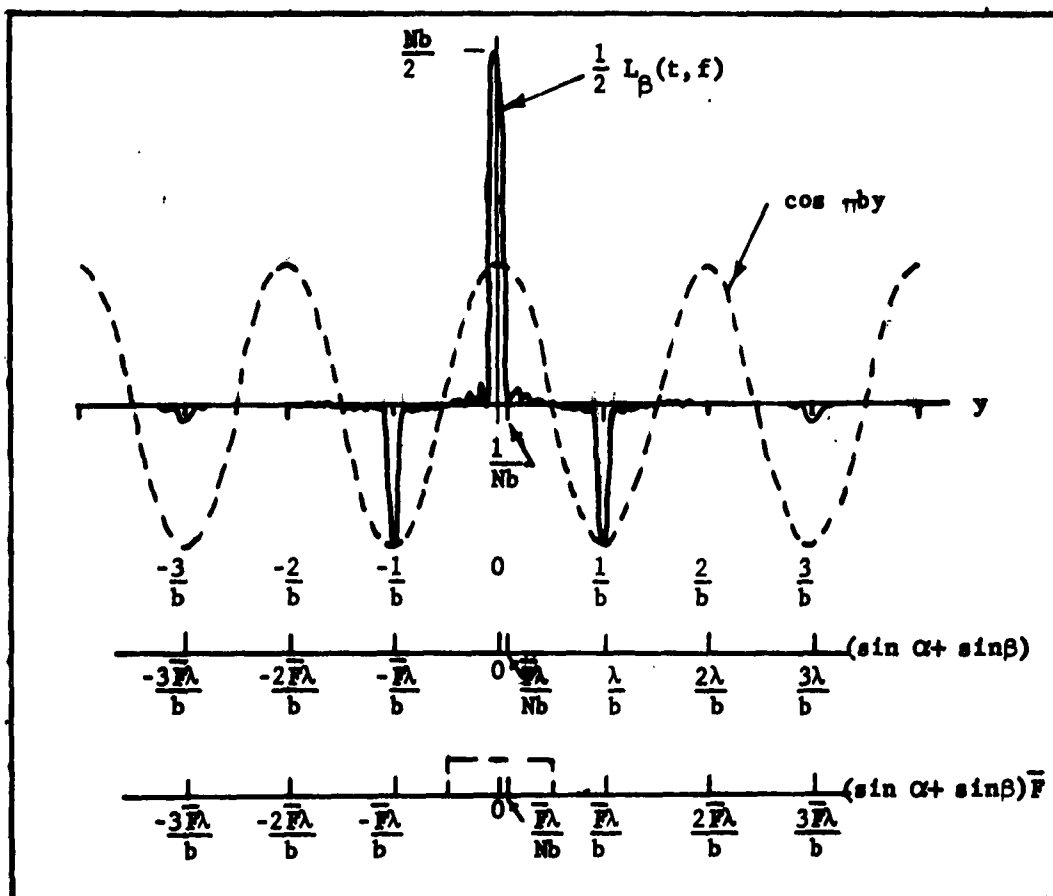
Fig. 26. A sketch of the time-varying part of the lamellar grating diffraction pattern for grating depth varying linearly in time, pictured at time t = 0. Three different abscissa variables of interest are shown. The dotted rectangle on the lower abscissa scale represents the image of the entrance slit in the plane of the exit slit, for the entrance slit width $\bar{F}\,y_b$.

The dotted rectangle on the abscissa labelled $(\sin\alpha + \sin\beta)\bar{F}$ corresponds to the approximate slit widths envisioned; i.e. of the order of $\frac{\bar{F}\lambda}{b}$. Hence the variation of phase across the exit slit

is appreciable. A response function $S_\beta(f,f_n)$ can be calculated from Eq. (5.25), noting that f and α are considered as parameters,

and y and ϵ as functions of β. Since Eq. (5.25) has the same form as Eq. (4.17), the results (4.24) and (4.33) apply directly. For two-sided operation with n = 13, Eq. (4.33) yields

$$S_\beta(f,f_n) = 2D(y)(\cos \pi by)S_0(f,f_n).$$

The sum of the contributions for all values of β is

$$S(f,f_n) = 2 \int_{y_3}^{y_4} S_\beta(f,f_n)dy = S_0(f,f_n)\left[2 \int_{y_3}^{y_4} D(y) \cos \pi by\, dy\right] , \tag{5.29}$$

in which the limits of integration depend on the relationship of the exit slit width to the wavelength and on α. The dependence of the integral on f comes about by this dependence of y_3 and y_4 on λ. For example, suppose that the exit slit width is set equal to

$$2(\sin \alpha + \sin \beta)\, \overline{F} = \frac{\overline{F}\lambda_n}{b} .$$

Then, for the value of α corresponding to the center of the entrance slit,

$$y_4 = -y_3 = \frac{\nu}{\overline{F}} (\sin \alpha + \sin \beta)\, \overline{F} = \frac{1}{2b}\frac{\nu}{\nu_n} = \frac{1}{2b}\frac{f}{f_n} . \tag{5.30}$$

To evaluate the integral in Eq. (5.29) the integrand can be written

$$D(y) \cos \pi by = \frac{Nb}{2} (\text{dif}^2 N by)(1 - \tan^2 \frac{\pi by}{2}) .$$

The integral becomes

$$\frac{e_1}{2} = \frac{1}{2} \int_{y_3}^{y_4} Nb\, \text{dif}^2 N by\, dy - \frac{1}{2} \int_{y_3}^{y_4} Nb\, \text{dif}^2 Nby\, \tan^2 \frac{\pi by}{2}\, dy , \tag{5.31}$$

which, by virtue of Eq. (5.18), is seen to consist of a term slightly less than 1/2, from which is subtracted a very small term. The factor of 1/2 reflects the fact that ideal modulation yields a modulation amplitude of only half the incident power. The fraction of the ideal modulation amplitude is then given by the quantity e_1. The limits of integration y_3 and y_4 also take into account the fact that the feet of $D(y)$ falling outside the limits imposed by the exit slit represent wasted power. This effect would be present even if the lamellar grating were replaced by a flat mirror of the same size. For a typical slit width such as that shown in Figure 25, twice the first integral of Eq. (5.31) is about 0.98, while twice the second integral is about 0.02, giving an efficiency of about 0.96. For longer wavelengths and narrower slits, the slit width limitation becomes dominant. With a slit of width $\frac{1}{2} \frac{\overline{F}\lambda}{b}$ the value of e_1 is approximately 0.94, while a slit width $\frac{1}{10} \frac{\overline{F}\lambda}{b}$ gives an efficiency of about 0.89. These efficiencies are nearly the same for all values of α allowed by the entrance slit, except those for which the central interference maximum falls near the exit slit edge, and these efficiencies may, therefore, be taken as approximately characteristic of all the radiation of a given wave number leaving the exit slit at a given instant.

By virtue of Eqs. (5.29), (5.30) and (5.31), the response function $S(f,f_n)$ obtained by taking into account these diffraction effects can now be written

$$S(f,f_n) = e_1(^f/f_n) \ S_0(f,f_n) \ . \tag{5.32}$$

Under the usual conditions of operation, the slits are set at approximately $\frac{\bar{F} \lambda_n}{b}$, so that in the neighborhood of the peak response the appropriate efficiency factor is probably not less than 0.96. The value of $e_1(\frac{f}{f_n})$ could be calculated for all values of f. It can be seen in Figure 26 that extending the integration to larger values of y would include the contributions of the odd lamellar grating orders, which are all modulated 180° out of phase with the zero order, and thus reduce $e_1(\frac{f}{f_n})$ substantially. But the overlapping of the lamellar grating orders due to the use of finite slit widths must now be taken into account and it is convenient to do the calculations in the more approximate way described in the next chapter.

SLIT CONSIDERATIONS

Modulation efficiencies for wavelengths less than λ_n

The reason for the choice of the value $\dfrac{\bar{F} \lambda_n}{b}$ for the modulator

slit widths becomes apparent upon consulting Figure 27, in which

$\dfrac{2}{Nb} D(y) \cos \pi$ by is reproduced as a broken curve along with rectangles

representing the images of the modulator entrance slit formed in the

plane of the exit slit by the different lamellar grating interference

orders. The area under a rectangle gives the relative modulated

power for a given lamellar grating order. That is, the ordinate is

relative modulated intensity (modulated power per unit slit width

relative to the zeroth order value) and the abscissa is the coordinate
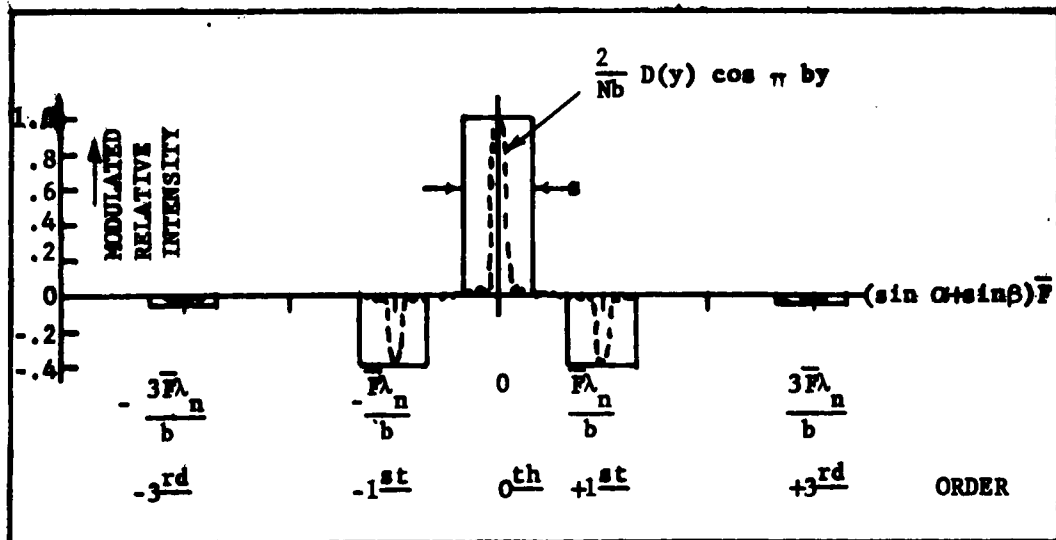
Fig. 27. Images of the modulator entrance slit formed in the plane
of the modulator exit slit by the various lamellar grating orders.
The broken line curve is $\dfrac{2}{Nb} D(y) \cos \pi$ by.

in the plane of the exit slit. A negative ordinate corresponds to out-of-phase or <u>counter-modulated</u> relative intensity. If the entrance slit width s and the exit slit width s_3 are made equal, $\dfrac{\overline{F}\,\lambda_n}{b}$ is the width for which the zeroth and $\pm$ 1st orders begin to overlap and for which s_3 begins to pass the $\pm$ 1st orders. When the modulator is used with a grating monochromator the wavelengths of most interest are $\dfrac{\lambda_n}{p}$ with corresponding modulation frequencies pf_n, where $p = 1,2,3,\ldots,$ and the slits are set at approximately $\dfrac{\overline{F}\lambda_n}{b}$. An approximation for the efficiency factor $e_1\!\left(\dfrac{f}{f_n}\right)$ for these frequencies can be obtained by simply subtracting the amount of counter-modulated odd order radiation leaving the exit slit from the amount of zero order radiation allowed through. The relative heights of lamellar grating orders $0, \pm 1, \pm 3, \pm 5$ are $1.00, .405, .045, .015$, respectively. Figure 28 illustrates the case $\lambda = \dfrac{\lambda_n}{2}$. The net power modulated in phase with
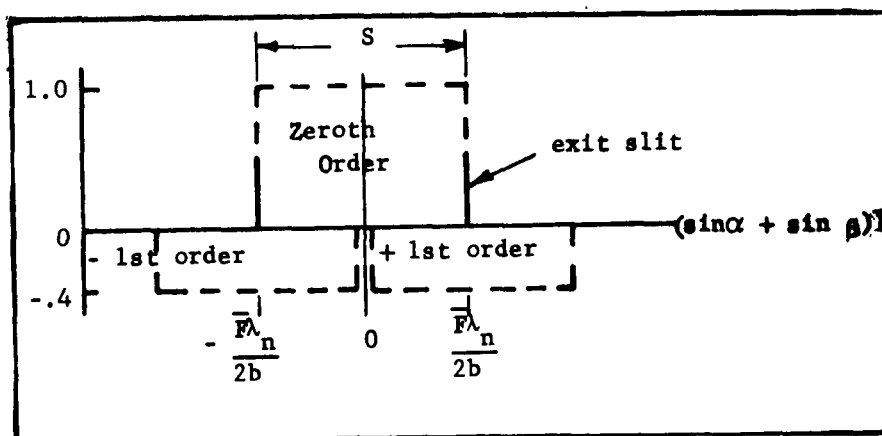
Fig. 28. Overlapping images of the entrance slit formed at the exit slit by first order and zeroth order of the lamellar grating for radiation of wavelength $\dfrac{\lambda_n}{2}$ when all slit widths are $\dfrac{\overline{F}\,\lambda_n}{b}$.

the rectifier is apparently proportional to $1.00 - .40 = 0.60$.

Table 1 gives some values of $e_1(\frac{f}{f_n})$ calculated in this way.

TABLE 1

The efficiency factor $e_1(\frac{f}{f_n})$ for
wavelengths corresponding to the
spectrometer grating orders

λ	f/f_n	$e_1(\frac{f}{f_n})$	λ	$\frac{f}{f_n}$	$e_1(f/f_n)$
λ_n	1	1.00	$\frac{\lambda_n}{6}$	6	0.29
$\frac{\lambda_n}{2}$	2	0.60	$\frac{\lambda_n}{7}$	7	0.26
$\frac{\lambda_n}{3}$	3	0.47	$\frac{\lambda_n}{8}$	8	0.24
$\frac{\lambda_n}{4}$	4	0.38	$\frac{\lambda_n}{9}$	9	0.22
$\frac{\lambda_n}{5}$	5	0.32	$\frac{\lambda_n}{10}$	10	0.20

Optimum slit widths for use with grating monochromator

In the following discussion the focal lengths of the modulator optics and the monochromator optics will be assumed to be equal. Suppose that the modulator is placed at the exit slit of the monochromator and the detector then follows the modulator.

Three slits are needed: the monochromator entrance slit, the modulator exit slit, and the common slit which serves as monochromator exit slit and modulator entrance slit. For maximum power transfer coupled with minimum spectral slit width, the monochromator slit widths should have the same value, s. Throughout this analysis s and s_3 will be assumed to be equal. In this case, neglecting the modulator for the moment, the output radiant flux is proportional to the product of s and the spectral passband, which itself is proportional to s. That is,

$$\Phi = K\ s^2\ ,$$

<div align="right">(6.1)</div>

and the flux for slit width s relative to the flux Φ_0 for some initial slit width s_0 is

$$\frac{\Phi}{\Phi_0} = \frac{s}{s_0}^2\ .$$

<div align="right">(6.2)</div>

The modulator exit slit s_3 does not affect the spectral passband but it does form the effective actual slit width of the system whenever it is less than s. Upper bounds on s and s_3 are set by the occurrence of overlapping lamellar grating orders. Quantitative relationships can be inferred from Figure 29. It is convenient to set

$$s_0 = \frac{\overline{F}\lambda\ n}{b}\ .$$

<div align="right">(6.3)</div>

Again relative modulated intensity is plotted versus $(\sin\alpha + \sin\beta)\ \overline{F}$. The condition for no counter-modulated power passing s_3 is seen from
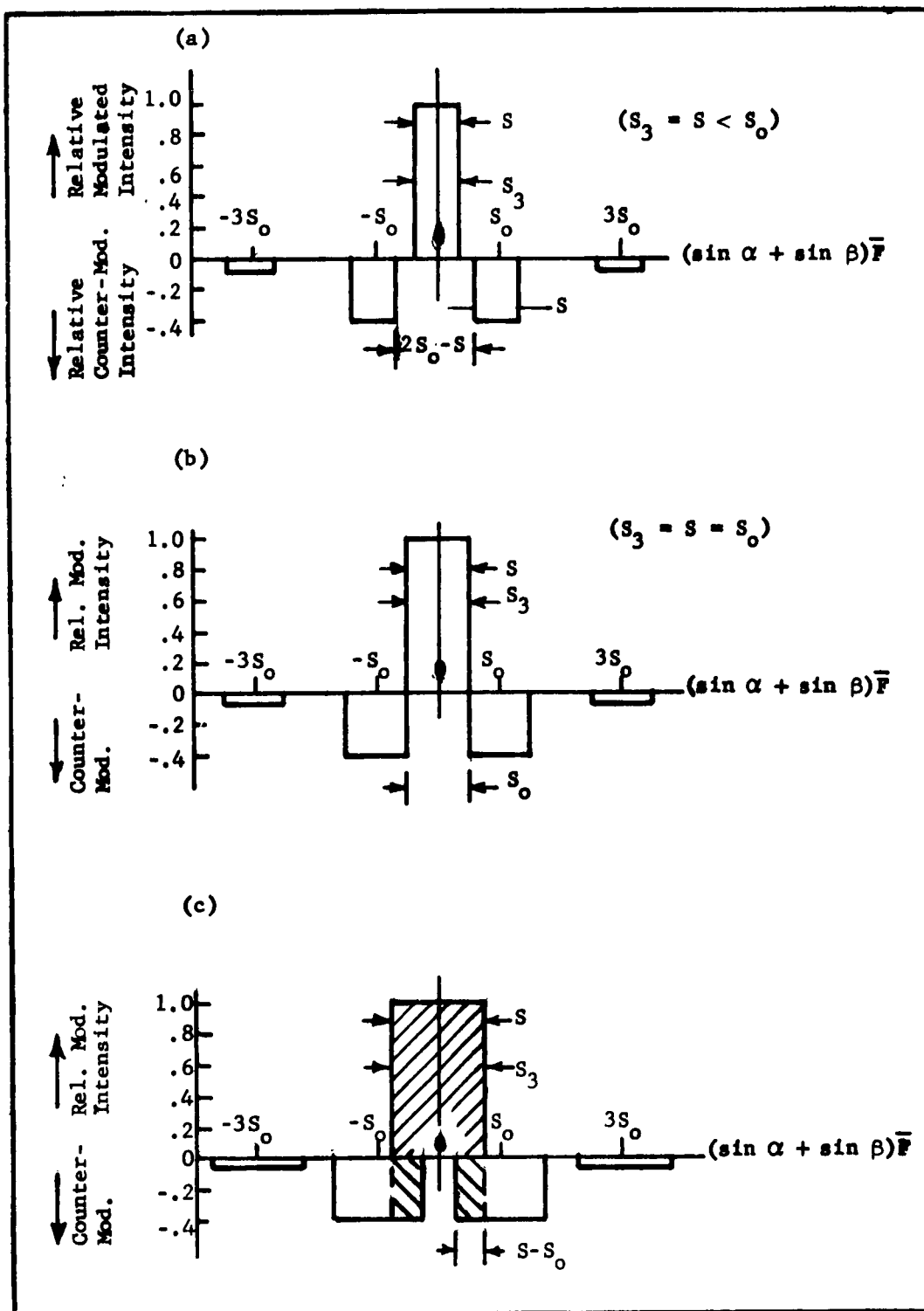
Fig. 29   Diagrams for making radiant flux calculations.

Figure 29(a) to be

$$s + s_3 \leq 2 \, s_o \, , \tag{6.4}$$

which reduces to

$$s = s_3 < s_o \tag{6.5}$$

when $s = s_3$, as shown in Figure 29(b).

The flux leaving s_3 will now be calculated for different conditions of interest. First suppose $s_3 = s$ and that they are increased from zero. The flux from the spectrometer increases as in Eq. (6.1); i.e., both the actual slit width and the spectral passband increase. For $s < s_o$ the flux leaving s_3 is given by the same expression. For $s > s_o$ counter-modulated power leaves s_3. The flux leaving s_3 relative to that when $s = s_3 = s_o$ is

$$\frac{\Phi}{\Phi_o} = \left(\frac{s}{s_o} \right)^2 \qquad (o < s < s_o) \tag{6.6}$$

$$= 0.2 \left(\frac{s}{s_o} \right)^2 + 0.8 \left(\frac{s}{s_o} \right) \quad (s_o < s < 3s_o) \tag{6.7}$$

Equation (6.6) is apparent from Figure 29(a) , while Eq. (6.7) is easily derived by use of Figure 29(c). The cross-hatched area below the axis must be subtracted from that above the axis to yield the net modulated power.

Next let s_3 be fixed at the value s_o and allow s to vary. For $s < s_o$ Eq. (6.1) applies. For $s > s_o$, only the spectral passband changes, the effective slit width remains s_o, and counter-modulated

power passes. The relative flux is, for $S = S_o$,

$$\frac{\phi}{\phi_o} = \left(\frac{s}{s_o}\right)^2 \qquad (0 < s < s_o) \qquad\qquad (6.8)$$

$$= 1.4\left(\frac{s}{s_o}\right)^2 - 0.4\left(\frac{s}{s_o}\right) \qquad (s_o < s < 3s_o). \qquad (6.9)$$

Finally, let s be fixed at the value s_o and vary s_3. The pass-band does not change. When $s_3 < s_o$, the flux is $K s_o s_3$. When $s_3 > s_o$, there is reduction of the net modulated power by counter-modulation. The relative flux is

$$\frac{\phi}{\phi_o} = \frac{s_3}{s_o} \qquad (0 < s_3 < s_o) \qquad\qquad (6.10)$$

$$= 1.4 - 0.4\left(\frac{s_3}{s_o}\right) \qquad (s_o < s_3 < 3s_o) . \qquad (6.11)$$

The results (6.6) through (6.11) are displayed in Figure 30. For comparison, Eq. (6.2), corresponding to the variation of s and s_3 together without the counter-modulation effect, is plotted also in the figure.
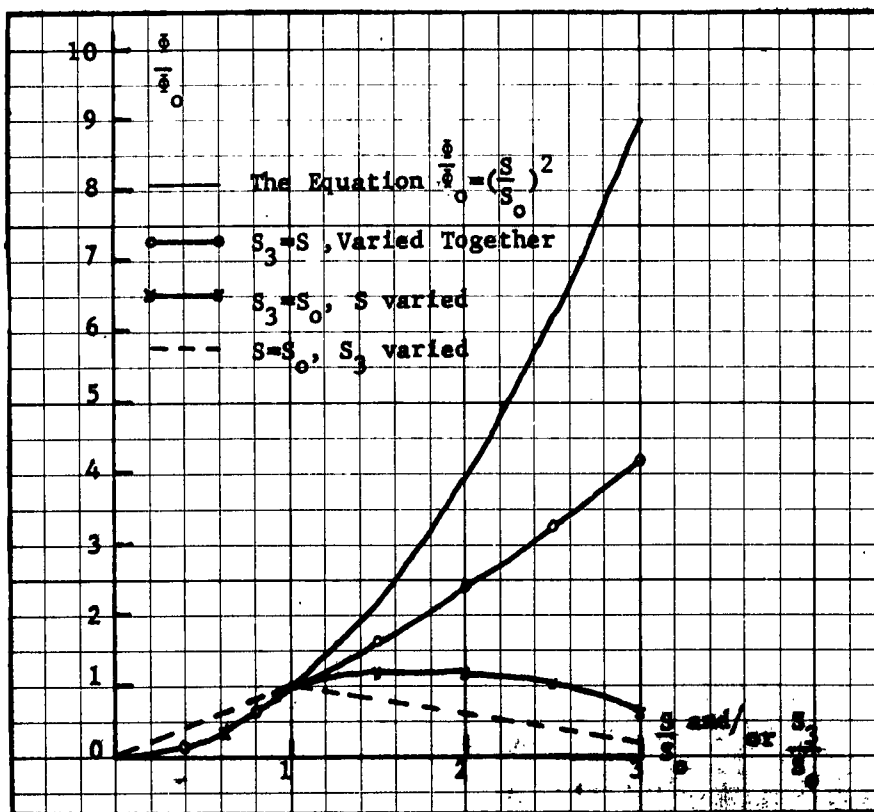
Fig. 30. The relative flux leaving the modulator exit
slit under various conditions explained in the text.

CHAPTER VII

DESCRIPTION AND MECHANICAL ALIGNMENT PROCEDURE

The optical plan and mechanical arrangement of the inter-
ferometric modulator appear in Figure 31. The lamellar grating
is irradiated by means of a standard Czerny-Turner arrangement
having an aperture ratio of approximately 4. The precise, adjust-
able, reciprocating motion required of the movable part G_2 of the
grating is obtained from the drive unit, indicated schematically
by the dashed enclosure in the figure, followed by a reduction
provided by the ratio bar R_2 pivoted at P. A cam within the drive
unit turns at constant speed, causing the cam follower to recip-
rocate with amplitude C_0 along the line AA making angle θ_n with the
transverse reference line shown. A component $C_0 \sin \theta_n$ of this
amplitude of motion is communicated to the drive rod R_1, which is
maintained parallel to the grating R_3. The coupling between R_1 and
R_2 is such that R_2 can slide lengthwise through the coupling unit
and can also rotate with respect to R_1. The coupling between R_2 and
R_3 is identical. With this arrangement, the displacement of R_1 and
that of R_3 form corresponding sides of similar triangles, so that
these displacements are proportional. The centers of R_1 and R_3 are
separated by a fixed distance l, while the perpendicular distance
B from P to the center of R_3 is adjustable. For a given setting of

94

Fig. 31. Optical and mechanical plan of interferometric modulator.

B, then, the reduction ratio is

$$\frac{B}{\ell + B} .$$

The amplitude of motion of the movable part of the grating is then

$$X_m = \frac{B}{\ell + B} (C_o \sin \theta_n), \qquad (7.1)$$

supposing the cam follower displacement to be zero at "mirror position" of the grating. For a given value of B, the maximum grating depth X_m can be varied continuously, at a rate which is slow relative to the reciprocating motion, by changing θ_n.

The photographs of Figure 32 show three views of the complete instrument, which is evacuable when the sides and top panels of its vacuum tank are set in place. The entire unit is portable and can be connected by means of bellows couplings to other similar vacuum tanks containing source or detector optics, a monochromator, or other optical components.

Modulator coupled with grating monochromator

This instrument is designed primarily to be used with the grating monochromator. The arrangement is depicted schematically in Figure 5 if the monochromator is inserted between source and modulator. Unless it is specified otherwise, the following discussion will refer to two-sided operation, defined previously. In this case, the cam follower has maximum displacement C_o on each side of its position of zero displacement corresponding to zero grating depth.

According to Eq. (5.3), the path difference corresponding to the grating depth in Eq. (7.1) must be

$$x_m = 2X_m \cos \alpha \qquad (7.2)$$
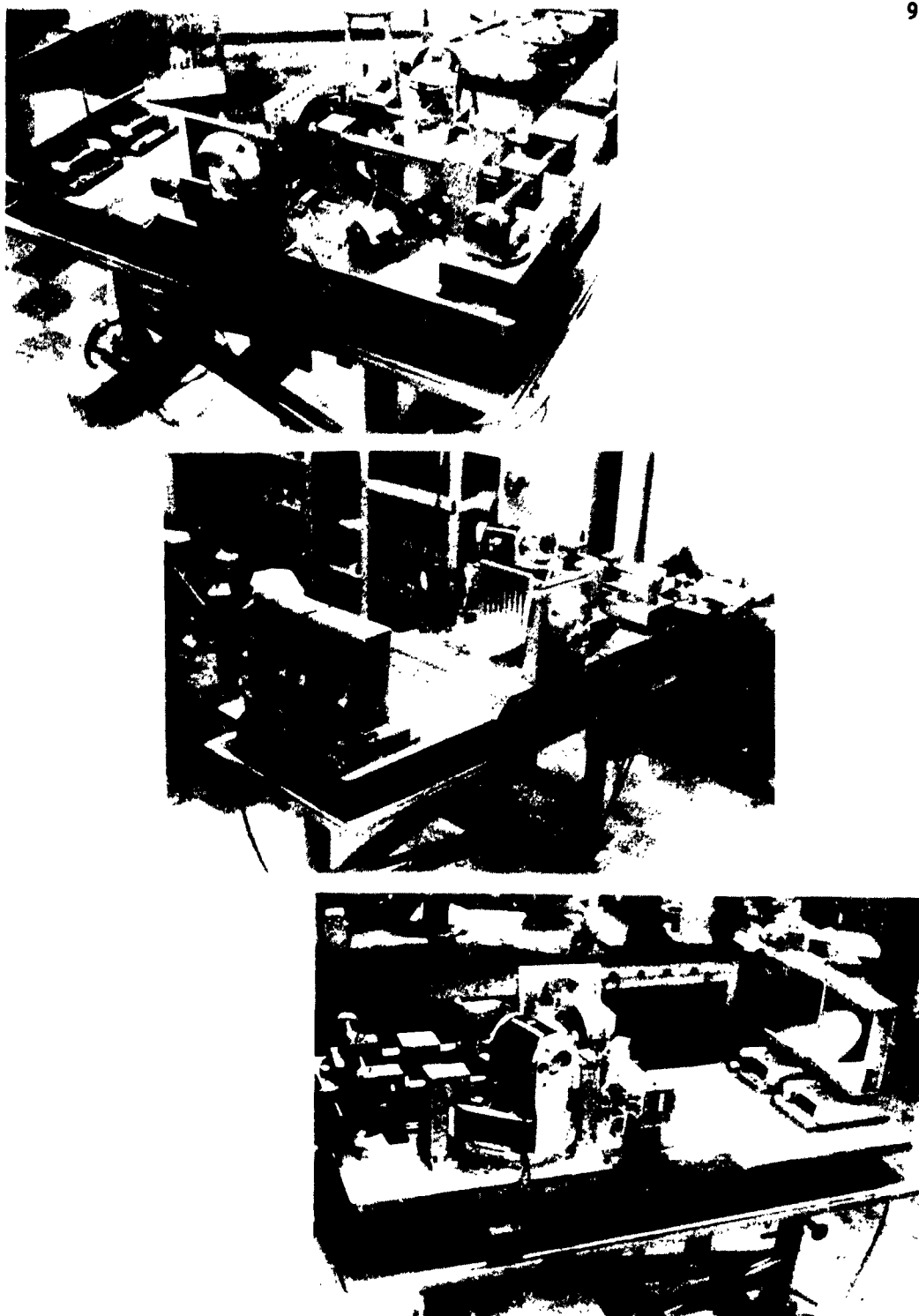
Fig. 32. Three views of the assembled
interferometric modulator with vacuum
tank sides and top removed.

Then, by use of Eq. (3.53) also, the wavelength of peak response

for a given setting of B and θ_n is

$$\lambda_n = (\frac{4 \cos \alpha}{n}) \frac{B}{\ell + B} (C_0 \sin \theta_n) \ . \qquad (7.3)$$

On the other hand, the band of wavelengths making up the first

order radiation leaving the monochromator exit slit is centered

about a wavelength

$$\lambda = 2d \cos \alpha \sin \theta \ , \qquad (7.4)$$

where d is the groove spacing of the dispersion grating and θ is

the grating angle measured from the central image position. The

monochromator has a Czerny-Turner arrangement nearly identical with

that of the modulator, so that the angle α is nearly the same in

both. The coupling condition then is

$$\lambda = \lambda_n \ , \qquad (7.5)$$

or

$$\frac{4BC_0}{n(\ell + B)} \cos \alpha \sin \theta_n = 2d \cos \alpha \sin \theta \ , \qquad (7.6)$$

which is equivalent to

$$\theta = \theta_n \ , \qquad (7.7)$$

$$B = \frac{\ell n}{\frac{2C_0}{d} - n.} \qquad (7.8)$$

In practice it is customary to express the monochromator wavelength

as

$$\lambda = \frac{1}{K} \sin \theta \ ,$$

where K (cm^{-1}) is the "grating constant", obtained experimentally

by measuring the values of θ corresponding to a number of calibration spectral lines. The coupling conditions become

$$\theta = \theta_n \; ,$$

<div align="right">(7.7)</div>

$$B = \frac{\ell \, n}{4C_0 K \cos \alpha - n}$$

<div align="right">(7.9)</div>

Ordinarily, ℓ, n, C_0, and α have fixed values so that to each dispersion grating, having constant K, there corresponds a different value of B. Listed below are the required B values for the existing dispersion gratings, for $n = 13$, $\ell = 8.000$ in, $C_0 = 1.000$ in, and $\cos \alpha = .985$:

dispersion grating (lines/in)	K (cm^{-1})	B (in)
180	35.98	.300
90	18.00	.622
45	8.86	1.374
20	4.015	3.826

The maximum design value for B is 6 in., which yields a maximum grating amplitude, by Eq. (7.1), of

$$(X_m)_{max} = \frac{3}{7} \text{ in.} = 21.77 \text{ mm.}$$

<div align="right">(7.10)</div>

In the photograph of Figure 33, the cam drive motor and the synchronous rectifier assembly are removed to reveal most of the other important parts, which are listed below the photograph. Detailed descriptions of the principal components follow.
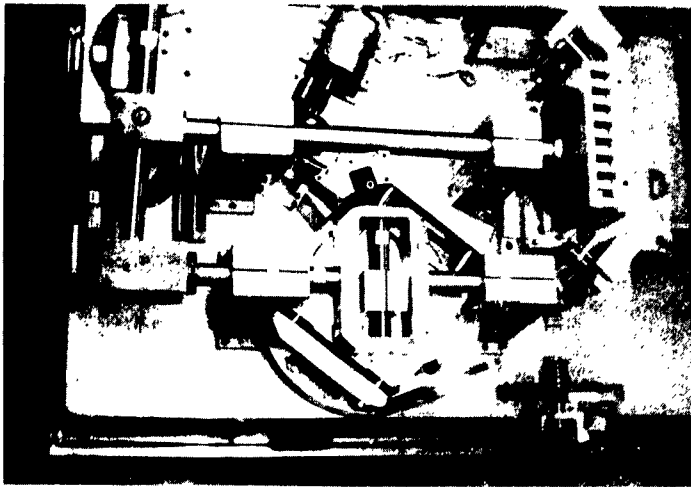
Fig. 33. Top view of the modulator with cam drive motor and recti-
fier assembly removed from the drive unit. A list of the main com-
ponents follows.

M	Fixed part of lamellar grating
D	Movable part of lamellar grating
K,L	Grating rod supports
G	Pivot bearing housing
F	Pivot ways
H	Ratio bar
Y,O	Coupling units
I,J	Drive rod supports
Z	Drive rod
W	Yoke
T	Yoke bar
S,R	Two parts of "coupling unit R"
P	Follower block
Q	Follower guide
A	Scanning drive selsyn

The lamellar grating and associated optics

The optical arrangements in modulator and monochromator are identical except that the 10 in. x 10 in. spherical mirrors in the monochromator have focal lengths of 100 cm, while the focal lengths of those in the modulator are 105 cm. All three slit openings used in the coupled combination are 2 in. long and continuously variable in width from zero to 20 mm. The dispersion gratings measure 9 in. wide by 7 in. high, which requires that the lamellar grating have at least these dimensions. The movable part has height 7-3/8 in. which is thus the effective height of the complete lamellar grating, and the overall width of the fixed part is 9-1/2 in. The useful width is 9 in. The two halves of the lamellar grating were separately machined from aluminum tool and jig plate, then clamped together with facets flush. The unit was then surfaced on a lathe and polished with rouge powder. The movable section of the grating is rigidly fastened to the grating rod, while the mounting for the fixed part allows six degrees of freedom, for bringing the two sets of facets into proper alignment.

The discussion at the beginning of chapter VI makes it clear that the period b of the lamellar grating is chosen to satisfy the condition

$$s_3 \leq \frac{\bar{F}\lambda_n}{b} \quad .$$

(7.11)

Inserting the values $\bar{F} = 105$ cm. and $b = 2.54$ cm. yields

$$s_3 \leq 41.4 \, \lambda_n \; .$$
<div align="right">(7.12)</div>

Since the monochromator has $\bar{F}' = 100$ cm, the corresponding monochromator slit widths should be

$$s \leq \frac{\bar{F}' \, \lambda_n}{b} = 39.4 \, \lambda_n = \frac{100}{105} \cdot s_3$$
<div align="right">(7.13)</div>

The spectral passband of the monochromator for such slit widths is then

$$\Delta \nu = \frac{\cot \theta}{2\bar{F}' \lambda_n} \cdot s = \frac{\cot \theta}{2b} = (0.197 \; cm^{-1}) \cot \theta \; .$$
<div align="right">(7.14)</div>

Some representative values are:

θ	$\Delta \nu$ (cm^{-1})
$10°$	1.12
$20°$	.54
$30°$	.34
$40°$	.23

These represent maximum spectral slit widths for efficient use of the modulator. Somewhat smaller spectral slit widths having been used successfully with a spectrometer with similar characteristics,[1] the value $b = 2.54$ cm represents a reasonable choice. A smaller value would allow use of lower resolution, if desirable, but would aggravate the shadowing problem, to be discussed in a later chapter.

---

1. R. A. Oetjen et. al., J. Opt. Soc. Am. 42, 559 (1952).

The ratio bar

A side view of the ratio bar assembly appears in Figure 34.

Fig. 34. View of ratio bar and pivot assembly with drive rod coupling unit removed.

H   Ratio bar
G   Pivot bearing housing
F   Pivot ways

The drive rod and coupling unit have been removed to allow a clearer view of the ratio bar H, the pivot bearing housing G, and the ways F along which the whole assembly can be moved, and to which it can be securely clamped by set screws not visible in the picture.

It will be shown in the next chapter that for acceptable performance the grating depth must be controlled to within a small fraction, for example 1/20, of a wavelength for the shortest wavelength radiation to be used. For $\lambda = 100 \mu$, the tolerance is thus about 0.2 mil. The ratio assembly is, therefore, designed for high rigidity and

maximum freedom from "play". The pivot bearing consists of two large ball bearings located several inches apart on the pivot spindle and duplexed and preloaded for "zero play". The coupling unit between grating rod and ratio bar can be seen most clearly in Figure 34 also. The ratio bar passes through an adjustable linear ball bushing[2] housed in a slotted cube which can be tightened around the ball bushing to make an arbitrarily close fit between bushing and ratio bar. The uncertainty in radial position then depends mainly on the uniformity of the balls, while low-friction linear motion is still allowed. The bushing housing is pivoted in its yoke by means of vertical pins and bushings. The grating rod slides through adjustable ball bushings housed in the supports K and L of Figure 33. Coupling unit O is identical to Y except that provision is made for adjusting the effective length of the drive rod Z, which is connected to the coupling unit by means of two large nuts screwed directly onto the threaded end of the drive rod.

The drive unit

The above reduction arrangement relaxes the tolerance requirements on the drive unit, pictured in Figure 35, with cam motor and rectifier removed. Even so, the large number of moving parts makes it necessary to keep tolerances low on the individual components. Whenever sliding motion is required, adjustable ball bushings are used; all radial bearings are duplexed and preloaded.

---

2. Thomson Industries, Inc., Manhasset, New York.
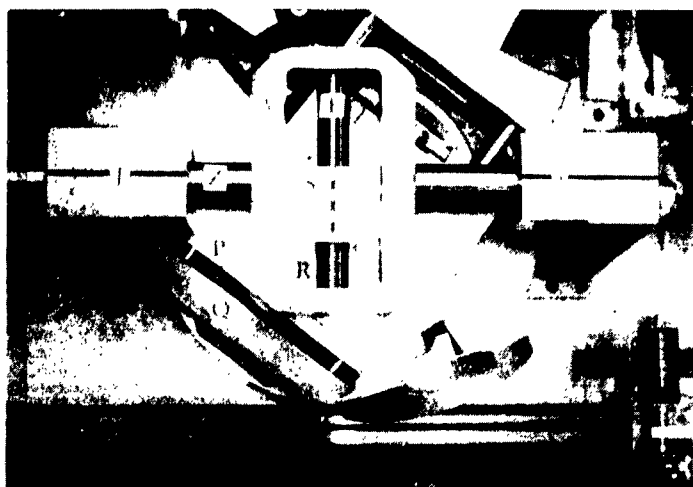
Fig. 35. Top view of drive unit with cam motor
and rectifier assembly removed.

I, J   Drive rod supports
   Z   Drive rod
   W   Yoke
   T   Yoke bar
S, R   Two parts of "coupling unit R"
   P   Follower block
   Q   Follower guide

The drive rod Z and yoke W move back and forth, through the
fixed supports I and J, under the influence of block S, which is
free to slide along the yoke bar T. The block S is pivoted on plate
R, clamped to the cam follower block P, which is constrained by
the two shafts of the follower guide Q to move along a straight line
determined by the orientation θ_n of the circular base plate to which
the follower guide is bolted. This coupling unit, consisting of
block S and plate R, will be referred to as "coupling unit R".
The plate R is mounted in ways on the follower block so that the
position of the coupling unit axis can be adjusted over a range some-

what greater than one inch. The angle θ_n may be taken to be the angle between the transverse shaft T and the follower guide shafts. If the follower block P moves a distance C_o along direction θ_n, block S must move a distance $C_o \sin \theta_n$ perpendicular to T. The circular base plate is labeled C in Figure 36. It carries the

Fig. 36. Enlarged view of drive unit with cam motor, drive rod and yoke removed, revealing

A   Cam
P   Follower block
Q   Follower guide
C   Follower guide base plate

follower guide and the complete cam drive assembly, is supported in a bearing identical to the above-described pivot bearing, and is rotated by means of a large worm gear and worm. The gear tooth ratio is 360:1. This, along with a second worm and gear, with ratio 15:1, provides an overall gear tooth ratio of 5400:1. The second worm shaft is driven by a selsyn which is linked to a

transmitter selsyn in the control panel. An identical driving arrangement is used for the grating table in the monochromator, so that the synchronization condition $\theta = \theta_n$ is fulfilled by driving both selsyns with the same transmitter.

The cam

The plate cam in the drive unit can be seen beneath the follower block in Figure 36 and is fully exposed in Figure 37 by the removal of the follower block and guide. In Figure 37,
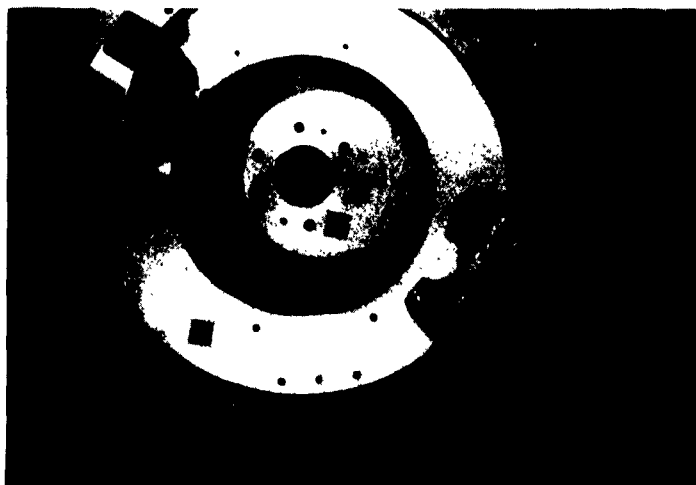
Fig. 37. Top view of cam, cam gear, and follower guide base plate, with follower and guide removed.

    A   Cam
    C   Cam gear
    D   Base plate

the cam A is bolted to the cam gear C, which is mounted in ball bearings concentric with the base plate bearing. In this figure the base plate is labeled D. Figure 38 shows follower and guide
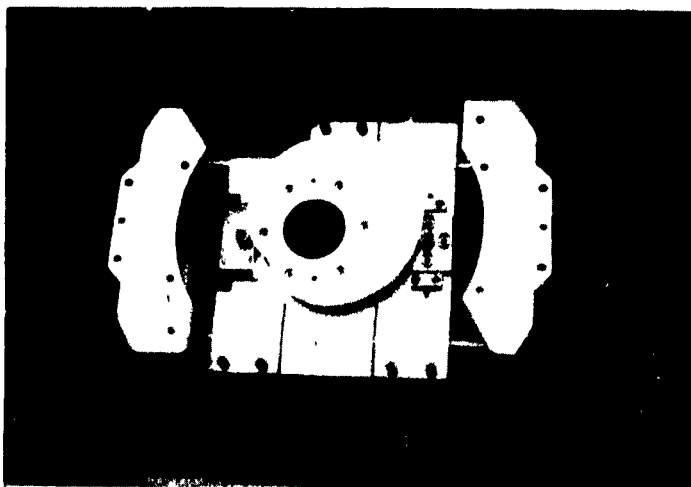
Fig. 38. Bottom view of follower and guide
with cam placed in approximate working
position.

    A   Cam
    P   Follower block
    Q   Follower guide

inverted to reveal the two 1/2 in. diameter cam rollers. The cam

is placed approximately in its correct working position relative

to the rollers. The roller on the right in the figure is bolted

to the follower block, while the left roller is spring loaded

against the cam. Both roller positions can be adjusted so that

a line through their centers passes through the axis of rotation

of the cam.

The cam is designed to produce the realistic follower motion

shown in Figure 39(a), consisting of two long linear portions and

short non-linear portions to provide finite accelerations during

Fig. 39. The cam follower displacement as a function of
time (a) for a complete grating cycle, with reversal regions
exaggerated, and (b) on an enlarged scale for the range
$(0 < t < \frac{T}{80})$.
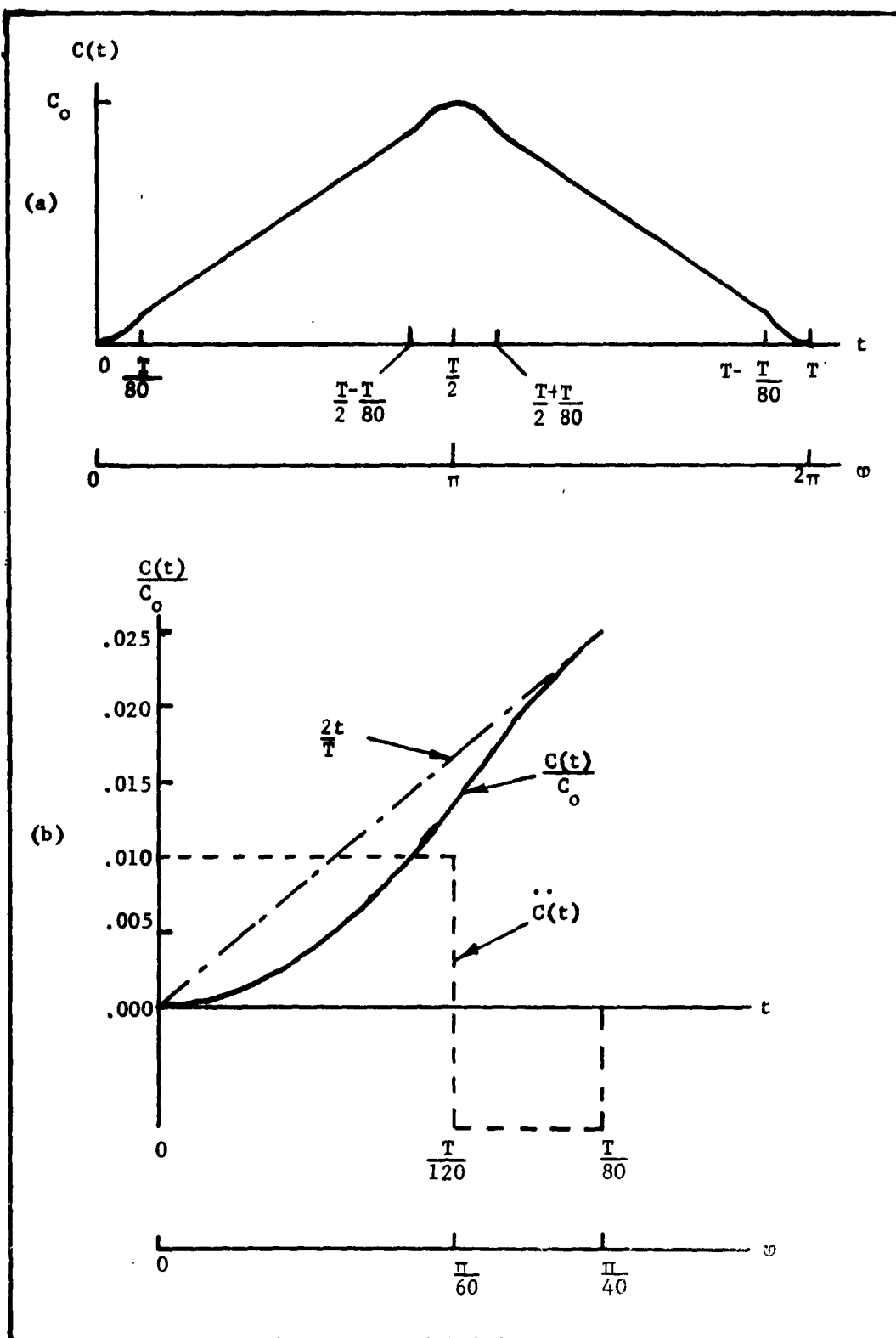
reversal of direction. The follower displacement $C(t)$ can be most conveniently described for one-sided operation. In this case the displacement is taken to be zero when the short radius of the cam is in contact with the fixed roller. With the cam in this position, the coupling unit R of Figure 35 is moved along the ways provided and clamped to the follower block with its axis coincident with the axis of θ_n; that is, with the axis of rotation of block S passing through the axis of the circular base plate. Then this cam position always corresponds to zero grating depth regardless of the value of θ_n. During the time interval $(0 < t < \frac{T}{2})$ the cam turns with constant speed through angle π and the follower attains its maximum displacement $C_o = 2.000$ in. The linear part of the displacement is

$$\frac{C(t)}{C_o} = \frac{2}{T} t \qquad \frac{T}{80} < t < \frac{T}{2} - \frac{T}{80} \qquad (7.15)$$

The non-linear part is shown in detail for the interval $(0 < t < \frac{t_o}{2})$ in Figure 39(b). The graph consists of two parabolic segments smoothly joined at $t = \frac{T}{120}$. The first parabolic segment has slope zero at $t = 0$ and the second one joins the straight line of Eq. (7.15) smoothly at $t = \frac{T}{80}$. The displacements for these intervals are

$$\frac{C(t)}{C_o} = 200 \left(\frac{t}{T}\right)^2 \qquad (0 < t < \frac{T}{120}) \qquad (7.16)$$

$$\frac{C(t)}{C_o} = -\frac{1}{40} + 6\frac{t}{T} - 160\left(\frac{t}{T}\right)^2 \qquad (\frac{T}{120} < t < \frac{T}{80}) . \qquad (7.17)$$

In the interval $(\frac{T}{2} - \frac{T}{80} < t < \frac{T}{2})$ the curve has this same shape,

but is inverted and reversed. Finally, the whole curve is symmetrical about the ordinate $t = \frac{T}{2}$. The acceleration $\ddot{C}(t)$ of the follower is shown, with arbitrary scale, as a dashed line in Figure 39(b). For $T = 1$ sec, the values $\ddot{C}(t)$ are 800 in/sec^2 and -640 in/sec^2.

In the case of two-sided operation, the follower moves between the limits $-C_O$ and $C_O = 1.000$ in. while the cam turns through angle π, during the time interval $(-\frac{T}{2} < t < \frac{T}{2})$. Thus the period of revolution of the cam must be $2T$ and the follower accelerations become 200 in/sec^2 and -160 in/sec^2. In this mode of operation, the mid position of the follower block corresponds to zero grating depth and the axis of the coupling unit R is moved to the center of the follower block. Then the grating always passes through "mirror position" when the follower is at the midpoint of its path, even though θ_n is varied.

The cam drive

A photograph, Figure 40, of the drive unit with the follower and guide and drive rod removed allows a clear view of the cam drive mechanism. The cam drive motor N is a 1/8 H.P., 1800 rpm, synchronous motor. The bevel gears I, J have a gear tooth ratio $\frac{T_I}{T_J} = \frac{13}{30}$, so that the synchronous rectifier shaft turns with gear J at 13 cps. Spur gear K is integral with gear J and meshes with spur gear L, which is on a common shaft with the pinion gear M, a helical spur gear mating with the cam gear C. The gear tooth

Fig. 40. View of cam drive motor, gear
train and rectifier assembly, with
follower and guide removed.

N   Cam motor
I,J Bevel gears
K,L Spur gears
M   Cam pinion gear
C   Cam gear
A   Cam

ratio $\frac{T_M}{T_C}$ is $\frac{2}{13}$, so that the cam speed is

$$\frac{2T_K}{T_L} \text{ cps.}$$ (7.18)

Provision is made for altering this gear tooth ratio to produce

the proper cam speed for the desired resolution in either the

two-sided or one-sided mode of operation. In both modes, once

the value of n is decided upon, the maximum path difference must

be

$$x_m = \frac{n \lambda_n}{2} \; , \tag{3.53}$$

and this value is obtained by adjusting B. The rectification frequency $f_n = \frac{n}{T}$ is set at 13 cps in the detection system used. Then

$$T = \frac{n}{f_n} = \frac{n}{13} \; \text{sec.} \tag{7.19}$$

For the one-sided mode, therefore, the gear tooth ratio for resolution n is

$$\frac{T_L}{T_K} = \frac{2n}{13} \quad . \tag{7.20}$$

For the two-sided mode it is

$$\frac{T_L}{T_K} = \frac{4n}{13} \quad . \tag{7.21}$$

The synchronous rectifier assembly is located just above bevel gear J in Figure 40. For phasing of the rectifier breakers with the amplifier output, the rectifier housing can be rotated by means of the worm and gear arrangement partly visible at the top of the picture.

Source, auxiliary filters, detector, amplifier and recorder

The source used with the modulator-monochromator arrangement is a 100-watt General Electric mercury lamp. Filtering out of radiation of wavelength shorter than $40 \, \mu$ is achieved with a 0.5mm crystal quartz window on the Golay detector and with black polyethylene. Amplification and rectification are performed with a Perkin-Elmer Model 107 amplifier and the standard Perkin-Elmer synchronous

rectifier assembly. A twin T filter is inserted between the second and third stages of this amplifier to reduce the frequency response near 39 cps. The rectified, filtered output is displayed on a Varian strip-chart recorder.

Mechanical alignment procedure

The following procedure has been found effective in bringing the mechanical components of the modulator into the correct alignment to produce the desired path difference variation. Unless otherwise indicated, two-sided operation with n = 13 is implied.

Centering of cam rollers on follower block

The goal here is to have the roller axes and the cam axis all in the same plane. But this is not a crucial adjustment and it is sufficient to locate the rollers midway between the follower guide shafts. With the follower guide removed as in Figure 38 this determination can be made by use of a 6-in. uniform cylindrical rod and vernier calipers.

Measurement of cam follower displacement

The parts are assembled as in Figure 32. The total tension of the three helical springs which hold the one roller against the cam should be 25 to 50 lbs. The cam is oriented with its shortest radius at the fixed roller. It is convenient to measure cam angle by means of the angular displacement of the large bevel gear J of Figure 40, always turning gear J in the same direction to avoid backlash in the

gears between J and the cam gear. A micrometer screw, mounted
beside the follower block on the circular base plate is used to
measure the displacement of a protrusion on the follower block
as bevel.gear J is turned. The exact cam angle corresponding
to the shortest radius is determined by obtaining equal follower
displacements for equal cam angles measured clockwise and counter-
clockwise from the initial position. Follower displacements are
then measured at perhaps 100 points as the cam is turned through
360°. Deviations from the calculated displacements reflect
irregularities in the cam contour, non-concentricity of cam and
cam bearing, mis-alignment of fixed cam roller, and gear imper-
fections.

Determination of follower guide orientation
corresponding to $\theta_n = 0$

The follower guide shafts are judged to be perpendicular
to the drive rod when a 0.0001 in. dial gage placed against the end
of the drive rod indicates the least motion while the cam makes
a complete revolution. This determination can be made with a pre-
cision of $\pm.003^{\circ}$ when backlash between the large worm and worm gear
is prevented. At this orientation of the follower guide, the
scanning drive counter is set at $\theta_n = 0$.

Positioning of coupling unit R

The cam is rotated exactly 90° from the shortest radius position
mentioned above, so that the follower block is then centered on the
base plate. The coupling unit is set approximately in the center of

the follower block. A dial gage measures the longitudinal displace-
ment of the drive rod and another measures the transverse displace-
ment of the coupling unit while θ_n is varied from $0°$ to $90°$. The
variations of these displacements as functions of θ_n allow a
determination of the corrections to make in the location of the
coupling unit. The correction perpendicular to the way bed is made
by inserting shims between the mating surfaces of way and way bed.
The positioning of the coupling unit is correct when variation of
θ_n from $0°$ to $90°$ produces a negligible motion of the drive rod --
i.e., of the order of 0.001 in. If desired, the proper positioning
for the one-sided mode of operation can now be obtained by holding
θ_n at $90°$ and moving the coupling unit exactly 1.000 in. along its
way bed, the distance being measured with a micrometer screw against
the end of the drive rod.

Determination of pivot position
corresponding to $B = 0$

First, with the cam at the mid-position and the coupling unit
centered as above, the ratio bar is made parallel to the pivot ways,
which are nominally perpendicular to the drive and grating rods. This
is a convenient, though not essential, adjustment since the ratio

$\frac{B}{\ell+B}$ is independent of the angular displacement of the ratio bar

about its pivot point. The adjustment is made by means of the large
nuts on the end of the drive rod and is checked by noting the lon-
gitudinal motion of the grating rod as the pivot is slid along its
way bed. After this perpendicularity is attained, changing B-values

necessitates only a very small adjustment in the fixed lamellar
grating position to regain mirror position.

The position of the pivot along its way bed for $B = 0$ is that
for which a maximum motion of the ratio bar ($\theta_n = 90^\circ$, cam turned
through 180°) produces the least longitudinal grating rod motion.
This position can be determined to $\pm$ 0.001 in. in this way and
is recorded as the distance B_0 between reference pins located
on the pivot bearing housing G of Figure 34 and on the instrument
bed plate. A given value of B is then obtained by sliding the pivot
to a new position such that the distance between reference pins
is $B + B_0$.

Adjustment of the fixed lamellar
grating to mirror position

With all the above adjustments made, with the desired value
of B, and with the cam at its mid-position (θ_n arbitrary), the
movable part of the lamellar grating is at mirror position. It
remains to make the facets of the fixed part flush with those of
the movable. Until a more nearly flat lamellar grating is constructed
it is sufficient to check this condition with a straight edge. A
final adjustment along the direction of the grating rod axis is then
made so that an interference maximum·occurs at $\theta_n = 0$ when the
lamellar grating is irradiated with relatively short wavelength
far infrared radiation.

ERRORS AND OTHER DEPARTURES FROM THE IDEALIZED CASE

In this chapter, the general results of chapter III are used to calculate or estimate the effects of specific variations from the ideal, inherent in the practical design of the instrument. The effects of possible errors in adjustment and of mechanical imperfections are also treated.

In addition to the modulator spectral response $S(\nu, \nu_n)$, the following quantities will usually be found useful:

1. The combined modulator-spectrometer spectral response $V_{2\Delta\nu}(\nu - \nu_a)S(\nu, \nu_n)$ for the first grating order,

2. The value of the modulator spectral response at ν_n, or $S(\nu_n, \nu_n)$,

3. The value of the modulator spectral response at the pth monochromator grating order, or $S(p\nu_n, \nu_n)$, for $p > 1$,

4. The instrumental line shape $S(\lambda_n, \lambda)$.

The spectrometer spectral response, for the first grating order only, may be approximated by the triangular function $V_{2\Delta\nu}(\nu)$, with half-width

$$\Delta\nu = \frac{S\nu_n}{2F' \tan\theta_n} . \tag{7.14}$$

Let the spectrometer input spectrum be $2P_0(\nu)$, where $P_0(\nu')$ is the spectral distribution on $(-\infty < \nu' < \infty)$. The spectrometer output

119

Both $V_{2\Delta\nu}(\nu - \nu_n)$ and $S(\nu, \nu_n)$ change width during scanning and, as will be seen in several examples in this chapter, $S(\nu, \nu_n)$ may also change shape.

The modulator output signal as function of ν_n can be calculated approximately by replacing $V_{2\Delta\nu}(\nu - \nu_n)$ in Eq. (8.1) by $\Delta\nu\ \delta(\nu-\nu_n)$, yielding

$$S(\nu_n) = 2\Delta\nu P_0(\nu_n) S(\nu_n, \nu_n) \qquad (8.3)$$

for the first grating order. The ideal spectral response $S_0(\nu, \nu_n)$ has a constant value for $\nu = \nu_n$ during scanning, but certain errors may produce a variation of $S(\nu, \nu_n)$ at this wave number. The quantity $S(\nu_n, \nu_n)$ is therefore of interest for such errors.

If the higher spectrometer grating orders are included in the calculation of the output signal, and if they too are approximated by delta functions, the result is

$$S(\nu_n) = \sum_p 2 P_0(p\nu_n) S(p\nu_n, \nu_n) , \qquad (8.4)$$

where $p = 1,2,3,\ldots$ is the grating order. The quantity $S(p\nu_n, \nu_n)$ is then a good indication of the modulator's ability to suppress the higher grating orders.

The instrumental line shape $S(\lambda_n, \lambda)$ of the modulator is of interest mainly because of its similarity to $S(\nu, \nu_n)$. For each type of error or other variation the relationship between these two functions is investigated to determine whether $S(\nu_n, \nu)$ can be inferred from the shape of $S(\lambda_n, \lambda)$. The measured modulator instrumental line shape obtained by scanning a fixed monochromator

output $V_{2\Delta\nu}(\nu - \nu_0)$ with the modulator is modified because of

the finite spectral width $\Delta\nu$. As an example Figure 41 shows how

$S_0(\nu, \nu_n)$ changes its half-width as scanning proceeds. A value

of $\Delta\nu$ somewhat larger than normal is illustrated. The curve

$S_0(\nu, \nu_n)$ is supposed to translate along the ν axis from right to

left as the modulator scanning variable $\lambda_n(=\frac{1}{\nu_n})$ increases from

$\frac{\lambda_0}{2}$ to $2\lambda_0$. The calculated output signal relative to that at

$\nu_n = \nu_0$ is

$$\frac{\int_0^\infty V_{2\Delta\nu}(\nu - \nu_0) \, S_0(\nu, \nu_n) \, d\nu}{\int_0^\infty V_{2\Delta\nu}(\nu - \nu_0) \, S_0(\nu, \nu_0) \, d\nu} , \qquad (8.5)$$

as a function of ν_n. Plotted versus λ_n, this expression is the

calculated equivalent of the measured instrumental line shape. Study

of Figure 41 reveals that, compared with the ideal instrumental line

shape $S_0(\lambda_n, \lambda_0)$, expression (8.5) has its zeros slightly shifted

away from λ_0, the shift being greatest near λ_0 and decreasing

uniformly for $\lambda_n < \lambda_0$ and for $\lambda_n > \lambda_0$. This effect is a result

of the decreasing height of the feet of $S_0(\nu, \nu_n)$ as ν departs

more and more from ν_n. The maximum value of expression (8.5) occurs

essentially at λ_0. The heights of its feet are approximately the same

as those of $S_0(\lambda_n, \lambda_0)$ for $\lambda_n < \frac{\lambda_0}{2}$, becoming greater than those

of $S_0(\lambda_n, \lambda_0)$ for $\lambda_n > \frac{\lambda_0}{2}$ and less than those of $S_0(\lambda_n, \lambda_0)$ for
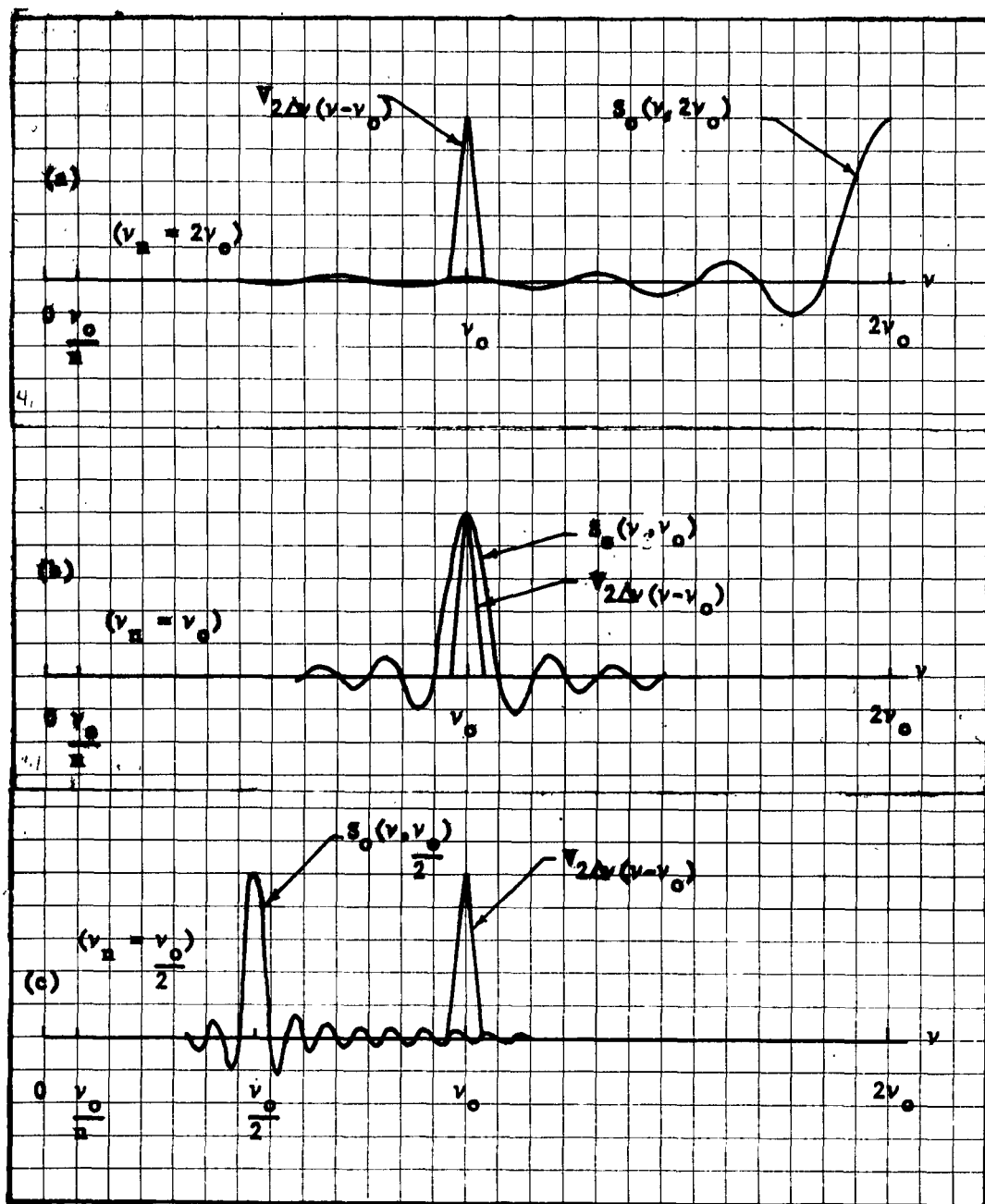
Fig. 41. Scanning the monochromator output
with the modulator.

$\lambda_n > \dfrac{\lambda_o}{2}$. This effect results from the change in width of

$S_0(\nu, \nu_n)$ as a function of ν_n.

A word of explanation should be included here also concerning the efficiency factor $e_1(\dfrac{f}{f_n})$. Logically it should be included in the response function as in Eq. (5.32), and therefore in the spectral response and the instrumental line shape. However, for convenience it will be regarded as a separate factor during the calculations of other effects. Since $\dfrac{f}{f_n} = \dfrac{\nu}{\nu_n} = \dfrac{\lambda_n}{\lambda}$, this efficiency factor becomes $e_1(\dfrac{\nu}{\nu_n})$ as a factor of $S(\nu, \nu_n)$ and the values in Table 1 are applicable if the slits are set at $\dfrac{\overline{F}\,\lambda_n}{b}$; it becomes $e_1(\dfrac{\lambda_n}{\lambda})$ as a factor of $S(\lambda_n, \lambda)$ and the values in Table 1 are applicable if the slits are continuously adjusted to the value $\dfrac{\overline{F}\lambda_n}{b}$ during scanning of the fixed line λ by the modulator. Ordinarily, the slits are set at the fixed value $\dfrac{\overline{F}\lambda}{b}$ under the latter conditions and, since there is no change of incident wavelength relative to the slit width, e_1 has the constant value $e_1(1)$.

Shift of wavenumber of peak response in $S_0(\nu, \nu_n)$

Even in the idealized case, the spectral response does not have its maximum value exactly at $\nu = \nu_n$, but at a slightly higher wavenumber. This is a consequence of the use of a finite maximum path difference, and is true also for interferometers used nonperiodically. For $n = 13$ the wavenumber shift is about one per cent of the half-width $\dfrac{\nu_n}{n}$ of the spectral response curve, hence is negligible. For larger values of n this percentage is still smaller.

Formulation of the
shadowing problem

The derivation of the intensity distribution for the lamellar grating in chapter V neglects the fact that the set of grating facets upon which the radiation first falls casts shadows on the other set of facets. This effect can be taken into account in an approximate fashion by considering only the zeroth order of interference and assuming rectilinear propagation of the radiation. The geometrical relationships are shown in Figure 42, for positive values of the grating depth X.
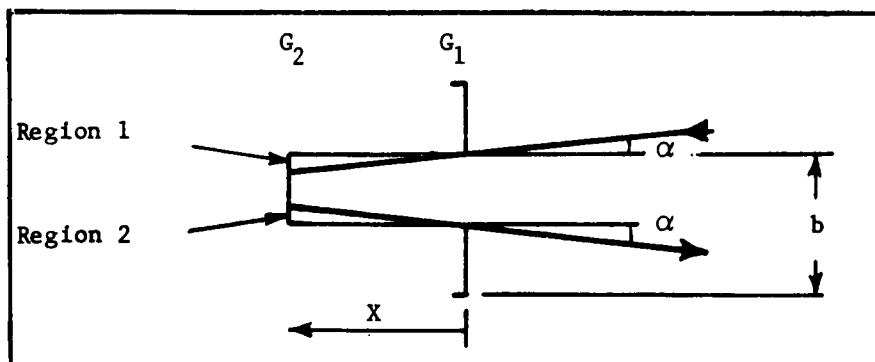
Fig. 42. Illustration of geometrical relationships involved in shadowing. The figure represents part of a cross section of the lamellar grating taken perpendicular to the facets.

Two facets of the front grating G_1 and one facet of the rear grating G_2 appear in horizontal cross section. Radiation is incident at angle α and specularly reflected. No radiation reaches region 1 of the rear facet and radiation falling on region 2 undergoes two reflections and returns to the source. The unused fraction of the area of this shadowed facet is given by

$$\frac{2 \text{ X } \tan \alpha}{b/2} \quad .$$

Since the path difference is $x = 2 \text{ X } \cos \alpha$, this fraction, which is applicable to the entire rear grating, becomes

$$\frac{2 \tan \alpha}{b \cos \alpha} \quad x \quad .$$

The fraction of the area of the rear grating which reflects radiation in the proper direction for interference with the front surface beam is then

$$1 - \sigma x , \tag{8.6}$$

where only positive values of x are considered, and

$$\sigma = \frac{2 \tan \alpha}{b \cos \alpha} \quad . \tag{8.7}$$

The values $\alpha = 9.79°$ and $b = 2.54$ cm yield a value $\sigma = 0.135 \text{ cm}^{-1}$.

As in chapter V the incident plane wave can be represented by the wave function

$$a = a_0 e^{i(\omega t - \frac{2}{\pi} \nu' \zeta)}$$

with average power $\frac{1}{2} a_0 a_0^*$. The sum of the wave functions representing the two reflected beams is then

$$a_1 = \frac{1}{2} a_0 e^{i(\omega t - 2\pi \nu' \zeta)} + \frac{1}{2} a_0 (1 - \sigma x) e^{i(\omega t - 2\pi \nu' x - 2\pi \nu' \zeta)} \tag{8.8}$$

The average power resulting from the superposition of these beams, relative to the incident average power is

$$\frac{a_1 a_1^*}{a_0 a_0^*} = \frac{1}{2} \left[1 - \sigma x + \frac{\sigma^2 x^2}{2} + (1 - \sigma x) \cos 2\pi \nu' x \right] , \tag{8.9}$$

for positive values of x. A similar analysis for negative values

of X and of x yields the following expression in place of Eq. (8.9),

applicable to the two-sided operation in which both positive and

negative x-values are encountered:

$$\frac{a_1 a_1^{*}}{a_0 a_0^{*}} = \frac{1}{2}\left[(1 - \sigma|x|) + (1 - \sigma|x|) \cos 2\pi\nu' x + \frac{\sigma^2 x^2}{2}\right].$$

$$(8.10)$$

This quantity as a function of time and frequency is obtained by

using the usual definitions, Eqs. (3.23) and (3.11). The transmission

function on the interval $(-\frac{T}{2} < t < \frac{T}{2})$ can then be defined as

$$L_1(t,f') = \left[(1 - \sigma_1|t|) + (1 - \sigma_1|t|) \cos 2\pi f't + \frac{\sigma_1^2 t^2}{2}\right] \cdot U_T(t),$$

$$(8.11)$$

in which $\sigma_1 = \frac{2 x_m}{T} \sigma$.

Consistent with the earlier definition of L_1, the factor $\frac{1}{2}$ in

Eq. (8.10) has been omitted in Eq. (8.11).

The spectral response function $S(\nu, \nu_n)$ which follows from

$L_1(t,f')$ is a sum of a number of sets of functions each set of functions

following from one term in $L_1(t,f')$. Each term in $L_1(t,f')$ produces

a set of spectral response functions with particular properties and

which, therefore, describe particular effects in the interferometer

operation. A description of these separate effects is given in the

following paragraphs.

<u>First shadowing effect</u>. -- The first term on the right hand side of Eq. (8.11) can be written

$$(1 - \sigma_1 |t|)U_T(t) = (1 - \sigma_1 \tfrac{T}{2})U_T(t) + \sigma_1 \tfrac{T}{2} V_T(t) \ ,$$

with Fourier transform

$$(1 - \sigma_1 \tfrac{T}{2}) \ T \ \text{dif} \ T \ f' + \frac{\sigma_1 T}{2} \cdot \frac{T}{2} \cdot \text{dif}^2 \frac{Tf'}{2} \ . \tag{8.13}$$

The function $(1 - \sigma_1 |t|) \ U_T(t)$ is exhibited in Figure 43. The contribution of this term to the response function $S(f,f_n)$ is

$$2(1 - \sigma_1 \tfrac{T}{2}) \ \text{dif} \ n + \sigma_1 \tfrac{T}{2} \ \text{dif}^2 \tfrac{n}{2} \ , \tag{8.14}$$

by use of Eq. (4.11).
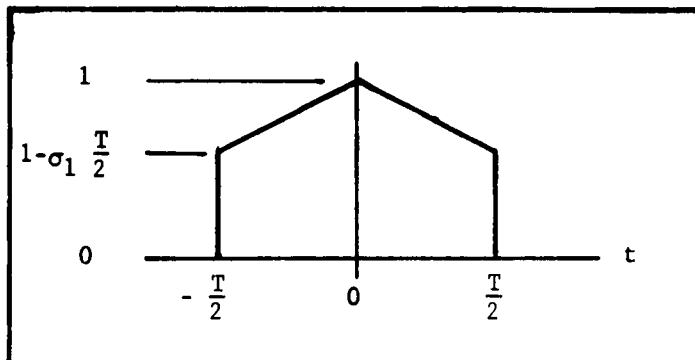
Fig. 43. The function $(1 - \sigma_1 |t|) \ U_T(t)$.

The first part of expression (8.14) vanishes, while the second part, in view of the discussion following Eq. (4.14), can be looked on as accidental apodization coupled with a constant term in the transmission function. It may be written

$$\left(\frac{2}{n\pi}\right)^2 \sigma x_m \quad ,$$

which reduces to the value $\dfrac{x_m}{3140\ cm}$ for $\sigma = .135\ cm^{-1}$ and $n = 13$.

For a given value of x_m, this corresponds to a very small additive constant in the spectral response $S(\nu, \nu_n)$. According to Eq. (3.55) the total contribution of such a term to the instantaneous recorded signal is its product with the total power in the input spectrum. This unwanted addition to the signal increases linearly as scanning proceeds to longer wavelengths. For an incident spectrum consisting, for example, of the band of wavelengths between 100μ and 1000μ in the radiation from a black body source at 1300° K or from a mercury arc source, the resulting "zero drift" can be quite large. If this same radiation is first dispersed by a grating monochromator, however, the effect is much reduced. To get the order of magnitude of this effect it is necessary to estimate the distribution of power among the radiation orders leaving the monochromator exit slit, for a given radiation source.

This problem has been discussed by Oetjen,[1] for black body radiation of wavelengths shorter than 100μ and an ideal echelette grating used at the blaze angle. From his analysis it can be inferred that for a black body source at 1300° K, in the wavelength region 100-1000μ, the relative power in a given grating order leaving the

---

1. R. A. Oetjen, et. al., J. Opt. Soc. Am. 42, 559 (1952).

exit slit is proportional to the cube of the order number, at the

blaze angle. A mercury arc with quartz envelope is known to have a

higher ratio of far infrared to near infrared radiation than such

a black body source. It has been suggested[2] that the wavelength

dependence of the spectral radiance of a mercury arc is λ^{-3} instead

of λ^{-4}. Even though this may not hold true at the long wavelength

end of the region under consideration, the gradual increase, with

increasing wavelength, of the reflectance of the reflection filters

(echelette filter gratings) and of the transmission of the trans-

mission filters (crystal quartz, carbon particles suspended in

polyethylene), as well as a probable increase in reflectance of the

dispersion grating itself for the longer wavelengths, makes it

appear reasonable to assume a λ^{-3} wavelength dependence for the

mercury arc radiation leaving the spectrometer exit slit. This

implies a power p^2 for the pth monochromator order relative to the

first order power. This approximation will be used throughout the

present chapter for determining the effect of a given error, or other

variation, on the modulator's performance as a filter. The p^2

relationship represents the most unfavorable power distribution

likely to be encountered in practice, since the higher orders decrease

more rapidly than the lower orders as the dispersion grating is turned

away from the blaze angle. Table 3 lists the power in the pth grating

---

2. T. K. McCubbin, Jr., "Far Infra Red Spectroscopy from 100
    to 700 Microns" (The Johns Hopkins University, Baltimore, Md.,
    1951).

order and the total power in all grating orders, relative to the power
in the first order, for the first ten dispersion grating orders.

TABLE 3

An estimate of the relative power reaching the modulator
for the various spectrometer grating orders

p	p^2	$\sum_{p=1}^{p} p^2$
1	1	1
2	4	5
3	9	14
4	16	30
5	25	55
6	36	91
7	49	140
8	64	204
9	81	285
10	100	385

Returning to the shadowing problem, the above results allow an
estimation of the "zero drift" when $\lambda_n = 1000 \, \mu$, there are ten
grating orders present in the monochromator output, and the source
is a mercury arc. The product of the total relative input power
385 and the appropriate term $\dfrac{x_m}{3140 \text{ cm}}$ in the spectral response

yields the value of the unwanted signal relative to the desired first-order signal, which is unity. The product is 0.0037 and negligible. A similar analysis for the term $\frac{\sigma_1^2 t^2}{2}$ in Eq. (8.11) reveals that it produces an even smaller effect.

Second shadowing effect. -- The principal term

$$(1 - \sigma_1 |t|) \cos 2 \pi f't \cdot U_T(t)$$

in the transmission function Eq. (8.11) has Fourier transform

$$(1 - \sigma_1 \tfrac{T}{2})T \text{ dif } Tf' + \sigma_1 \tfrac{T^2}{4} \text{ dif}^2 \tfrac{Tf'}{2} * \tfrac{1}{2}\left[\delta(f'-f) + \delta(f'+f)\right],$$

easily obtained by means of Eqs. (8.13) and (2.30). Neglecting the smaller contributions just described, the response function is, by virtue of Eq. (4.11),

$$S(f,f_n) \doteq (1 - \sigma_1 \tfrac{T}{2})\left[\text{dif } T(f - f_n) + \text{dif } T(f + f_n)\right]$$

$$+ \tfrac{1}{2}\sigma_1 \tfrac{T}{2}\left[\text{dif}^2 \tfrac{T}{2}(f - f_n) + \text{dif}^2 \tfrac{T}{2}(f + f_n)\right] \quad . \quad (8.15)$$

In consequence of definitions (3.52), (3.53) and (8.12), the spectral response is

$$S(\nu, \nu_n) \doteq (1 - \tfrac{n\sigma}{2\nu_n})S_0(\nu, \nu_n) + \tfrac{n\sigma}{4\nu_n}S_1(\nu, \nu_n) \tag{8.16}$$

where

$$S_1(\nu, \nu_n) = \text{dif}^2 \tfrac{n}{2\nu_n}(\nu - \nu_n) + \text{dif}^2 \tfrac{n}{2\nu_n}(\nu + \nu_n) .$$

$$\tag{8.17}$$

The functions $S_0(\nu, \nu_n)$ and $S_1(\nu, \nu_n)$ may be seen in Figures 21(a)

and 17, respectively, for n = 13. The most significant feature of Eq. (8.16) is the reduction of the maximum value by the amount

$$\frac{n \ \sigma}{4} \ \lambda_n \ .$$

Table 4 gives the values of this quantity for $\sigma = .135 \ cm^{-1}$ and representative values of n and λ_n.

TABLE 4

The quantity $\dfrac{n \ \sigma \ \lambda_n}{4}$ for representative

values of n and λ_n

λ_n \ n	13	26	52	104
100 μ	.0044	.0088	.0176	.035
500 μ	.022	.044	.088	.0176
1000 μ	.044	.088	.176	.352
4.4 mm	.193			

The efficiency of the modulator is not seriously reduced in the range 100-1000 μ with low resolution, but for higher resolution or longer wavelengths the reduction is significant.

Because of the presence of $S_1(\nu, \nu_n)$ in the spectral response, it does not pass through zero at $\nu = p \nu_n$. That is,

$$S_1 \ (p \nu_n, \nu_n) = (\frac{2}{\pi n})^2 \ \frac{2(p^2 + 1)}{(p^2 - 1)^2} \ . \tag{8.18}$$

For a monochromator output having a p^2 spectral distribution, the contribution of the pth order to the modulator output signal for a given λ_n or ν_n is then

$$p^2 \frac{n\sigma}{4\nu_n} \cdot S_1(p \nu_n, \nu_n) e_1(p) = \frac{2\sigma}{\pi^2} \frac{\lambda_n}{n} \left[\frac{(p^2+1) p^2}{(p^2-1)^2} \right] e_1(p),$$

(8.19)

if it is assumed that the monochromator and modulator slits are set at $\frac{F\lambda_n}{b}$ so that the efficiency factors e_1 from Table 1 are applicable. The bracketed factor in Eq. (8.19) has order of magnitude unity, so that for $\sigma = .135$ cm^{-1} the whole expression reduces to approximately

$$.03 \frac{\lambda_n}{n \text{ cm.}} e_1(p) ,$$

which is negligibly small even for $\lambda_n = 4.4$ mm, n = 13 and p = 2.

The dependence on λ_n of shadowing effects such as that represented by Eq. (8.19) follows directly from the presence of λ_n in the coefficients of $S_0(\nu, \nu_n)$ and $S_1(\nu, \nu_n)$ in Eq. (8.16), and is of course expected on the basis of the geometry of the shadowing process. The occurrence of ν_n in these coefficients causes a change in shape of $S(\nu, \nu_n)$ as ν_n is varied. In this connection it is interesting to write down the expression for the corresponding apparent spectrum of a monochromatic line of wavelength λ,

$$S(\lambda_n, \lambda) \doteq (1 - \frac{n\sigma \lambda_n}{2}) S_0(\lambda_n, \lambda) + \frac{n\sigma \lambda_n}{4} S_1(\lambda_n, \lambda) , \quad (8.20)$$

and note that, since it is normally plotted versus λ_n, it has a slightly different shape from that of the spectral response $S(\nu, \nu_n)$.

Grating reversal

The nonlinear parts of the path difference curve near the reversal points are expected to alter the response function. The contribution to the response function can be calculated exactly by setting up the transmission function $\cos 2\pi\nu x(t)$, where $x(t)$ is defined by equations like (7.15), (7.16), (7.17), and then taking the Fourier transform. The order of magnitude of the effect can be arrived at by approximating the parabolic segments by straight line segments and using the results at the end of chapter IV.

The part of the path difference function near the reversal at $T/2$ is plotted in Figure 44 for two-sided operation. In this case, the cam makes one half revolution during one grating cycle of period T. An angle of $4.5°$ is occupied by the reversal curve for each $90°$ of cam angle. The corresponding time interval is thus $T/40$, as indicated in the figure. The curve $\frac{2x_m}{T} t$ and the parabolic segments are shown as broken lines, while the approximating segments are continuous lines. In terms of the symbols defined in chapter IV, the approximating segment between $\frac{T}{2} - \frac{T}{40}$ and $\frac{T}{2} - \frac{T}{100}$ is characterized by

$$\tau_1 = \frac{T}{2} - \frac{T}{40}$$

$$\tau_2 = \frac{T}{2} - \frac{T}{100}$$

$$\tau_0 = 0.015\ T$$

$$\tau = \frac{T}{2}(1 - 0.035) = 0.4825\ T$$

$$x_1 = 0.01\ x_m \quad . \tag{8.21}$$
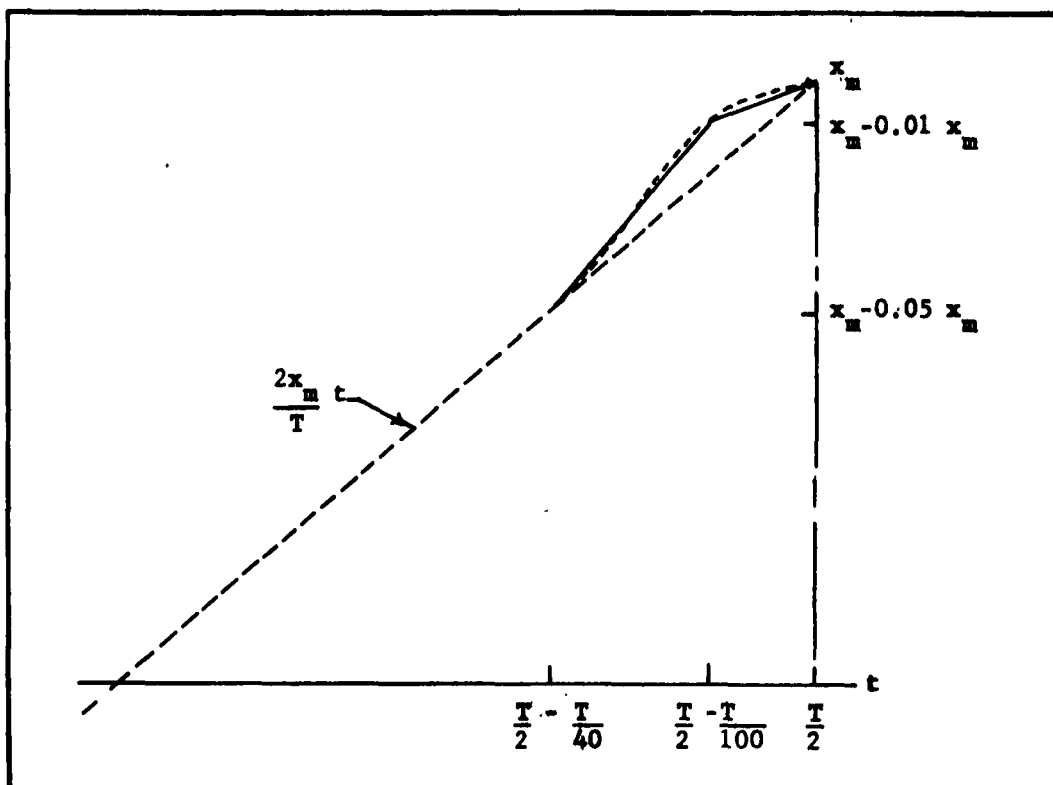
Fig. 44. Path difference _versus_ time near the reversal point at t = T/2, for two-sided operation. The line $\frac{2x_m}{T}$ t and the parabolic segments are shown as broken curves, the approximating segments as continuous lines.

This segment of the path difference function has associated with it a contribution $\Delta S(v\nu, v\nu_n)$ to the spectral response. The quantity $\Delta S(v\nu, v\nu_n)$ is obtainable from Eq. (4.43) by means of the substitution $f = v\nu$. If, in addition, the definitions (4.38) and (4.40) for v, v_1, ϵ, and μ are used, $\Delta S(v\nu, v\nu_n)$ can be written

$$\Delta S(v\nu, v\nu_n) =$$

$$\frac{|\tau_o|}{2T} \left\{ \cos\left[2\pi\left(v\tau + \frac{x_1}{2}\right)\left(\nu - \frac{\nu_n}{1+\frac{x_1}{2v\tau}}\right)\right] \text{dif}\left[\tau_o(v+v_1)\left(\nu - \frac{\nu_n}{1+\frac{v_1}{v}}\right)\right]\right.$$

$$\left. + \cos\left[2\pi\left(v\tau + \frac{x_1}{2}\right)\left(\nu + \frac{\nu_n}{1+\frac{x_1}{2v\tau}}\right)\right] \text{dif}\left[\tau_o(v+v_1)\left(\nu + \frac{\nu_n}{1+\frac{v_1}{v}}\right)\right]\right\} .$$

$$(8.22)$$

Consider the two factors in the first term of Eq. (8.22). The dif function has a half-width in ν-space of

$$\frac{1}{\tau_o(v+v_1)} \quad , \qquad (8.23)$$

which is the reciprocal of the total change in path difference during the time interval τ_o. Since $\tau_o << T$, this half-width is large compared with that of $S_o(\nu, \nu_n)$. For the values of τ_o, τ and x_1 given in (8.21), the half-width is $50 \frac{\nu_n}{n}$. The central maximum of the dif function occurs at

$$\nu = \frac{\nu_n}{1+\frac{v_1}{v}} \quad , \qquad (8.24)$$

which is the proper wave number for complete modulation at frequency f_n when the path difference varies at the rate $v + v_1$. In the present example, Eq. (8.24) yields $\nu = \frac{3}{4}\nu_n$. The cosine factor in Eq. (8.22) has "period" in ν-space of

$$\frac{1}{v\tau + \frac{x_1}{2}} \quad . \qquad (8.25)$$

This is the reciprocal of the path difference at time $t = \tau$ of the grating cycle. Since τ in this case is nearly equal to $T/2$, the cosine factor varies rapidly as a function of ν, the "period" being $\frac{1}{.485} \frac{\nu_n}{n}$. The argument of the cosine function is zero at

$$\nu = \frac{\nu_n}{1 + \frac{x_1}{2\nu\tau}} \, . \tag{8.26}$$

For the values of x_1 and τ being considered, this yields $\nu \doteq \nu_n$. The second term in Eq. (8.22), if it were plotted for negative values of ν, would have a graph which is a mirror image, with respect to the line $\nu = 0$, of the graph of the first term. The value of the second term on $(0 < \nu < \infty)$ is by no means negligible, because of the large half-width of the dif function.

To obtain the net effect of the variation from the perfect triangular grating motion, the contribution

$$\Delta S_0(\nu\nu, \nu\nu_n) = \frac{|\tau_0|}{2T} \left\{ \cos 2\pi\nu\tau(\nu - \nu_n) \operatorname{dif} \nu\tau_0(\nu - \nu_n) \right.$$

$$\left. + \cos 2\pi\nu\tau(\nu + \nu_n) \operatorname{dif} \nu\tau_0(\nu + \nu_n) \right\} \, , \tag{8.27}$$

obtained from Eq. (4.44), must be subtracted from ΔS. The cosine and dif functions of Eq. (8.27) are centered at wave numbers $\pm \nu_n$ and have "period" and half-width $\frac{1}{.4825} \frac{\nu_n}{n}$ and $\frac{200}{3} \frac{\nu_n}{n}$, respectively. Calculated values of $4(\Delta S - \Delta S_0)$ are given in Table 5 for $\nu = p\nu_n$, under the column headed $\tau = .4825 \, T$.

TABLE 5

Approximate spectral response contributions
produced by grating reversal, for
wave numbers p ν_n.

p	$4(\Delta S - \Delta S_0)$ $(\tau=.4825T)$	$4(\Delta S - \Delta S_0)$ $(\tau=.4975T)$	$S(vp\nu_n, \nu\nu_n)$	$e_1 S(vp\nu_n, \nu\nu_n)$	$p^2 e_1 S(vp\nu_n, \nu\nu_n)$
1	.00610	.00238	.00848	.00848	.0084
2	-.00202	-.00622	-.00824	-.00495	-.0198
3	.00252	.01190	.01542	.00723	.0652
4	.00842	-.01762	-.00920	-.00350	-.0560
5	-.01270	.02244	.00974	.00311	.0780
6	.01414	-.02512	-.01088	-.00315	-.1136
7	-.00294	.01268	.02242	.00582	.2860
8	.00034	-.01153	-.02272	-.00500	-.3480
9	.00412	.00947	.02306	.00505	.4100
10	-.00692	-.00702	-.02096	-.00420	-.4192
Total for orders 2-10 ------				.00041	-.1006

The approximating segment lying between $\frac{T}{2}$ and $\frac{T}{2} - \frac{T}{100}$ has

$$\tau_1 = \frac{T}{2}$$

$$\tau_2 = \frac{T}{2} - \frac{T}{100}$$

$$\tau_0 = -\frac{T}{100}$$

$$\tau = \frac{T}{2}(1 - \frac{1}{200}) = 0.4975 \, T$$

$$x_1 = 0.01 \, x_m \tag{8.28}$$

Values of $4(\Delta S - \Delta S_0)$ calculated for this segment are entered in Table 5 under the column headed $\tau = 0.4975 \, T$. The sums of the contributions made by the two approximating segments are also tabulated, under the column headed $S(v \, p \nu_n, v \nu_n)$. The factor of 4 has been inserted because the grating cycle defined on $(-\frac{T}{2} < t < \frac{T}{2})$ contains two reversal regions: the one shown in Figure 44 and a similar one at $t = -\frac{T}{2}$, defined such that $x(t) = -x(-t)$. The latter reversal region has the same effect on the spectral response as the former, which introduces a factor of two. This pair of reversal regions occurs twice during the time 2T, introducing a second factor of two.

The last two columns of Table 5 refer to the use of the modulator as a filter for a spectrometer with a uniform and a p^2 power distribution, respectively, and with slits set at $\overline{F} \lambda_n$.

$\overline{b}$

Undue significance should not be attached to the particular numbers displayed in Table 5; they should be taken only as typical values. The exact values obtained depend on the choice of τ_2, the position of

the apex of the triangular approximation to the nonlinear section of the path difference curve. The $p = 1$ contribution is necessarily positive and there is a strong tendency toward alternation of signs such that the pth contribution has the sign $(-1)^{p-1}$ for any reasonable choice of τ_2 which makes the triangle appear to approximate the shape of the parabolic segments. An exact calculation for the parabolic curves would be of little more significance since, as it happens, the actual contour of the cam does not conform exactly to the contour designed to produce the parabolic segments in the curve of path difference. An immediate conclusion to be drawn from the table is that the desired output signal produced by the first order of the monochromator is not diminished, but slightly increased, by the finite reversal time. However, the additional contributions made by the higher monochromator orders can be quite large when these orders are stronger than the first order. The differences in sign make the expected net increment of signal attributable to orders 2-10 less than the increments due to some of the individual orders. The presence of a strong absorption line at, for example, $\nu = 7\nu_n$, could alter this net increment by a factor of 4 perhaps.

For a given cam, the quantity x_1 is proportional to x_m and both these quantities are inversely proportional to ν_n. Thus if $\nu = p \, \nu_n$ is substituted into Eqs. (8.22) and (8.27), the increments $\Delta S - \Delta S_0$ are independent of the scanning variable ν_n. However, if modulator and monochromator are scanning in synchronism, the power distribution

in the monochromator orders is changing continuously, even in the absence of absorption bands. This causes a gradual change in the net higher order signal contribution due to finite reversal time, from a value of the order of 10% at blaze down to something less than .05% sufficiently far from blaze that the power distribution is approximately uniform. If an absorption line is present in the input spectrum at any of the wave numbers $p\nu$ for $p > 1$, the result is a spurious positive or negative "line" located at $\nu_n = \nu$ in the record of signal versus ν_n.

Electrical filtering and synchronous rectification in practice

So far the electrical filters in the detection system have been represented by the rectangular functions $U_w(f')$ of Eq. (3.30) and $U_{w_0}(f')$ of Eq. (3.39). In this section, the properties of actual filters are taken into account. Practical considerations involved in synchronous rectification are also discussed.

The detector-amplifier frequency response.-- In actuality, the frequency response of the detection-amplification combination should be represented not by the function $U_w(f')$ but by an empirical function $G(\frac{f'}{f_n})$, which has the value unity near the frequencies $\pm f_n$ and falls off gradually at other values of f'. In addition, the various frequency components of the signal passing through the system may undergo different phase shifts. Eq. (3.32) should therefore be written

$$F_3(t) = \frac{1}{T} \sum_{q=-q'}^{q'} G(\frac{q}{n}) P_1(\frac{q}{T}) e^{+2\pi i q \frac{t}{T}} * \delta(t - t_q) . \qquad (8.29)$$

Then Eq. (3.30) is replaced by the transform of $F_3(t)$,

$$P_3(f') = \frac{1}{T} \sum_{q=-q'}^{q'} G(\frac{q}{n}) \, P_1(\frac{q}{T}) \, e^{-2\pi i t_q \frac{q}{T}} \, \delta(f' - \frac{q}{T}) . \tag{8.30}$$

In these equations the qth frequency component of $F_3(t)$ has undergone a phase shift $2\pi \frac{t_q}{T}$ relative to the rectifier. The procedure outlined in Eqs. (3.33)-(3.42) then leads to the following equation in place of Eq. (3.43):

$$F_5(t) = \frac{1}{T} \sum_k (\text{dif} \frac{k}{2} - \text{dif} \, k) \, P_1(-\frac{kn}{T}) \, G(-k) \, e^{-2\pi i \frac{knt_q}{T}} , \tag{8.31}$$

and finally the response function, Eq. (3.51), may be replaced by

$$S(f, f_n) = \cos 2\pi f_n t_n \left[\text{dif} \frac{n}{f_n} (f-f_n) + \text{dif} \frac{n}{f_n} (f + f_n) \right]$$

$$- \frac{1}{3} G(3) \cos 6\pi f_n t_{3n} \left[\text{dif} \frac{n}{f_n}(f-3f_n) + \text{dif} \frac{n}{f_n} (f + 3f_n) \right]$$

$$+ \frac{1}{5} G(5) \cos 10\pi f_n t_{5n} \left[\text{dif} \frac{n}{f_n}(f-5f_n) + \text{dif} \frac{n}{f_n} (f + 5f_n) \right] + \dots \tag{8.32}$$

Part of this curve is sketched in Figure 45 for $t_n = t_{3n} = 0$, $n = 13$ and $G(3) = 1$. The rectification function is $R_0(t)$.

Suppose the synchronous rectifier to be correctly phased with the f_n component of the amplifier output; i.e., $t_n = 0$. Then if the $3f_n$ component has undergone a phase shift relative to the f_n component during detection and amplification, Eq. (8.32) shows that its influence is diminished by the phase factor $\cos 6\pi f_n t_{3n}$. Similar statements apply to the higher harmonics of f_n. Since these phase shifts are

largely unknown, however, they will be omitted in subsequent
expressions of the response function, spectral response and
instrumental line shape, and it will be kept in mind that the
actual influence of these harmonics will in general be less than
that predicted.

An estimate of the actual function $G(\frac{f'}{f_n})$ can be obtained
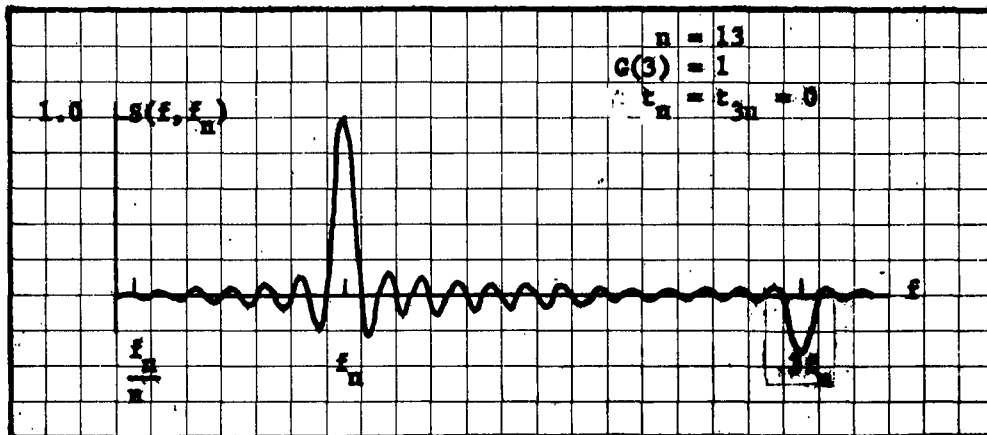
Fig. 45. A sketch of the response function when the
detector-amplifier bandpass is unlimited and the recti-
fication function is $R_0(t)$.

by taking the product of the frequency response of the Golay detector
into the measured voltage gain of the amplifier. The frequency response
of the Golay detector used was not measured but is expected to decrease
even more rapidly at higher chopping frequencies than the frequency
response used in these calculations.[3]

---

3. Detector data obtained from:
   Final Report on Comparative Testing of Thermal Detectors,
   NDRC Contract OEM sr-1168, The Ohio State University,(1946).

The twin T filter in the amplifier is at present tuned to minimize the gain at 45 cps. Measurements made for this condition indicate that tuning the filter to shift this minimum to 39 cps would produce the approximate detector-amplifier frequency response $G\left(\frac{f}{f_n}\right)$ given in Table 6 for the first 10 harmonics of f_n = 13 cps. A knowledge

TABLE 6

The estimated detector-amplifier frequency response
and the modulator response function at the harmonics
of f_n; The resulting signal increments produced
by the higher monochromator orders at blaze

f cps	harmonic f/f_n	$G\left(\frac{f}{f_n}\right)$	$S(f,f_n)$	$e_1 S(f,f_n)$	$e_1 p^2 S(f,f_n)$
13	1	1.00	1.00	1.00	1.00
26	2	.61	0	0	0
39	3	.017	-.006	-.003	-.024
52	4	.055	0	0	0
65	5	.045	.009	.0035	.07
78	6	.035	0	0	0
91	7	.030	-.004	-.001	-.05
104	8	.020	0	0	0
117	9	.013	.0015	.0003	.03
130	10	.010	0	0	0

of $G\left(\frac{f}{f_n}\right)$ allows calculation of the response function $S(f,f_n)$ at these harmonics. This also is tabulated, along with $e_1\left(\frac{f}{f_n}\right)S(f,f_n)$,

the signal contribution made by the pth radiation order from the monochromator assuming a uniform power distribution; and finally $e_1 p^2\ S(f, f_n)$, the signal contribution of the pth order at blaze. The spectral response, with $t_{3n} = t_{5n} = \ldots = 0$,

$$S(\nu, \nu_n) = S_0(\nu, \nu_n) - \frac{1}{3} G(3) \left[\text{dif}\ \frac{n}{\nu_n}(\nu - 3\nu_n) \right.$$
$$\left. + \text{dif}\ \frac{n}{\nu_n}(\nu + 3\nu_n) \right] + \ldots \quad , \quad (8.33)$$

obtained from Eq. (8.32) by use of definition (3.52), has the same shape as $S(f, f_n)$. Hence the quantities $S(p\nu_n, \nu_n)$ and $p^2\ S(p\nu_n, \nu_n)$ have the same values as those listed in the table for the response function. Again, the unwanted contributions made by the higher monochromator orders are expected to be appreciable only at blaze.

The expression for the apparent spectrum $S(\lambda_n, \lambda)$ of a monochromatic line of wavelength λ is derived from $S(\nu, \nu_n)$ by replacing ν and ν_n by $1/\lambda$ and $1/\lambda_n$, respectively. The result is

$$S(\lambda_n, \lambda) = S_0(\lambda_n, \lambda) - \frac{1}{3} G(3) \left[\text{dif}\ \frac{n}{\lambda}(\lambda_n - 3\lambda) + \text{dif}\ \frac{n}{\lambda}(\lambda_n + 3\lambda) \right]$$
$$+ \ldots \quad ,$$
$$(8.34)$$

which has the same functional form as Eq. (8.33).

Phasing and shape of the rectification function.-- According to Eq. (8.32), if the terms in $G(3)$, $G(5)$, etc. are negligible, the spectral response becomes

$$S(\nu, \nu_n) = \cos 2\pi f_n t_n\ S_0(\nu, \nu_n) . \quad (8.35)$$

The output signal for a given ν_n is, by Eq. (3.55),

$$S(\nu_n) = \cos 2\pi f_n t_n \int_0^\infty 2P_o(\nu) \, S_o(\nu, \nu_n) \, d\nu \quad . \tag{8.36}$$

In the absence of errors, therefore, correct rectifier phasing maximizes the output signal at any chosen modulator setting ν_n.

The actual rectification function $R_o'(t)$ used is shown in Figure 46. It is an even function having the values shown in the figure.
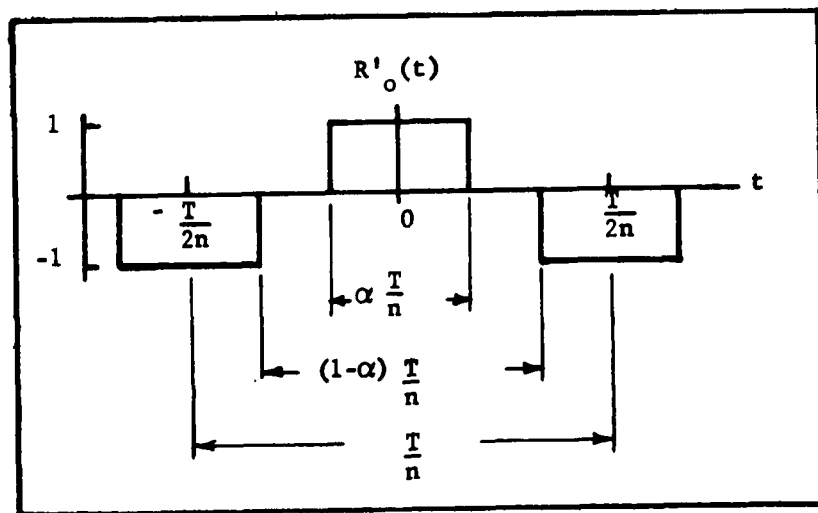
Fig. 46. The actual rectification function $R_o'(t)$.
It is symmetrical about the ordinate $t = 0$.

It may be defined by the following expression:

$$R_o'(t) = \left[-U_{\frac{T}{n}}(t) + U_{\frac{T}{n}(1-a)}(t) + U_{\frac{aT}{n}}(t) \right] * \sum_{k=-\infty}^{\infty} \delta(t - \frac{kT}{n}) \quad , \tag{8.37}$$

having Fourier transform

$$R'(f') = \left[-\text{dif } k + (1-a) \, \text{dif } k(1-a) + a \, \text{dif } a \, k \right] \cdot \sum_{k=-\infty}^{\infty} \delta(f' - \frac{k}{T} \frac{n}{T}) . \tag{8.38}$$

The coefficients of the delta functions reduce to zero for even values of k and to

$$\frac{2}{\pi k} \sin \pi ka \quad \text{for } k = \pm 1, \pm 3, \pm 5, \ldots \quad . \tag{8.39}$$

The parameter a can be chosen to suppress some of the unwanted odd harmonics. For example, the value $a = \frac{1}{3}$ yields the following co-efficients:

k	$\frac{2}{\pi k} \sin \pi k \, a$	$(a = \frac{1}{3})$
± 1	$\sqrt{3}/\pi$	
± 3	0	
± 5	$-\sqrt{3}/5\pi$	
± 7	$\sqrt{3}/7\pi$	
± 9	0	
± 11	$-\sqrt{3}/11\pi$	

Such a rectification function completely eliminates the 3rd and 9th harmonic contributions listed in Table 6. However, if the rectifier adjustment is in error by $\frac{1}{30}$ cycle, i.e., if $a = \frac{1}{3} \pm \frac{1}{30}$, the co-efficient $\frac{2 \sin \pi k a}{\pi k}$ for $k = 3$ has the value $\mp \frac{2}{3\pi} \sin 18^\circ$, which is some improvement over the $a = \frac{1}{2}$ value of $\frac{2}{3\pi}$. The adjustment to $a = \frac{1}{3}$ must be made accurately to obtain the desired rejection of higher harmonics.

The coefficient $\frac{\sqrt{3}}{\pi}$ for $k = \pm 1$ and $a = \frac{1}{3}$ is to be compared with the value $\frac{2}{\pi}$ for $a = \frac{1}{2}$, which has been used throughout the calculations in previous chapters. For a comparison of interferometric modulation

with square wave chopping in which only the first harmonic is amplified and synchronously rectified, the coefficient $\frac{2}{\pi} \sin \pi a$ is multiplied by an additional factor $\frac{4}{\pi}$ for the square wave case.

The post-rectification low-pass filter.-- The frequency response of the post-rectification low-pass filter is represented in Eq. (3.39) by $U_{W_0}(f')$. In reality it may pass a small fraction of the $\pm \frac{1}{T}$ frequency components in the rectifier output. The effect of this can be seen most clearly by reference to Figure 14. When the modulator is set for maximum response at wave number ν_n an incident wave number ν near $\nu_n + \frac{\nu_n}{n}$ has strong modulation frequency components $\pm (f_n + \frac{1}{T})$ and also much weaker components $\pm (f_n - \frac{1}{T})$, as shown in Figure 14(a). Synchronous rectification shifts the $\pm (f_n + \frac{1}{T})$ components to $\pm \frac{1}{T}$, respectively, and shifts the $\pm (f_n - \frac{1}{T})$ components to $\mp \frac{1}{T}$, respectively. This is depicted in Figure 14(c) and (d). The sum of the amplitude of the $\frac{1}{T}$ component and that of the $-\frac{1}{T}$ component reaches a maximum for an incident wave number very near $\nu_n + \frac{\nu_n}{n}$. This maximum value is equal to that of the steady signal at peak response, i.e., when the incident wave number is ν_n. A similar maximum occurs for an incident wave number very near $\nu_n - \frac{\nu_n}{n}$. Thus the $\frac{1}{T} = 1$ cps variation in the recorded signal can have a maximum amplitude equal to the steady signal at $\nu = \nu_n$ multiplied by the relative frequency response, at 1 cps, of the actual filter used. Inadequate filtering of this component is expected to show up clearly near the first zeros on either side of the central maximum of the apparent spectrum $S_0(\lambda_n, \lambda)$ of a monochromatic line. Also,

when monochromator and modulator are scanning simultaneously and the spectral response is $S_0(\nu, \nu_n)$, the incident wave number ν_n does not produce a 1 cps modulation frequency component, but all other wave numbers in the monochromator spectral passband do so. On the other hand, if for some reason $P_1(f',f)$ does not pass through zero at $q\frac{f_n}{n}$ for integral $q = \pm n$, then even radiation of wave number ν_n contributes to the 1 cps component.

Error in positioning of midpoint of motion of movable grating relative to fixed grating: "x_0 error"

This type of error corresponds to a translation of the limits of variation of the path difference, for which the response function is derived in chapter IV. The path difference contains a small additive term x_0 which is essentially constant during a complete grating cycle. Since each part of the grating cycle is affected by this error, it may be expected to have a relatively strong influence on the modulator's performance. Such an "x_0 error" will be present in some measure despite careful adjustment of the fixed grating relative to the movable and despite a careful attempt to position the axis of coupling unit R of Figure 35 directly above the cam and follower guide axis; furthermore, thermal expansion of the drive rod and grating rod and other parts, and shifting of components by vibration, may introduce an x_0 error after an optimum alignment has been attained. The two-sided and one-sided modes of operation will be discussed separately.

Two-sided operation.-- The appropriate spectral response, value

of the spectral response at ν_n, and instrumental line shape follow immediately from the response function of Eq. (4.34):

$$S(\nu, \nu_n) = \cos 2\pi\gamma \frac{\nu}{\nu_n} \, S_0(\nu, \nu_n) \quad , \tag{8.40}$$

$$S(\nu_n, \nu_n) = \cos 2\pi\gamma \quad , \tag{8.41}$$

$$S(\lambda_n, \lambda) = \cos 2\pi\gamma \frac{\lambda_n}{\lambda} \, S_0(\lambda_n, \lambda) \, . \tag{8.42}$$

In these equations

$$\gamma = x_0/\lambda_n \quad . \tag{4.20}$$

The detailed shapes of these curves depend on whether x_0 is a constant independent of λ_n or is proportional to λ_n, making γ constant. If the error is in the positioning of the fixed grating, or in any of the linkage between the grating and the sine-producing mechanism, then x_0 is constant. An error in positioning of coupling unit R produces an x_0 which varies linearly as scanning proceeds, hence is proportional to λ_n.

The spectral response curve has the same shape as $S(f, f_n)$ of Eq. (4.34) and may be obtained from the curves of Figure 21(a), since for a given ν_n the ratio γ is constant with respect to changes in ν. The obvious effects of the cosine factor in Eq. (8.40) are a reduction of the spectral response at ν_n, a very slight shift in the wave number of maximum response, and a suppression of the subsidiary maxima and minima at regular intervals along the ν axis. These

effects are identical for corresponding positive and negative values

of x_0. The reduction at ν_n is $\cos 2\pi\gamma$ and amounts to 0.866 for

$\gamma = 1/12$. The magnitude of the actual error X_0 in displacement

of the grating for this value of γ is $X_0 = {}^\lambda n/24$.

Some representative values are:

λ_n	X_0 $(\gamma = \frac{1}{12})$
100 μ	.00016 in.
500 μ	.0008 in.
1000 μ	.0016 in.

For γ less than about 1/4, the shift of the peak is always

toward smaller values of ν . When n = 13 and γ = 1/12, the calcu-

lated shift is nearly sufficient to neutralize the opposide shift

already present in $S_0(\nu, \nu_n)$ as a result of the finite maximum path

difference. For γ = 1/6 and n = 13, the calculated shift is about

$.03 \frac{\nu_n}{n}$.

The zeros of $S(\nu, \nu_n)$ still occur at integral multiples of $\frac{\nu_n}{n}$,

and in particular at p ν_n, so that the feet of the curve near these

points are, if anything, reduced. The general tendency of the cosine

factor in the interval (o $<\nu< 2 \nu_n$) for γ = 1/12, for example, is

to restore symmetry about $\nu = \nu_n$.

The combined spectral response $V_{2\Delta\nu}(\nu - \nu_n)S(\nu, \nu_n)$, with

finite slit widths, has practically no shift for $\gamma = \frac{1}{12}$, since both

factors are very nearly symmetrical in the region of overlapping. For

$\gamma = 1/6$, the center of area under the curve $V_{2\Delta\nu}S$ is shifted toward

smaller wave numbers by about $0.01 \frac{\nu_n}{n}$.

Eq. (8.41) indicates that during scanning with the modulator-spectrometer combination, the x_0 error introduces a factor $\cos 2\pi \frac{x_0}{\lambda_n}$ in the recorded signal, in the limit of vanishing spectrometer slit width. This factor varies during scanning if x_0 is constant, but remains constant if x_0 is proportional to λ_n.

The instrumental line shape given in Eq. (8.42) has the same shape as the spectral response if x_0/λ_n is constant. However, if x_0 is a constant error, then for a fixed λ the cosine factor of Eq. (8.42) becomes the constant factor less than unity, $\cos 2\pi \frac{x_0}{\lambda}$.

In the presence of an x_0 error, the correct rectifier phasing is still obtained by maximizing the output signal. For, suppose the rectifier and the qth component of the amplifier output differ in phase by $2\pi\frac{t_q}{T}$ as in Eq. (8.29). If the proper expression for $P_1(f',f)$ for this case is obtained from Eqs. (4.22) and (4.30) and inserted into Eq. (8.30), the resulting response function again has the constant factor $\cos 2\pi f_n t_n$ (assuming $w < 3f_n$ and $w_0 < \frac{2}{T}$). The minimizing of x_0 and the phasing of the rectifier are therefore independent adjustments, assuming that x_0 is known to be a small fraction of the wavelength.

One-sided operation.-- For this mode of operation the spectral response, the value of the spectral response at ν_n, and the instrumental line shape are obtained from Eq. (4.24). They are, for n = 13:

$$S(\nu, \nu_n) = \sin 2\pi(\gamma+\tfrac{n}{4})\frac{\nu}{\nu_n} \left[\text{dif } \tfrac{n}{2\nu_n}(\nu - \nu_n) - \text{dif } \tfrac{n}{2\nu_n}(\nu + \nu_n) \right],$$

$$(8.43)$$

$$S(\nu_n, \nu_n) = \sin 2\pi (\gamma + \tfrac{n}{4}) = \cos 2\pi\gamma \quad, \qquad (8.44)$$

and

$$S(\lambda_n, \lambda) = \sin 2\pi (\gamma + \tfrac{n}{4})\frac{\lambda_n}{\lambda} \left[\text{dif } \tfrac{n}{2\lambda} (\lambda_n - \lambda) - \text{dif } \tfrac{n}{2\lambda} (\lambda_n + \lambda) \right].$$

$$(8.45)$$

The spectral response has the same shape as $S(f, f_n)$ of Figure 21(b), plotted for $\gamma = \frac{1}{12}$. The rapidly varying sine factor causes a relatively large shift in the wave number of peak response and introduces a strong asymmetry about the ordinate $\nu = \nu_n$. For $\gamma = \frac{1}{12}$, the peak response has the value 0.96 and is shifted by about 0.24 $\frac{\nu_n}{n}$ toward smaller wave numbers; the response at ν_n is 0.866, the same as for two-sided operation. The zeros of the curve no longer must occur at even multiples of $\frac{\nu_n}{n}$. For example, $\gamma = \frac{1}{12}$ yields a value -0.057 for the response at 2 ν_n.

An error such that $\gamma = 1/6$ produces a peak response of 0.87 shifted by 0.45 $\frac{\nu_n}{n}$ toward shorter wave number and a response of 0.500 at ν_n. A negative value of γ, corresponding to an average location of the movable grating too near the fixed grating by a distance $\left|x_0\right|$, causes a shift of the peak response toward higher wave numbers.

The quantity $S(\nu_n, \nu_n)$ is the same, for n = 13, as in the two-sided mode. The instrumental line shape of Eq. (8.45) has the same shape as the spectral response curve of Eq. (8.43) if x_0/λ_n is constant. If x_0 is constant, the sine factor of $S(\lambda_n, \lambda)$ can be

written $\sin 2\pi \left(\dfrac{x_o}{\lambda} + \dfrac{n \lambda_n}{4} \right)$, which gives $S(\lambda_n, \lambda)$ a slightly different shape from that of $S(\nu, \nu_n)$.

Small irregularities in path difference repeated at intervals of 2T: "x_1 error"

Imperfections in the cam contour and cam gear are largely responsible for this type of error. Because of the superiority of two-sided operation, from the point of view of x_o errors, that mode only will be treated here. In this case a single irregularity on the cam produces a path difference irregularity once in a time 2T. The results embodied in Eqs. (4.43)-(4.46) and (8.22)-(8.27) apply immediately, if the imperfections are approximated by linear segments like those shown in Figure 22. Equations (8.22) and (8.27) could again be used to make approximate calculations for an irregularity having specific values of τ, τ_o and x_1. However, it is possible to draw some general conclusions when x_1 is sufficiently small by putting these equations into a different form. Using the relation $\nu = \dfrac{n}{T \nu_n}$ and setting $\nu = p \nu_n$, where p may be thought of as a continuous variable, of which integral values $p = 1, 2, \ldots 10$ may eventually be selected, the portion $(\Delta S)^+$ of ΔS having minus signs in the arguments can be combined with the similar portion of ΔS_o to yield

$$(\Delta S - \Delta S_o)^+ = $$

$$\frac{\tau_o / |\tau_o|}{2\pi n(p-1)} \left\{ \cos 2\pi \left[n \frac{\tau}{2}(p-1) \frac{pnx_1}{4x_m} \right] \cdot \frac{\sin 2\pi \left[\frac{n}{2} \frac{\tau_o}{T}(p-1) + \frac{pnx_1}{4 x_m} \right]}{1 + \frac{T}{\tau_o} \cdot \frac{x_1}{2x_m} \cdot \frac{p}{p-1}} \right\}$$

$$- \frac{\tau_0/|\tau_0|}{2 \pi n(p-1)} \left\{ \cos 2\pi \; n \; \frac{\tau}{T} \; (p-1) \; \sin 2\pi \frac{n}{2} \; \frac{\tau_0}{T} \; (p-1) \right\} \quad . \quad (8.46)$$

For sufficiently small values of $\frac{x_1}{x_m}$ and for p confined to the range ($2 \leq p \leq 10$), the first term of Eq. (8.46) differs from the second term by an amount small compared to unity, provided also that $\frac{|\tau_0|}{T}$ is large enough that the denominator of the first term does not differ too much from unity. For very small values of $\frac{|\tau_0|}{T}$, the quantity $(\Delta S - \Delta S_0)^+$ becomes very small because the denominator of the first term becomes large and the argument of the sine factor in the second term becomes small. Intermediate values of $\frac{|\tau_0|}{T}$, such that the denominator of the first term lies between 1.00 and 5.00, for example, yield a similar small value for the whole expression. The exact value of $(\Delta S - \Delta S_0)^+$ depends on $\frac{\tau}{T}$ also, but a maximum value $(\Delta S - \Delta S_0)^+_{max}$ can be found which is independent of both τ_0 and τ .

Direct measurements of cam follower displacements show that a typical x_1 error caused by cam imperfections has an amplitude, relative to the maximum path difference, of $\frac{x_1}{x_m} = 0.0015$. The small additional angle in the arguments of the cosine and sine functions of Eq. (8.46) thus has a value no greater than

$$2\pi \; \frac{pn \; x_1}{4 \; x_m} \doteq 18° \qquad (8.47)$$

for p = 10 and n = 13 and the arguments of the preceding paragraph can be used to establish a maximum value for $(\Delta S - \Delta S_0)^+$. A similar

result holds for the portions of Eqs. (8.22) and (8.27) having plus signs in the arguments. It is safe to say, then, that the maximum contribution to be expected is

$$(\Delta S - \Delta S_o)_{max} = 2(\Delta S - \Delta S_o)_{max}^+ .$$

For an x_1 error such that $\frac{x_1}{x_m}$ is of the order of 0.0015 or smaller, for arbitrary τ and τ_o, and for $2 \leq p \leq 10$, the result is

$$(\Delta S - \Delta S_o)_{max} = \frac{1}{2} \cdot \frac{x_1}{x_m} \cdot \frac{p}{p - 1} . \tag{8.48}$$

This is independent of n as long as the expression on the left hand side of Eq. (8.47) is substantially less than 90°. For the nominal value $\frac{x_1}{x_m} = 0.0015$, the maximum contribution is 0.0015 at $p = 2$ and 0.0008 at $p = 10$. A calculation of the contribution at $p = 1$ based on Eqs. (8.22) and (8.27) yields even smaller values.

The cam follower measurements reveal that there are about 10 x_1-type irregularities having $\frac{x_1}{x_m}$ of the order of 0.0015 and about 30 smaller ones having $\frac{x_1}{x_m} = 0.0005$ on the average. The distribution of these irregularities with respect to size, duration, and time of occurrence is more random than regular. If it is recalled that the above calculated contributions to the signal are maximum values and that the magnitudes and signs of the actual contributions are quite sensitive functions of x_1, τ, and τ_o, it becomes reasonable to expect a total contribution not much exceeding the value 0.0015 for a given p. Of course, there is a finite possibility that the total contribution is much greater than this, and for that reason these cam irregulari-

ties should be reduced, by additional care in machining.

The two halves of the cam are made unsymmetrical by the presence of these x_1 irregularities. Thus asymmetry of the cam or other mechanical components not only produces unwanted contributions to the spectral response, but, according to the discussion following Eq. (4.42) introduces a $\frac{1}{2T}$ frequency component into the rectifier output.

Periodic errors of period less than 2T

An x_1 error repeated exactly during each half revolution of the cam corresponds to an error of period T, for two-sided operation, and produces just twice the contribution to the spectral response as the same error with period 2T. Conceivably, an x_1 error can occur with such a frequency and with the proper phase relation relative to the rectifier to accumulate a large error signal. In general, the frequencies of most concern are submultiples of the rectifica-tion frequency 13 cps, since variations in the transmission function $L_1(t,f')$ at these frequencies have 13 cps Fourier series components. Calculations made by P. B. Burnside show that cosinusoidal periodic errors in the path difference, having amplitudes of the order of 0.005 x_m, can produce contributions of the order of 0.05 to the spectral response for certain values of p.[*] Although periodic errors are undoubtedly present, caused, for example, by slight imperfections in the cam drive gears, their amplitudes are apparently much smaller than the x_1 errors already discussed, since no definite periodicity is evident in the measured cam follower displacements.

[*] Private communication.

Errors in synchronization
of scanning drives

Errors $\Delta\theta$, $\Delta\theta_n$ and ΔB in the monochromator grating angle θ, the modulator scanning angle θ_n and the ratio arm B, respectively, produce a shift of the apparent wave number of input radiation of a given wave number. The error $\Delta\theta$ produces directly a wave number error, in terms of the half-width $\frac{\nu_n}{n}$ of $S(\nu, \nu_n)$,

$$(\Delta\nu)_\theta = (-n \cot\theta \, \Delta\theta) \frac{\nu_n}{n} , \qquad (8.49)$$

obtained from Eq. (7.4). Even if the modulator is properly adjusted for wave number ν_n the shift is determined essentially by Eq. (8.49), because of the relatively large passband of the modulator.

On the other hand, if the monochromator is in correct adjustment so that its spectral response for input radiation of wave number ν_n is $V_{2\Delta\nu}(\nu - \nu_n)$, then an error $\Delta\theta_n$ or ΔB causes a shift of $S(\nu, \nu_n)$ with respect to $V_{2\Delta\nu}(\nu - \nu_n)$. An error $\Delta\theta_n$ causes a shift of $S(\nu, \nu_n)$ given by

$$(\Delta\nu_n)_{\theta_n} = (-n \cot\theta_n \, \Delta\theta_n) \frac{\nu_n}{n} , \qquad (8.50)$$

based on Eq. (7.3). Values of $(\Delta\nu_n)_{\theta_n}$ from Eq. (8.50) are given below for n = 13, for selected values of θ_n, and for $\Delta\theta_n = 0.025°$, the measured uncertainty in θ_n in the instrument at present:

θ_n	$(\Delta\nu_n)_{\theta_n}$
10°	$0.032 \frac{\nu_n}{n}$
20°	$0.015 \frac{\nu_n}{n}$
30°	$0.010 \frac{\nu_n}{n}$

The combined modulator-monochromator spectral response has its center of area shifted by an amount depending on the ratio $\dfrac{(\Delta\nu)_{mod}}{\Delta\nu}$ listed in Table 2. For example, a calculation for n = 13, $\dfrac{(\Delta\nu)_{mod}}{\Delta\nu}$ = 2, and $(\Delta\nu_n)_{\theta_n}$ = 0.1 yields an effective wave number error of approximately 0.01 $\dfrac{\nu_n}{n}$.

The shift of $S(\nu, \nu_n)$ with respect to $V_{2\Delta\nu}(\nu - \nu_n)$ produced by an error in B follows from Eq. (7.3):

$$(\Delta\nu_n)_B = \left[-\frac{n\ell}{\ell+B} \cdot \frac{\Delta B}{B} \right] \frac{\nu_n}{n} \quad .$$

In practice the value of ΔB is no greater than 0.002 in. and could be made smaller if necessary. The shift $(\Delta\nu_n)_B$ for $\Delta B = 0.002$ in. is given below for three of the monochromator gratings:

grating lines/in.	B in.	$(\Delta\nu_n)_B$
180	0.300	0.084 $\frac{\nu_n}{n}$
90	0.622	0.039 $\frac{\nu_n}{n}$
45	1.374	0.016 $\frac{\nu_n}{n}$

Again the effective wave number error is of the order of one tenth of this shift.

The sources of errors

The mechanical components which are the sources of errors may be classified according to the types of errors already discussed and they also fall into three groups distinguished by the associated amplitude

of motion. The three distinct amplitudes are X_m, $C_0 \sin \theta_n$ and C_0.

Components associated with the amplitude X_m. -- These are the
pivot ways, the pivot bearing, the coupling unit on the grating rod,
and the fixed grating. The measured uncertainty ΔX in the position
of the movable grating due to these sources is of the order of
0.00015 in. The path difference error relative to the wavelength
is then

$$\frac{\Delta x}{\lambda_n} \doteq \frac{7.5 \text{ microns}}{\lambda_n} \quad ,$$

which is therefore most important at the shorter wavelengths. The
most likely types of errors from these sources are x_1 errors at
grating reversal and constant x_0 errors.

Components associated with the amplitude $C_0 \sin \theta_n$. -- Deviations
from straightness of the yoke bar and inaccuracy in the bearings of
coupling unit R and in the bushings of the coupling unit on the drive
rod result in errors which may be denoted by $\Delta(C_0 \sin \theta_n)$. The
corresponding error in path difference is

$$\Delta x = (2 \cos \alpha) \frac{B}{\ell + B} \, \Delta(C_0 \sin \theta_n) \, ,$$

while, according to Eq. (7.3),

$$\lambda_n = \frac{4 \cos \alpha}{n} \, \frac{B}{\ell + B} \, C_0 \sin \theta_n \quad .$$

Then

$$\frac{\Delta x}{\lambda_n} = \frac{n}{2} \, \frac{\Delta(C_0 \sin \theta_n)}{C_0 \sin \theta_n} \quad .$$

This quantity is independent of the reduction ratio $\frac{B}{\ell + B}$ but does vary during scanning, becoming large for small values of θ_n. The measured magnitude of $\Delta(C_o \sin \theta_n)$ is about 0.0003 in., for which

$$\frac{\Delta x}{\lambda_n} \doteq \frac{1}{90} \quad \text{when} \quad \theta_n = 10^o \; .$$

A slightly different result holds for the following three sources of error: the positioning of coupling unit R on the follower block along a line perpendicular to the follower guide shafts, radial play in the follower ball bushings, and deviations from straightness of the follower guide shafts. The path difference error is

$$\Delta x = \frac{(2 \cos \alpha)B}{\ell + B} \cos \theta_n \cdot (\text{error})$$

and

$$\frac{\Delta x}{\lambda_n} = \frac{n}{2} \frac{(\text{error})}{C_o \tan \theta_n} \quad .$$

Again the measured error is about 0.0003 in. Of course the positioning error of coupling unit R can be eliminated by proper adjustment.

Components associated with the amplitude C_o. -- All the parts engaged in moving the follower block belong in this group, for which

$$\frac{\Delta x}{\lambda_n} = \frac{n}{2} \frac{\Delta C_o}{C_o} \quad .$$

These errors are independent of both B and θ_n.

Ideally, the radius of the fixed cam roller measured at the instantaneous line of contact between roller and cam should be constant. The measured total variation is 0.0005 in. This produces a series

of x_1 errors of varying duration since the cam roller angular speed is not constant. Most of the follower displacement error can be traced to the cam itself which, as noted earlier, has a number of x_1 irregularities as large as 0.0015 in., besides the non-linear reversal regions. In addition, the average cam radius is about 0.0007 in. larger than it was designed to be. This is equivalent to an x_0 error such that $\gamma = \frac{1}{200}$, which is negligible. The follower displacement measurements alluded to were made in such a way that backlash in the cam drive gears did not affect the results, but any other gear imperfections are included in these measurements.

The backlash in the gear train between the cam drive motor and the cam corresponds to a follower displacement error of 0.0008 in., which can be responsible for random x_1 errors of about half the magnitude of the cam errors.

The net power required of the cam drive motor is only enough to overcome friction of all moving parts. The torque required during the constant-velocity motion is also small, but during grating reversal the motor experiences a torque pulse which undoubtedly sets up an oscillation of the rotor relative to the rotating field. The phase of this oscillation is keyed to the reversal points, but the frequency is likely to vary because of variations of line voltage, friction, etc. As yet no measurements of this effect have been attempted.

CHAPTER IX

EXPERIMENTAL RESULTS

A preliminary evaluation of the interferometric modulator's

performance has been made and the results are discussed below.

The overall attenuation of the desired radiation

In the following experimental investigation the modulator was

located at the exit slit of the spectrometer, which was equipped

with conventional filters for producing nearly pure (estimated at

greater than 95%) first order radiation. The radiation could be

chopped by means of an auxiliary chopper or by interferometric

modulation. In the latter case the modulator was used in the two-

sided mode with n = 13.

From the standpoint of geometrical optics the modulator optical

system is a one-to-one transfer between monochromator and detector

units, except for the slight difference in focal lengths. (This has

not yet been verified experimentally, since the quality of the over-

all optical alignment may be different before and after insertion of

the modulator into the system. The modulator unit should be inserted

and removed several times and the performance of the system as a

conventional spectrometer evaluated for both arrangements to get

a good estimate of this insertion factor.) Since the mirrors are

164

all practically 100% reflecting for far infrared radiation, the principal source of attenuation is the lamellar grating, which is sufficiently smooth, but not sufficiently flat, to be a perfect reflector when adjusted to mirror position. That is, not all the facets can be made to fall into alignment at once, so that a part of the "mirror" surface acts as a lamellar grating of depth comparable to the wavelength and diffracts some of the radiation into the $\pm$ first and higher lamellar grating orders, which are intercepted by the exit slit jaws when $s_3 \leq \frac{F\lambda}{b}$. This effect was investigated for wavelength λ by using the auxiliary chopper to obtain a signal, with the lamellar grating at mirror position and the slit widths equal to $\frac{F\lambda}{b}$. This signal was then compared with that obtained when a flat mirror was placed in front of the lamellar grating. These "reflectances" are entered in Table 7 for the wavelengths 90μ and 320μ. The value for 4.4 mm radiation was obtained in a similar manner using a microwave harmonic generator as source. When the exit slit width was increased beyond $\frac{F\lambda}{b}$, allowing some of the $\pm$ first order radiation to be detected, the "reflectance" was increased by as much as 5% for a 50% increase in s_3.

A measure of the completeness of destructive interference, or the depth of modulation, was obtained by again using the auxiliary chopper and slowly varying the path difference through successive multiples of $\lambda/2$. The difference between the observed maximum and minimum signals divided by the maximum signal was taken to be the

TABLE 7

Measured values of lamellar grating "reflectance",
depth of modulation, and the modulated signal
relative to the chopped signal
at selected wavelengths

λ	Lamellar Grating "Reflectance"	Depth of Modulation	Modulator Signal / Chopper Signal
90μ	0.80		
130μ			0.85
173μ		0.80	
195μ		0.85	0.85
320μ	0.85	0.90	0.95
4.4 mm	1.00	1.00	

depth of modulation. For this measurement it was essential to have

pure first order radiation and to have $s_3 \leq \dfrac{\overline{F}\lambda}{b}$. Table 7 shows

an increasing depth of modulation with increasing λ , which is con-
sistent with the increasing "reflectance".

The signal obtained by interferometric modulation, the chopper

having been removed, relative to the signal produced by chopping,

with the lamellar grating fixed at mirror position, is tabulated also.

This is expected to be proportional to the depth of modulation and

is seen to be approximately so. The absolute values of these signal

ratios are not significant because separate rectification systems

were used in obtaining the two signals. However, the noise level of the modulator signals was usually about 1.4 times the noise level of the chopper signal. Until this noise is reduced, therefore, the net effect of substituting the modulator for the chopper is a reduction of the signal to noise ratio by a factor of about 0.70 at 320 μ. Even so, this compares favorably with the reduction in signal produced by the conventional reststrahlen, transmission, and grating filters necessary to obtain comparable purity of radiation. The factor of 0.70 can apparently be increased by 10% by construction of a lamellar grating of sufficient flatness. A further increase may be expected if mechanical vibrations transmitted to the optical components and the detector can be reduced.

Measurement of the instrumental line shape by scanning the fixed-wavelength output of the monochromator

The instrumental line shape was measured by scanning the fixed-wavelength output of the monochromator with the modulator, which was adjusted for two-sided operation with n = 13. A band of first order radiation at λ = 169.9$\pm$ .25μ from the 90 line/in. dispersion grating of the spectrometer was isolated by the traditional filtering--KRS-5, black polyethylene, a 145 line/in. filter grating and a crystal quartz window on the Golay detector. The slits were all set at 20.00 mm, giving a calculated spectral slit width of 1.83 cm^{-1} and a ratio $\frac{(\Delta\nu)\text{mod}}{\Delta\nu}$ of 2.5. Since the mercury arc source did not completely fill the entrance slit, $\Delta\nu$ was actually somewhat smaller than this. The ratio arm B was set at 2.000 in., making $\frac{n \lambda_n}{\lambda}$ = 117.80 sin θ_n, by Eq. (7.3). The complete system was evacuated and

and λ_n was varied from zero to $\frac{41}{13}\lambda$ by varying θ_n from zero to 20.4°.

The resulting relative signal is plotted in Figures 47 and 48, in which the calculated function $S_0(\lambda_n, \lambda)$ also appears, as a broken line curve. The lack of agreement between the two curves for $\lambda_n < \frac{3\lambda}{n}$ can be traced partly to the increased effect of certain previously-discussed mechanical errors at these small values of $\theta_n (\le 1.5°)$ and partly to an inadequate signal to noise ratio. The rms noise level was approximately 1% of the maximum signal. The enhancement of the peaks between $\frac{3\lambda}{n}$ and $\frac{7\lambda}{n}$ is consistent with the presence of several per cent of second order and several per cent of third order radiation in the spectrometer output, the central maxima for these orders being at $\lambda_n = 6.5\frac{\lambda}{n}$ and $4.33\frac{\lambda}{n}$, respectively. The increments to the measured instrumental line shape at these values of λ_n amount to about half these percentages because of the increased counter-modulation effect for the shorter wavelength radiation. The presence of this higher order radiation was observed consistently in the three separate runs already mentioned.

In the range $10\frac{\lambda}{n} < \lambda_n < 16\frac{\lambda}{n}$ the whole experimental curve appears to be shifted to greater wavelengths by approximately $0.08\frac{\lambda}{n}$, as determined primarily by the positions of the zeros and the extrema of the curve. Two runs made under these same conditions and one run made with $\lambda = 160\mu$ showed similar shifts. This shift is barely within the experimental error; the monochromator wavelength error 0.25μ corresponds to a shift of $0.02\frac{\lambda}{n}$, the error $\Delta\theta_n$ in the
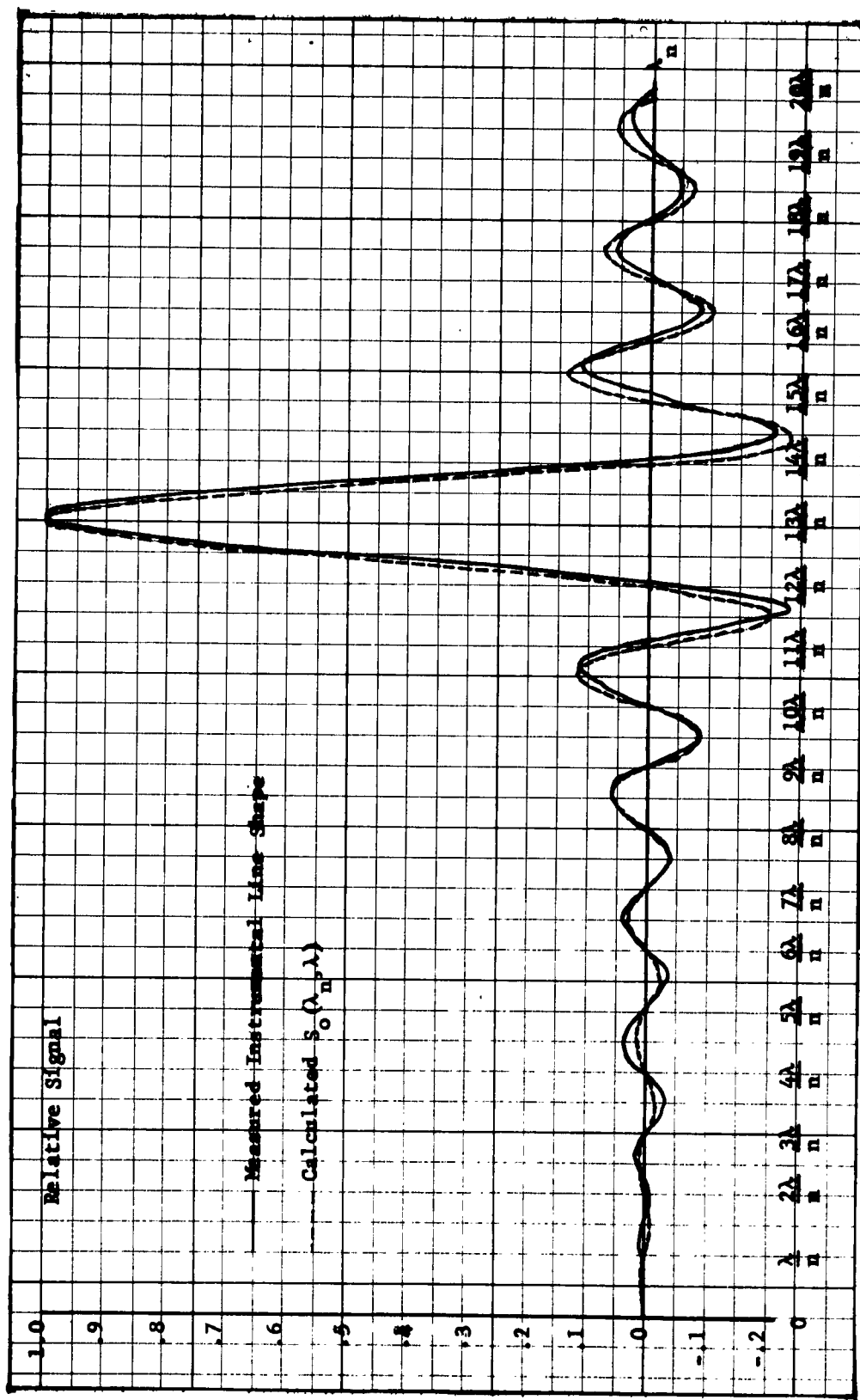
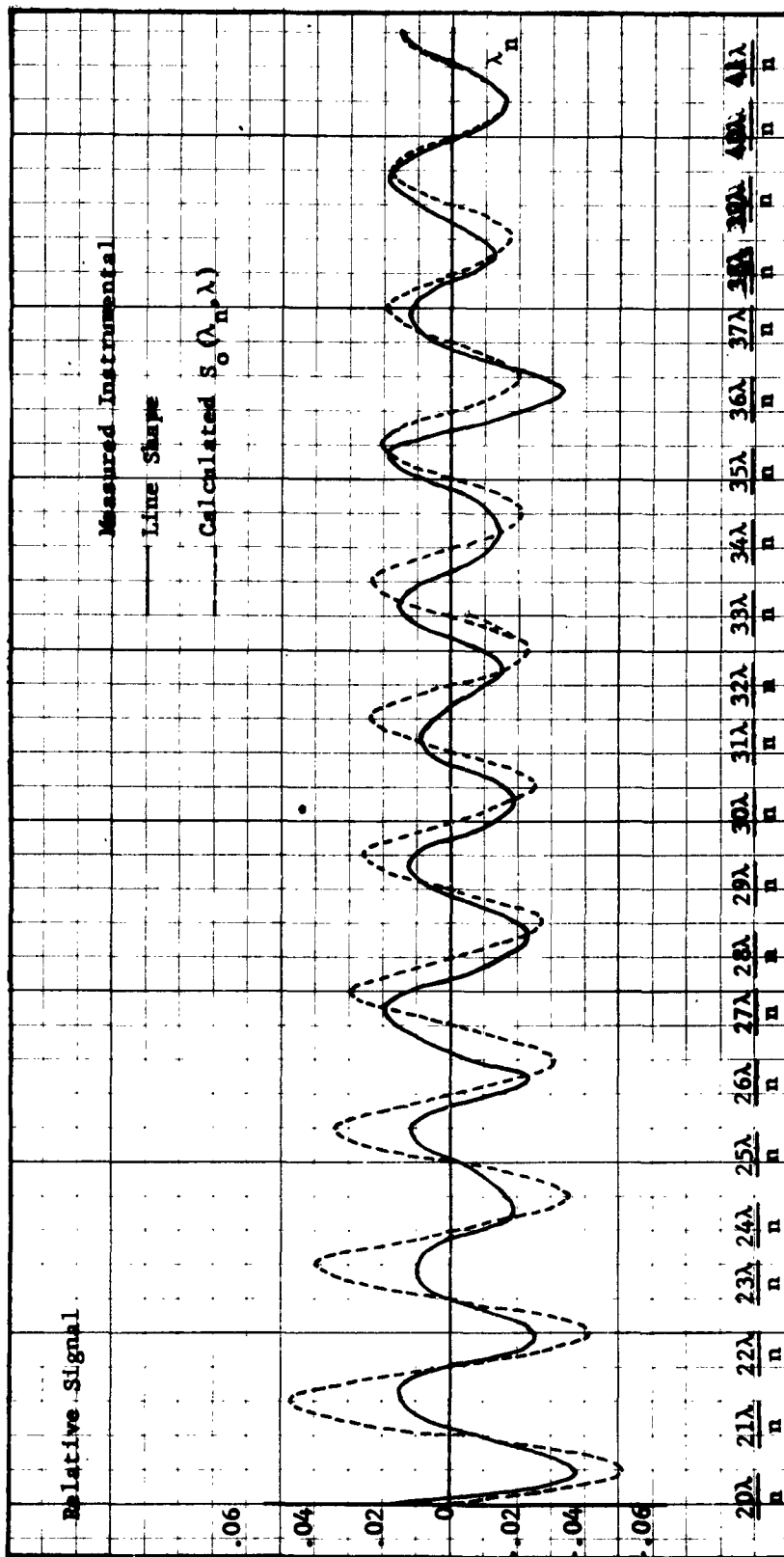Fig. 47. The calculated and measured instrumental line shape on $(0 < \lambda_n < \frac{20\lambda}{n})$.

Fig. 48. The calculated and measured instrumental line shape on $\left(\frac{20\lambda}{n} < \lambda_n < \frac{41\lambda}{n}\right)$.

scanning drive at $\theta_n \doteq 6°$ could produce a shift of $0.05 \frac{\lambda}{n}$, while an error of 0.002 inch in B corresponds to a shift of $0.01 \frac{\lambda}{n}$. The shift in the combined spectral response $V_{2\Delta\nu}(\nu - \nu_n) \, S(\nu, \nu_n)$ resulting from the shift under discussion is considerably smaller than $0.08 \frac{\lambda_n}{\lambda}$, but can and should be made smaller still by reducing the scanning drive error. Spring loading of the large worm gear may be the solution to this problem.

The slight broadening, or increase in the spacing of the zeros, to be expected because of the finite value of $\Delta\nu$ is too small to be observed with certainty. However, the increasing suppression of the feet for increasing λ_n is apparent and of the correct order of magnitude for λ_n as large as $22 \frac{\lambda}{n}$. The details of the curve between that point and $41 \frac{\lambda}{n}$ remain unexplained. Instead of diminishing uniformly with increasing λ_n, the feet appear to maintain nearly a constant amplitude until at $35 \frac{\lambda}{n}$ they again coincide approximately with $S_0(\lambda_n, \lambda)$. It is difficult to associate this with passage of a 39 cps component by the amplifier since, according to Figure 45, a small inverted dif curve of half width $\frac{\lambda}{n}$ should then appear at $39 \frac{\lambda}{n}$. (No significant difference in signal was observed when the region near $39 \frac{\lambda}{n}$ was scanned with the 39 cps filter disconnected from the amplifier circuit; apparently the normal amplifier-detector passband is sufficiently narrow, and the shape of the rectification function sufficiently like that described in chapter VIII, to eliminate the 39 cps component.) An x_0 error with

γ constant at about $\frac{1}{8}$ would account roughly for the observed variation in the amplitudes of the feet, but it would also invert the portion of the curve between $26 \frac{\lambda}{n}$ and $78 \frac{\lambda}{n}$. No such inversion appears in the measured curve.

In any event, the significance of this long wavelength end of the curve is somewhat questionable because the temperature rise of the $\frac{1}{8}$ h.p. cam drive motor operated in vacuum may have become sufficient to cause heating and thermal expansion of the mechanical parts of the modulator. The signal at $\lambda_n = \lambda$ decreased by 5% during the run in question and continued to decrease with time. The most obvious mechanism for this effect was expansion of the drive rod, which is near the motor and became noticeably warm during the run. This caused an x_0 error independent of λ_n. The 5% signal decrease corresponds to $\gamma = \frac{1}{17}$. The $\frac{1}{8}$ h.p. motor used in the tests has been replaced by a $\frac{1}{25}$ h.p. water-cooled motor and these gross temperature effects have consequently disappeared.

The instrumental line shape was also measured using as input the effectively monochromatic 3.3 mm wavelength fourth harmonic from a microwave harmonic generator. The modulator wavelength λ_n was varied from zero to $29 \frac{\lambda}{n}$. Although the signal to noise ratio and the stability of the signal were not sufficiently good for detailed measurements, the feet of the measured curve at the larger values of λ_n, in particular near $26 \frac{\lambda}{n}$, were not significantly larger than those of $S_0(\lambda_n, \lambda)$.

Effectiveness of the modulator
as a filter

The instrumental line shape measurements indicate that the
spectral response has the predicted order of magnitude in the neigh-
borhood of the second and third spectrometer orders. The monochroma-
tor-modulator combination has been used to scan most of the water
vapor absorption spectrum from 100-1000 μ . In the regions of most
strong first order absorption lines the output signal was zero to
the precision allowed by the noise level. Very near blaze measurable
higher order contributions were observed. Three examples may be cited.
First, at λ = 259.7μ , far from the balze wavelength of 400 μ of the
45 line/in. dispersion grating, an absorption line yielded zero
signal at atmospheric pressure and 47 units of signal with the
instrument evacuated. The rms noise level was about 1.5 units. The
higher order signal contribution was then certainly no greater than
3% of the total signal and the purity of the radiation, or the ratio
of the first order signal to total signal, was at least 97%.

Second, at λ = 174.4μ , which is closer to the blaze wavelength
of 200 μ of the 90 line/in. grating, a similar test revealed a purity
of at least 96%. An independent measurement of the total higher
order radiation, provided mainly by the atmospheric windows at 87.2
and 58.1μ , showed that the modulator in effect multiplied this
radiation by a factor less than 0.008.

Third, measurements made on the absorption line at 400.8μ ,
at the blaze of the 45 line/in. grating, showed a definite higher
order contribution which was negative in polarity and reduced the

purity to 90 %. The size of this higher order contribution can be attributed partly to the highly non-uniform spectral distribution of the higher order radiation, caused by the presence of the absorption lines which form the sides of the higher order windows. Under this circumstance the higher order contribution to the integral of the product of the input spectral distribution with the combined spectral response function is not necessarily negligible even if the modulator spectral response curve passes through zero at $2\nu_n$, $3\nu_n$, etc. It is in this situation that apodization is desirable.

x_o error

The results of deliberately introducing an x_o error into the path difference, for two-sided and for one-sided operation, are found in Figure 49(a) and (b), respectively. In both cases the error was such that x_o/λ was constant. In the first case the thermal expansion of the drive rod had produced an x_o error such that $\dfrac{x_o}{\lambda} = \dfrac{1}{5}$, which was increasing slightly during scanning, but which yielded essentially $S_o(\lambda_n, \lambda)$ multiplied by $\cos 2\pi \dfrac{x_o}{\lambda}$, in agreement with Eq. (8.42). The radiation used was the 170μ monochromator output obtained by the filtering already described. The calculated positions of the zeros and the central maximum are marked below the curve. The curve for the one-sided case was obtained by scanning a fixed harmonic generator line of wavelength $\lambda = 4.38$ mm, with the fixed part of the lamellar grating set 0.0145 in. from its usual position in a direction away from the spherical mirrors, i.e., so that $\dfrac{x_o}{\lambda}$ was equal to $-\dfrac{1}{6}$. The resulting instrumental line shape is violently
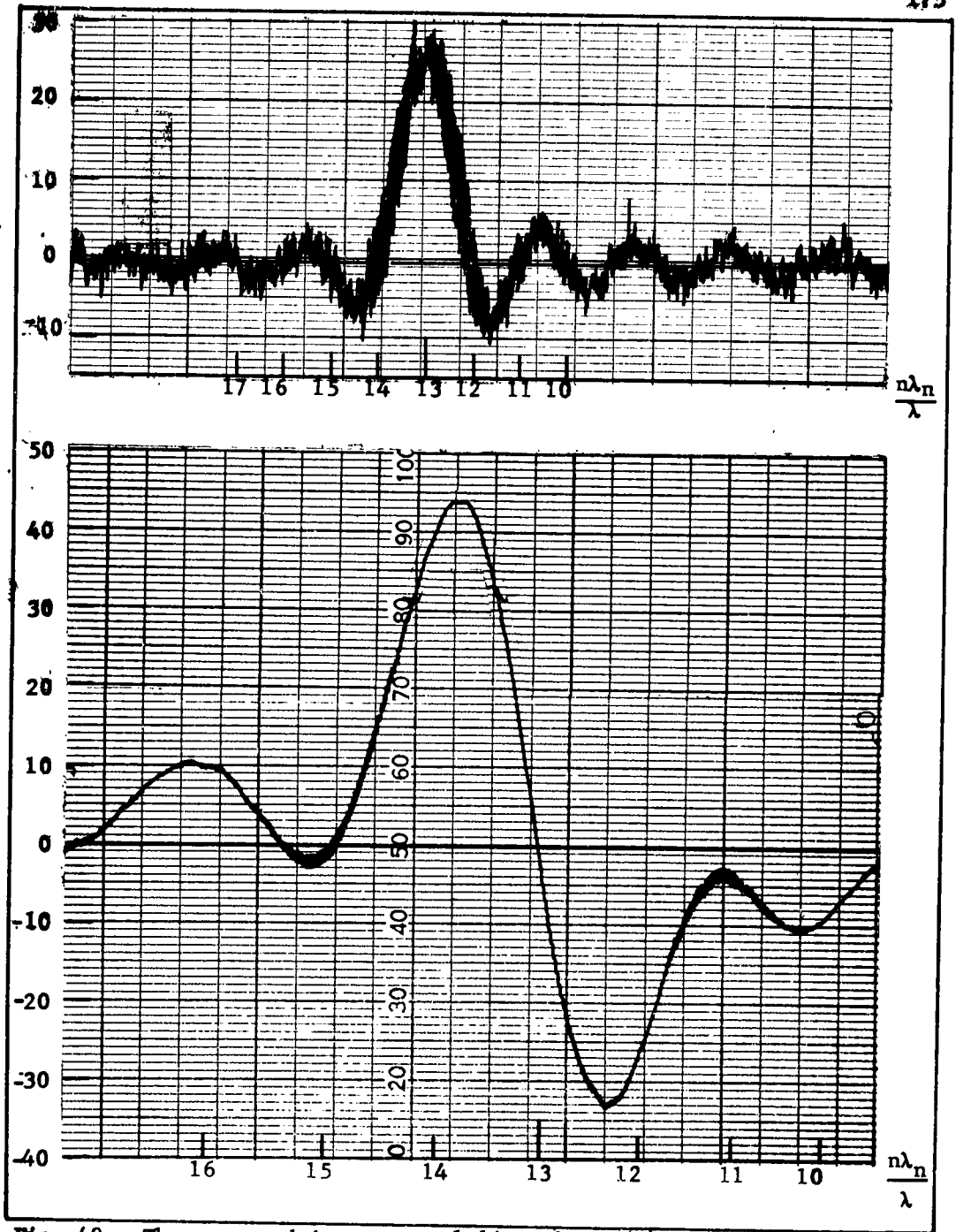
Fig. 49. The measured instrumental line shape (a) in the presence of an x_0 error such that $x_0/\lambda = 1/5$, operating in the two-sided mode, and (b) when $x_0/\lambda = -1/6$, operating in the one-sided mode.

skewed with positive peak shifted to higher wavelengths, as predicted
by Eq. (8.45). The calculated positions of the zeros and central
maximum for the error-free case entered below the curve may be in
error by as much as $\frac{1}{5}$ of the half width since a non-synchronous
motor was used for scanning.

1 cps and $\frac{1}{2}$ cps components in the recorder input

Observations of the 1 cps component in the input to the recorder
made while scanning the harmonic generator output with the modulator
operating to mirror position agree well with the predictions out-
lined in chapter VIII. For example, in Figure 49(b), the broadening
of the trace was observed to be caused by a 1 cps variation in the
signal. It is greatest not at, but adjacent to, large signal maxima
or minima as expected.

In the modulator-monochromator arrangement the Golay detector
was effectively rigidly attached to the modulator and was jarred
slightly each time the lamellar grating reversed. This occurred once
each second and caused a 1 cps variation in the recorder pen motion
even with zero radiation signal. The recording of Figure 49(a) shows
this microphonic noise throughout, as well as strong 1 cps and $\frac{1}{2}$ cps
components in the central region because of the finite monochromator
passband and the x_0 error. The recorder variations due to the latter
two causes are not troublesome when the modulator and monochromator
scan in synchromism, since then $\Delta\nu$ is made smaller and the x_0 error
made insignificant. The microphonic noise can be filtered out by
decreasing the passband v_0, but it is preferable to eliminate the

cause by redesigning the cam so that the reversal time is larger,

the acceleration of the cam follower smaller. The effect of the

resulting increase in non-linear path difference variation may then

have to be reduced by apodization of some form.

Variation of output radiant flux with slit widths

The predictions of chapter VI have been verified experimentally.

First it was necessary to correct for the fact that the image of the

mercury lamp source at the monochromator entrance slit was only 18 mm

wide and was not uniform in intensity over its whole width. This

correction was obtained as follows. With the modulator and monochro-

mator in their usual tandem arrangement, but with the lamellar grating

fixed at mirror position, the radiation was chopped by means of the

auxiliary 13 cps chopper. All three slit widths were kept equal and

the output signal, taken to be proportional to the radiant flux, was

recorded versus slit width $s = s_3$. For $s \leq 7$ mm the flux was pro-

portional to s^2 with good precision but for 7 mm $< s < 20$ mm the

increase in flux was less rapid. The ratio of the measured relative

flux Φ/Φ_o to the quantity $(s/s_o)^2$ is the desired correction factor,

plotted in Figure 50 versus slit width in mm.

Then the opaque chopper was removed. Modulator and monochromator

were both adjusted permanently for the wavelength $172.5\,\mu$, which was

pure first order radiation, making $\dfrac{\overline{F}\lambda}{b} = s_o = 6.9$ mm. The 5%

difference in focal lengths of the monochromator and modulator

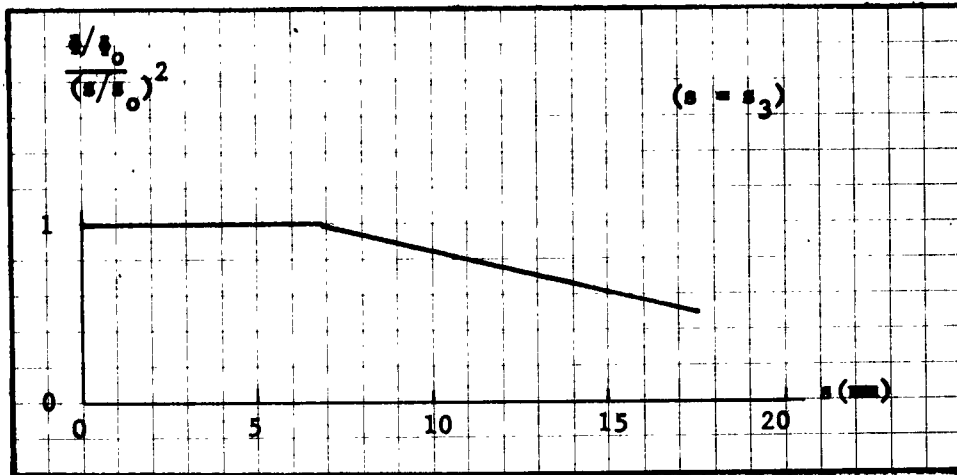collimating mirrors was neglected in all slit width calculations.

Fig. 50. The ratio of the measured relative flux to $(^s/_{s_o})^2$ as a function of slit width; opaque chopper used.

The three possibilities for which the expressions for the flux are given by Eqs. (6.6)-(6.11) were investigated. The flux Φ_o was identified with the signal obtained for $s = s_3 = s_o = 6.9$ mm. For a given sequence of slit settings the relative flux Φ/Φ_o was then calculated and plotted versus the appropriate variable slit width s or s_3. In all cases the spectrometer slit widths s were kept equal. First all slit widths were maintained equal and varied step-wise from 3 mm to 17.5 mm. The results appear in Figure 51. The solid line is the calculated curve corresponding to Eq. (6.6) in the range $o < s < 6.9$ mm and to the product of Φ/Φ_o of Eq. (6.7) and the correction factor of Figure 50 in the range 6.9 mm $< s <$ 17.25 mm. Figure 52 shows the experimental points for the case in which s_3 was fixed at $s_o = 6.9$ mm and s was varied. The calculated curve is obtained from Eq. (6.8) for $s = s_o$ and from the corrected Eq. (6.9) for
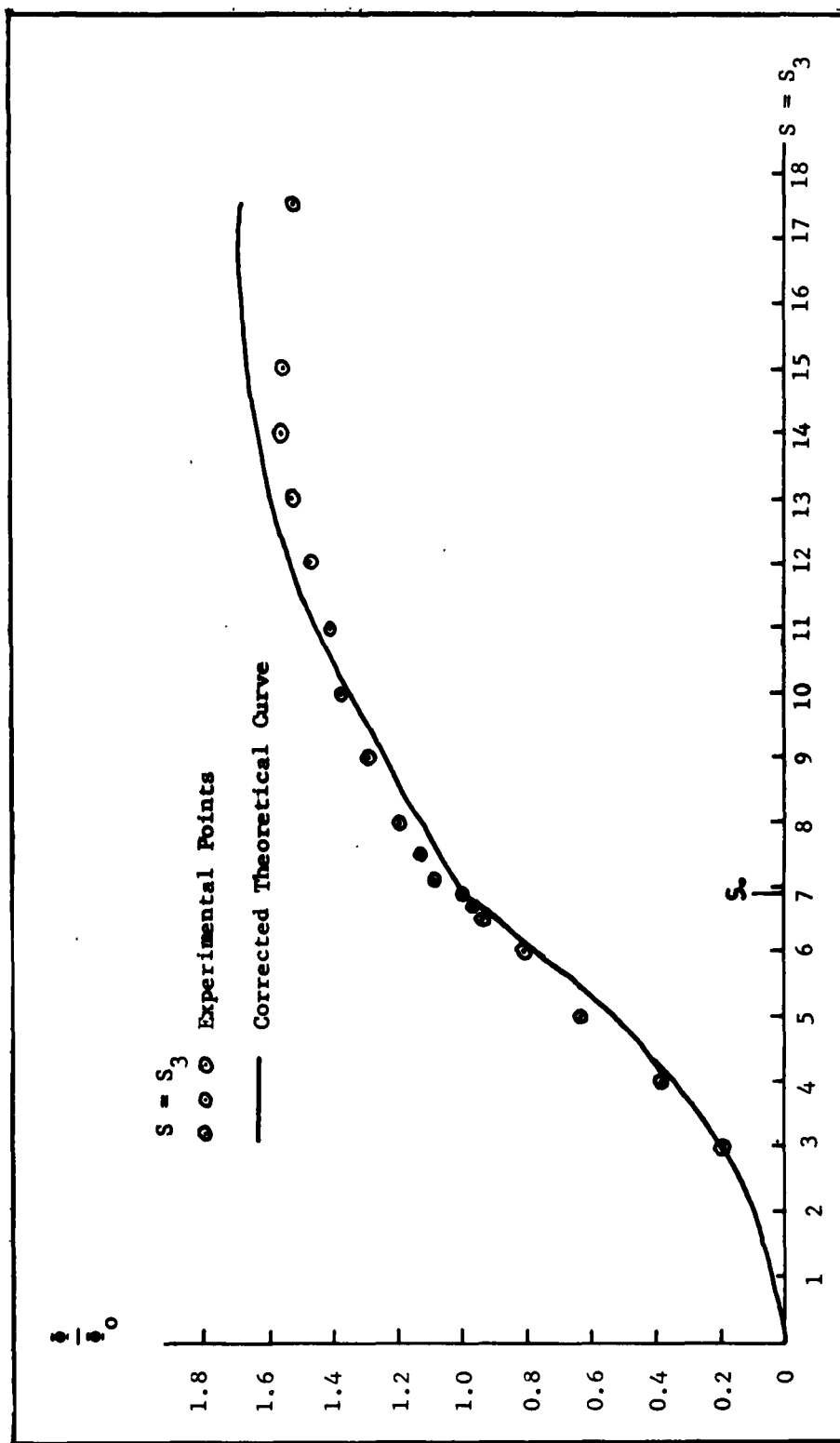
Fig. 51. Calculated and experimental values of the output relative radiant flux as a function of slit width; s_o = 6.9 mm; $s = s_3$.
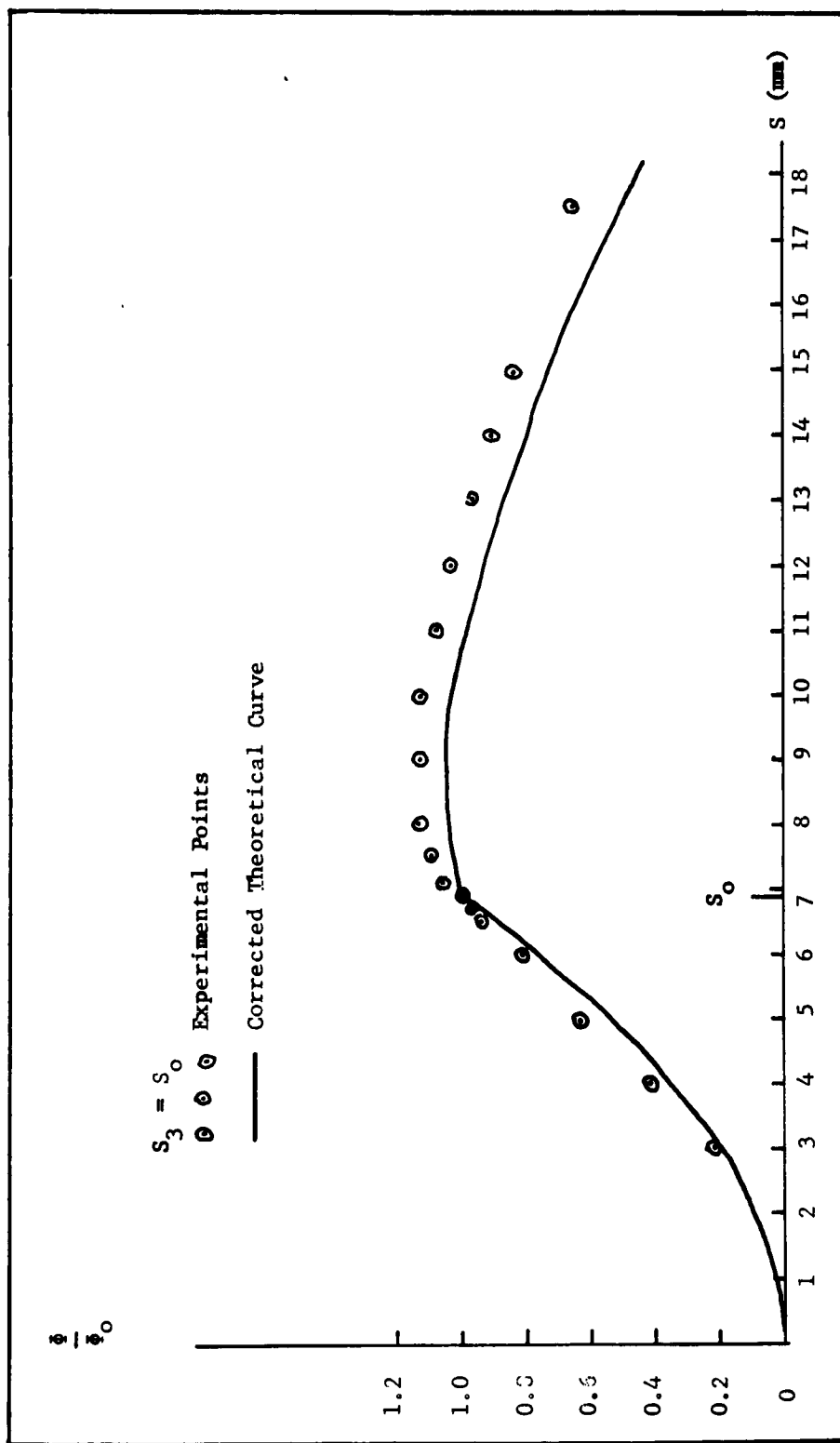
Fig. 52. Calculated and experimental values of the output relative radiant flux as a function of monochromator slit width; $s_3 = s_o = 6.9$ mm.

$s < s_0$. Finally, measurements were made with $s = s_0$ and s_3 variable. Figure 53 contains these results, along with the calculated curve which is given by Eq. (6.10) for $s_3 < s_0$. For $s_3 > s_0$ the corrected Eq. (6.11) applies. In this last figure the maximum relative flux occurs for $s_3 = 7.5$ mm instead of 6.9 mm. This is to be expected since, because of the larger modulator focal length, the value of s_3 equivalent to a given s is 1.05 s as in Eq. (7.13). The measured relative flux of Figure 53 is a direct measurement of the efficiency factor e_1. When corrected for the difference in focal lengths, the experimental value of Φ/Φ_0 at $s_3 = 2s_0$ is 0.67, which is to be compared with the calculated value 0.60 in Table 1.

Conclusions

The following corrections will improve the performance of the modulator and also reduce the uncertainty in the interpretation of results of testing: the lamellar grating should be made more nearly flat, backlash in the cam drive gear train should be reduced, and the cam irregularities should be removed.

The instrumental line shape measurements bear out the superiority of the two-sided mode of operation. The choice of $n = 13$ keeps shadowing effects small and allows the modulator and monochromator to be kept synchronized easily. The x_0 errors can be reduced to acceptable values by suitable adjustments. Assuming the corrections mentioned above to be made, the signal to noise ratio appears to be limited by microphonic noise and general mechanical instability caused by the accelerations during grating reversal.
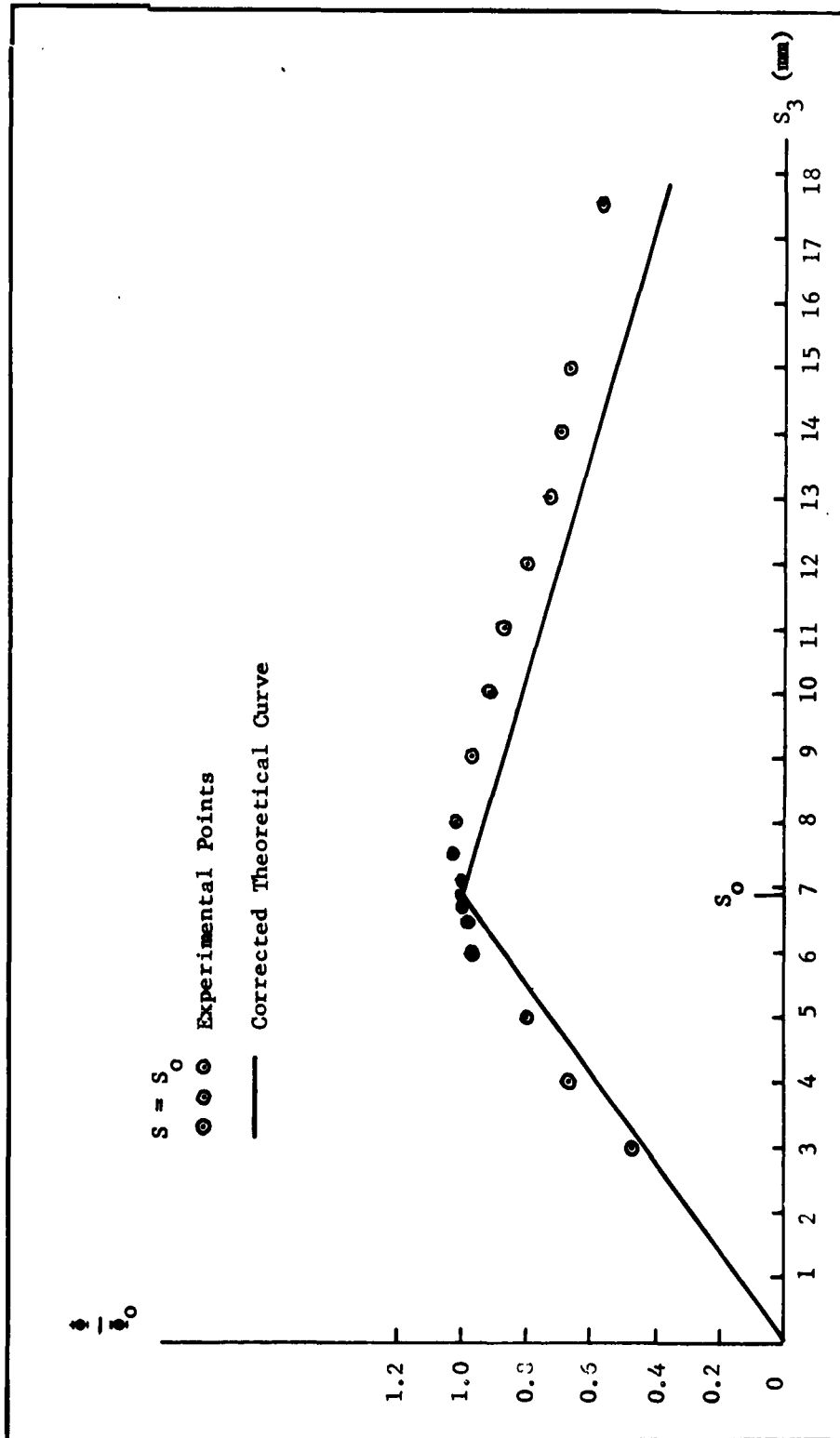
Fig. 53. Calculated and experimental values of the output relative radiant flux as a function of modulator exit slit; $s = s_o = 6.9$ mm.

This can be alleviated by operating at n = 26, which allows a cam speed of $\frac{1}{4}$ cps instead of $\frac{1}{2}$ cps and would not seriously affect synchronization. Also the cam can be reshaped to reduce the reversal accelerations.

BIBLIOGRAPHY

Books

Adams, E. P., and Hippisley, R. L., Smithsonian Mathematical Formulae
        and Tables of Elliptic Functions (Smithsonian Institu-
        tion, Washington, 1922).

Born, M., and Wolf, E., Principles of Optics (Pergamon Press, New York,
        1959).

Blackman, R. B., and Tukey, J. W., The Measurement of Power Spectra
        (Dover Publications, Inc., New York, 1959).

Lighthill, M. J., Introduction to Fourier Analysis and Generalized
        Functions (Cambridge University Press, 1958).

Pipes, L. A., Mathematics for Engineers and Physicists (McGraw-Hill
        Book Company, Inc., New York, 1946).

Strong, J., Concepts of Classical Optics (W. H. Freeman and Company,
        San Francisco, 1958).

Periodicals

Connes, J., J. phys. radium 19, 197 (1958).

Connes, P., Optica Acta 4, 136 (1957).

_____, Revue D'optique 38, 157 (1959).

_____, Revue D'optique 38, 416 (1959).

_____, Revue D'optique 39, 402 (1960).

Fellgett, P., J. Phys. Rad. 19, 187 (1958).

Gebbie, H., Roland, G., and Delbouille, L., Nature 191, 264 (1961).

Gebbie, H., Stone, N., and Walshaw, C., Nature 187, 765 (1960).

Genzel, L., J. Mol. Spect. 4, 241 (1960).

Genzel, L., and Weber, R., Z. angew. Physik 10, 127 (1957).

Genzel, L., and Weber, R., Z. angew. Physik 10, 195 (1957).

184

Happ, H., and Genzel, L., Infrared Physics 1, 39 (1961).

Jacquinot, P., J. phys. radium 19, 223 (1958).

Jacquinot, P., Reports on Progress in Physics 23, 267 (1960).

Oetjen, R. A., et al., J. Opt. Soc. Am. 42, 559 (1952).

Strong, J., J. Opt. Soc. Am. 44, 352 (1954).

Strong, J., J. Opt. Soc. Am. 47, 354 (1957).

Strong, J., and Vanasse, G., J. Opt. Soc. Am. 49, 844 (1959).

Strong, J., and Vanasse, G., J. Opt. Soc. Am. 50, 113 (1960).

Tinkham, M., Bull. Am. Phys. Soc. 6, 112 (1961).

Vanasse, G., Strong, J., and Loewenstein, E., J. Opt. Soc. Am. 49, 309 (1959).

Reports

"Final Report on Comparative Testing of Thermal Detectors", NDRC Contract OEM sr-1168, The Ohio State University (1946).

McCubbin, T. K. Jr., "Far Infra Red Spectroscopy from 100 to 700 Microns" (The Johns Hopkins University, Baltimore, Md., 1951).